

eScholarship@UMassChan

Modulating Influenza and Heparin Binding Viruses' Pathogenesis with Extrinsic Receptor Decoy Liposomes: A Dissertation

Item Type	Doctoral Dissertation
Authors	Hendricks, Gabriel L.
DOI	10.13028/M2V319
Publisher	University of Massachusetts Medical School
Rights	Copyright is held by the author, with all rights reserved.
Download date	2026-04-12 12:11:08
Link to Item	https://hdl.handle.net/20.500.14038/32028

**Modulating Influenza and heparin binding viruses' pathogenesis with extrinsic receptor
decoy liposomes**

A Dissertation Presented

By

Gabriel L. Hendricks

Submitted to the Faculty of the

University of Massachusetts Graduate School of Biomedical Sciences, Worcester

in partial fulfillment of the requirements for the degree of

DOCTOR OF PHILOSOPHY

June 28th 2013

Immunology and Virology Program

Modulating Influenza and heparin binding viruses' pathogenesis with extrinsic receptor decoy liposomes

A Dissertation Presented

by

Gabriel L. Hendricks

The signatures of the Dissertation Defense Committee signifies completion and approval as to style and content of the Dissertation

Robert Finberg, M.D., Thesis Advisor

Evelyn Kurt-Jones, Ph.D, Thesis Advisor

Jennifer Wang, M.D., Member of Committee

Masanori Terajima, Ph.D., Member of Committee

Peter Newburger, M.D., Member of Committee

Kenneth McIntosh, M.D., Member of Committee

The signature of the Chair of the Committee signifies that the written dissertation meets the requirements of the Dissertation Committee

Raymond Welsh, Ph.D., Chair of Committee

The signature of the Dean of the Graduate School of Biomedical Sciences signifies that the student has met all graduation requirements of the school.

Anthony Carruthers, Ph.D.,
Dean of the Graduate School of Biomedical Sciences

Immunology and Virology Program
June 28th 2013

Copyright Information

The chapters of this dissertation have appeared in the following publications/manuscripts:

Hendricks, G.L., Weirich, K.L., Viswanathan, K., Li, J., Shriver, Z.H., Ashour, J., Ploegh, H.L., Kurt-Jones, E.A., Fygenon, D.K., Finberg, R.W., Comolli, J.C., Wang, J.P. (2013).

Sialylneolacto-N-tetraose c (LSTc)-bearing Liposomal Decoys Capture Influenza A Virus. *J Biol Chem* 288, 8061-8073. DOI: 10.1074/jbc.M112.437202

Acknowledgements

I would like to thank all the people who have taught, helped, supported, and encouraged me throughout my graduate career and research.

I would like to especially thank my mentors, Dr. Robert Finberg and Dr. Evelyn Kurt-Jones for their advice, and encouragement. I have grown immensely as a scientist while under their tutelage and will be forever grateful for their guidance, scientific discussion and teaching me the little-known tidbits of the scientific research field.

I thank my thesis advisory committee members, Dr. Raymond Welsh, Dr. Susan Swain, Dr. Jennifer Wang, Dr. Masanori Terajima and Dr. Daniel Libraty for advice, support and direction during my career at UMass. I would also like to thank my additional defense committee members Dr. Peter Newburger and Dr. Kenneth McIntosh, who agreed to participate as my outside examiner, taking time out of his busy schedule to take part in my defense.

I would like to thank the University of Massachusetts and all of the support staff that performs the day-to-day tasks that make research possible. I would like to thank the core facilities that without, many of my experiments would be next to impossible to do, and to the administrative staff who have aided me in finalizing the requirements for graduation.

I would like to thank the many current and former members of the Finberg Lab. Thank you Shenghua, Jennifer, Ping, Anna, An, Megan, Glennice and Serena. I would also like to thank my fellow graduate students, those who have moved on before me, Matt and Christine who I have hoped to emulate. And to those that continue help each other in our journey to a doctorate, Ryan, Glen, Milan and Chris. Thank you for your advice, entertaining conversations and many science jokes, especially the thorough discussion of the pros and cons of tanning in the tissue culture hood.

I would like to thank my collaborators and members of the ENVELOP team, Dr. Fyngenson and her lab for all their help and discussion on the science of lipids and liposomes. Thank you for making all of the many, many liposome preparations over the years. Thank you to Dr. Zachary Shriver and his lab for the LSTc, LSTa and HS-octa glycolipids, that without, this project would not be possible. And I would like to thank Dr. Jim Comolli and Draper Laboratories for coordinating the project.

Finally, I would like to thank my all of my friends and family. I would not be where I am today if it were not for the love and support of my family and friends. They have always listened to my many gripes about in-depth problems that exist in biomedical research, and who most likely had little idea what I was talking about. But, more importantly, I want to thank you for your continued support during my long graduate career and always encouraging me after a bad experiment. Last, and most important of all, I would like to thank Heather Kolpa for making the last two years the best years of my life, and the running-est. It has been great to share my life with her, especially a fellow scientist and graduate student. I have become a better person and scientist with her, at home, at lab and at running, and I love and thank her dearly for that.

Abstract

Influenza is a severe disease in humans and animals, causing upwards of 40,000 deaths every year in America alone. Influenza A virus (IAV) also causes periodic pandemics every 10 to 50 years, killing millions of people. Despite this, very few effective therapies are available. All strains of IAV are prone to developing resistance to antibodies due to the high mutation rate in the viral genome. Because of this mutation rate, a yearly vaccine must be generated before every flu season, and efficacy varies year to year. IAV has also mutated to escape several of the clinically-approved small molecule inhibitors. A therapeutic agent that targets a highly conserved region of the virus could bypass resistance and also be effective against multiple strains of IAV. IAV attachment is mediated by many individually weak hemagglutinin–sialic acid interactions that all together make a strong attachment to a host cell. Polymerized sialic acid analogs can recreate these interactions and block infection. However, they are not ideal therapeutics due to solubility issues and *in vivo* toxicity. We used liposomes as a novel means for delivery of the sialic acid-containing glycan, sialylneolacto-N-tetraose c (LSTc). LSTc-bearing decoy liposomes form multivalent, polymer-like interactions with IAV. Decoy liposomes competitively bind IAV in hemagglutination inhibition assays and inhibit infection of target cells in a dose-dependent manner. LSTc decoy liposomes co-localize with IAV, while control liposomes do not. Inhibition is specific, as inhibition of Sendai virus and respiratory syncytial virus is not observed. In contrast, monovalent LSTc does not bind IAV or inhibit infectivity. LSTc decoy liposomes prevent the spread of IAV during multiple rounds of replication *in vitro* and extend survival of mice challenged with a lethal dose of virus. Considering the conservation of the hemagglutinin binding pocket and the ability of decoy liposomes to form high-avidity

interactions with IAV hemagglutinin, our decoy liposomes have potential as a new therapeutic agent against emerging strains.

Table of Contents

Title Page.....	i
Signature Page.....	ii
Copyright Information.....	iii
Acknowledgements	iv
Abstract	vi
Table of Contents	viii
List of Figures	xi
List of Tables.....	xiii
List of Abbreviations.....	xiv

Chapter I Introduction

A. Influenza the pathogen.....	1
B. Influenza the virus.....	3
Viral binding.....	6
Influenza A virus internalization	7
C. The immune response to Influenza A virus	10
Innate response to IAV	10
Adaptive immune response to IAV.....	13
Pulmonary recovery after IAV infection	15
D. Combating influenza – chasing a moving target.....	17
Small molecule inhibitors	17
Antibody therapeutics	19
Decoy receptors	20
Influenza virus decoy receptors	21
Sialylated decoy liposomes.....	22
E. Model systems for studying Influenza	24
F. Thesis objectives.....	27

Chapter II

Materials and Methods.....	29
----------------------------	----

Chapter III

Use of sialic acid containing decoy liposomes to prevent influenza A virus infection

Preface.....	42
Introduction.....	43
Results.....	44
Generation of decoy liposomes containing the sialic acid moiety LSTc or LSTa.....	44
Decoy liposomes containing LSTc bind to different strains of IAV	47
Decoy liposomes containing LSTc co-localize with IAV and inhibit binding of IAV at the surface of A549 human lung epithelial cells.....	51

LSTc decoy liposomes co-localize specifically to IAV infected A549 cells.....	55
Decoy liposomes containing LSTc prevent IAV infection of MDCK cells	58
Decoy liposomes containing LSTc do not prevent infection of respiratory syncytial virus in Vero cells	62
Functionalized decoy liposomes are not toxic <i>in vitro</i> or <i>in vivo</i>	62
Decoy liposomes containing LSTc remain active for long periods.....	63
Decoy liposomes containing LSTc block viral growth of Influenza A virus in MDCK cells	66
Decoy liposomes containing LSTc extend survival of Influenza A virus-infected mice	68
Decoy liposomes are not effective as therapeutics or prophylactics for Influenza A virus infection	74
Discussion	76

Chapter IV

Optimizing the anti-influenza A virus liposome platform

Introduction.....	87
Results.....	88
Large, low curvature decoy liposomes are more efficient at inhibiting IAV	88
Osmotic crushing slightly improves the efficacy of LSTc decoy liposomes.....	90
Increasing the fluidity of the liposome lipid bilayer increases efficacy of LSTc decoy liposomes	92
PEGylation of decoy liposomes abrogates their inhibitory properties	94
Additional decoy liposome surface negative charge does not increase IAV inhibition	96
Combining decoy liposomes and the NA inhibitor oseltamivir increases decoy liposome efficacy.....	98
Decoy liposomes with the α 2-3 linked SA-containing glycolipid inhibit IAV	100
Decoy liposomes with the α 2-3 linked SA glycan inhibit influenza virus infectivity	102
LSTc- and LSTa-containing decoy liposomes synergistically inhibit IAV infectivity	104
Discussion	107
Generation of liposome formulations for enhanced IAV inhibition.....	107
Decoy liposomes with α 2-3 linked SA inhibit IAV binding and infectivity	111

Chapter V

Heparin sulfate decoy liposomes inhibit respiratory syncytial virus and herpes simplex virus

Preface.....	113
Introduction.....	114
Results.....	116
Heparin sulfate oligosaccharide liposomes.....	116
Heparin and HS-octa inhibition is specific for HS-binding viruses	117
Decoy liposomes with HS-octa inhibit Respiratory syncytial virus	119
Decoy liposomes containing HS-octa block Respiratory syncytial virus growth.....	122
Decoy liposomes with HS-octa liposomes inhibit Herpes Simplex Virus	124
Decoy liposomes containing HS-octa block herpes simplex virus replication.....	126
Decoy liposomes with HS-octa inhibit human parainfluenza virus 3 hemagglutination....	127
Discussion.....	131

Chapter VI

Conclusions and Future Directions.....	136
--	-----

Appendix A

RIP3-dependent programmed necrosis is required for a proper danger signal during influenza A virus infection

Introduction.....	145
Materials and Methods.....	146
Results.....	148
RIP3 ^{-/-} mice have increased pulmonary pathology after IAV infection	148
RIP3 ^{-/-} mice have higher viral titers from IAV infection.....	148
RIP3 ^{-/-} mice a dysregulation of pulmonary infiltrates after IAV infection.....	152
IAV induces less early cytokine and chemokine production in mice lacking RIP3	154
Discussion.....	158

List of Figures

Chapter 1

- Figure 1.1 Influenza A Virus structure and genome..... 4
Figure 1.2 Infection and replication cycle of IAV and the current drug targets..... 8

Chapter 3

- Figure 3.1 Summary of decoy liposome construction..... 45
Figure 3.2 LSTc decoy liposomes bind directly to influenza A virus..... 52
Figure 3.3 LSTc-containing decoy liposomes inhibit binding of influenza A virus to A549 cells.
..... 54
Figure 3.5 LSTc decoy liposomes selectively inhibit influenza A virus infection of MDCK cells.
..... 59
Figure 3.7 LSTc-containing decoy liposomes are stable..... 67
Figure 3.8 Inhibition of influenza A virus replication by LSTc decoy liposomes..... 69
Figure 3.10 Mice that received LSTc decoy liposomes do not have altered viral titers or IL-1 β
levels four days post influenza A virus infection..... 73
Figure 3.11 Therapeutic or prophylactic treatment of infected mice with LSTc decoy liposomes
is not protective..... 75
Figure 3.12 Summary: LSTc-containing decoy liposomes inhibit influenza A virus binding and
infection..... 77

Chapter 4

- Figure 4.1 Larger decoy liposomes with less surface curvature are more efficient at inhibiting
influenza A virus..... 89
Figure 4.2 Osmotic crushing does not significantly affect influenza A virus inhibition..... 91
Figure 4.3 Increasing fluidity of the decoy liposome's surface increases efficacy..... 93
Figure 4.4 Addition of PEG reduces decoy liposome's inhibitory properties..... 95
Figure 4.5 Increasing negative charge of decoy liposomes does not affect influenza A virus
inhibition..... 97
Figure 4.6 Combining LSTc decoy liposomes with the NA inhibitor oseltamivir improves decoy
inhibition of influenza A virus..... 99
Figure 4.7 LSTa decoy liposomes inhibit influenza A virus infection of MDCK cells..... 103
Figure 4.8 Combining LSTc- and LSTa-containing decoy liposomes increases inhibition of
influenza A virus..... 105

Chapter 5

- Figure 5.1 Heparin sulfate and HS-octa specifically inhibit RSV and HSV infection of Vero
cells..... 118
Figure 5.2 HS-octa decoy liposomes inhibit RSV and HSV infectivity..... 121
Figure 5.3 RSV replication in Vero cells is blocked by HS-octa decoy liposomes..... 123
Figure 5.4 HS-octa decoy liposomes inhibit HSV infectivity..... 125
Figure 5.5 HS-octa decoy liposomes inhibit replication and HSV-induced cytotoxicity of Vero
cells..... 128

Appendix A

Figure 1. Wide field H&E staining of infected mouse airways.....	149
Figure 2. Detailed H&E staining of infected mouse lungs.	150
Figure 3. RIP3 ^{-/-} mice have higher viral titers after IAV infection.....	151
Figure 4 RIP3 ^{-/-} mice have dysregulated leukocyte influx after IAV infection.....	153
Figure 5 RIP3 ^{-/-} mice have a delayed cytokine profile early after IAV infection.....	156

List of Tables

Chapter 3

Table 3.1 Assessment of different decoy liposome formulations by hemagglutination inhibition assay..... 49

Table 3.2 Assessment of 7.5 mol% LSTc decoy liposomes by hemagglutination inhibition assay of multiple strains of influenza A virus and sendai virus. 50

Chapter 4

Table 4.1 Assessment of LSTa decoy liposomes by hemagglutination inhibition assay of multiple strains of influenza A virus. 101

Chapter 5

Table 5.1 Assessment of HS-octa decoy liposomes by hemagglutination inhibition assay of human parainfluenza virus 3..... 129

List of Abbreviations

Beijing: Influenza A/Beijing/262/95 (H1N1)
CCF: Cross-correlation function
DAMP: Danger-associated molecular pattern
DOPC: (1, 2-dioleoyl-sn-glycero-3-phosphocholine),
DOPE: 1,2-dioleoyl-sn-glycero-3-phosphoethanolamine
DOPG: (1, 2-dioleoyl-sn-glycero-3-[phospho-rac-(1-glycerol)]) (sodium salt)
GAG: Glycosaminoglycan
Gal: Galactose
HA: Hemagglutinin
HAI: Hemagglutinin Inhibition
HSV: Herpes simplex virus
HS: full-length heparan sulfate
HS-octa: heparan octasaccharide
IAV: Influenza A Virus
LSTa: Sialylneolacto-N-tetraose a
LSTc: Sialylneolacto-N-tetraose c
LD₉₀: 90% Lethal Dose
RIP3: Receptor-interacting serine/threonine-protein kinase 3
MDCK: Madin-Darby canine kidney
MFI: Mean fluorescence intensities
MOI: multiplicity of infection
NA: Neuraminidase
NAi: Neuraminidase inhibitor
OD: Optical Density
PAMP: Pathogen-associated molecular pattern
Phillippines: Influenza A/Philippines/2/82/X-79
PIV3: Parainfluenza virus 3
PR/8: Influenza A/Puerto Rico/8/34 (H1N1)
PRRs: Pattern recognition receptors
RSV: Respiratory syncytial virus
SeV: Sendai virus (Cantell)
SEM: Standard Error of Mean
TLR: Toll-like receptor
WSN-647: Influenza A/WSN/33 (H1N1)
X-31: Reassorted influenza with PR/8 internal genes and HA and NA genes from influenza A/Aichi/68 HA and NA genes (H3N2)

Chapter I

Introduction

Influenza A virus (IAV), a member of the orthomyxovirus family, causes upper and lower respiratory tract infections ranging from mild, non-life threatening illness to lethality (Sullivan 1996). IAV also causes periodic pandemic outbreaks, which are an ever-present danger in a modern, interconnected world. Historically, IAV pandemics have occurred with alarming speed and extremely high mortality rates. Unfortunately the vaccine and therapeutics currently available for influenza are not sufficient to block the spread of a newly emerged strain to which the general population has no pre-existing immunity. In order to generate more effective therapeutics, it is vital to fully understand influenza biology and to pursue therapeutics against all conserved regions of IAV proteins.

A. Influenza the pathogen

Influenza causes up to 40,000 deaths per year in the United States alone (Sullivan 1996), and many more worldwide. Most human infections consist of a sudden and acute fever, usually lasting three days, along with muscle pain and fatigue. The majority of IAV infections are self-limiting and do not require hospitalization, but potentially life-threatening complications such as pneumonia, bronchitis and secondary bacterial infections can occur. Those who are at increased risk of mortality from IAV include patients with cardiopulmonary and other chronic diseases, young children and the elderly (Cox and Subbarao 2000) Although seasonal influenza is not usually lethal in the general population, newly emerged pandemic strains have caused upwards

of 20-fold increased IAV-related mortality in the otherwise healthy, general population (Simonsen, Clarke et al. 1998).

IAV pandemics have occurred in the past at intervals of 10 to 50 years, and they present a public health risk. The most recent pandemic was a triple reassortment H1N1 virus from human, swine and avian IAV species. It began in Mexico in 2009 and quickly spread around the globe, ultimately claiming over 18,500 lives in the first 12 months alone (Dawood, Iuliano et al. 2012). Three IAV pandemics have occurred during the previous century: the 1918 H1N1, the 1957 H2N2, and the 1968 H3N2 pandemics, each differing in severity and mortality rates. The 1918 pandemic caused the highest mortality as compared to mortality from seasonal IAV (Cox and Subbarao 2000; Potter 2001). All three recent pandemics were antigenically novel, and they were all shown to bind to the canonical α 2-6 and α 2-3 linked SA (Glaser, Stevens et al. 2005; Pappas, Viswanathan et al. 2010; Lin, Xiong et al. 2012).

The speed of IAV spread allows it to become pandemic when there are too few individuals with cross-reactive antibodies present in the general population. IAV strains evolve to avoid existing antibody responses in the population by two general mechanisms, antigenic drift and antigenic shift. Antigenic drift occurs when point mutations accumulate in circulating strains, allowing the strain to avoid pre-established immunity (Potter 2001), and antigenic shift occurs when an entire gene segment is swapped between two strains, often the immunodominant proteins HA or NA (La Gruta, Kedzierska et al. 2007). Pandemic strains are thought to typically result from antigenic shift. Both mechanisms of antigenic change result in escape of antibody neutralization, allowing new strains to re-infect the general population. IAV can spread from an infected individual two days post-infection, while a new antibody response requires five to seven days for maturation and viral clearance (Fields, Knipe et al. 2013). The quick spread of IAV

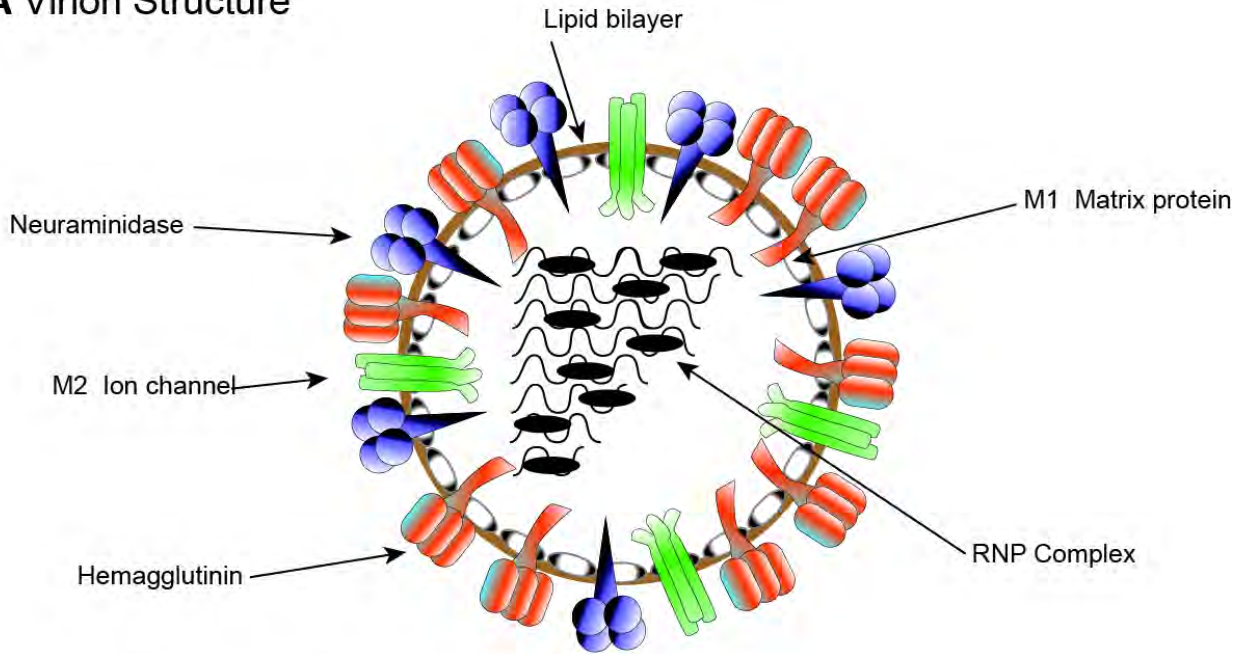
makes it a very dangerous virus that has killed millions in the past, and will kill millions in the future.

B. Influenza the virus

IAV is a member of the *orthomyxaviride* family of negative-sense, segmented, single-stranded RNA viruses and it contains eight gene segments, encoding at least twelve proteins (Figure 1.1A). The major surface protein of IAV is the adhesion and fusion protein, hemagglutinin (HA). HA binds as a homotrimer to cell surface sialic acid (SA) on glycoproteins and glycolipids. After endocytosis, HA also undergoes a pH-dependent conformational change and fuses the viral membrane with the endosomal membrane. HA is the immunodominant antigen and the majority of neutralizing antibodies made by B-cells are against one of the five major antigenic sites on the globular head of HA. IAV has two minor surface proteins: neuraminidase (NA) and matrix protein 2 (M2). NA releases progeny virus from infected cells by cleaving surface SA bound to HA on the budding virion. The M2 protein is a proton channel, responsible for viral uncoating (Jing, Ma et al. 2008). IAV is divided into subtypes based on antibody binding to HA and NA. Currently seventeen HA and nine NA subtypes have been described. Individual strains of IAV are described as the combination of HA and NA subtypes that they possess, for example, the two major subtypes that circulate in the human population is H1N1 and H3N2 IAV. H2N2 IAV have circulated through the human population this century, and were responsible for the 1957 pandemic, but currently no longer infects humans (Krause, Tsibane et al. 2012). The reason for the disappearance of this strain from the human population is currently not understood, but raises concern of its reemergence and pandemic potential due to

Figure 1.1 Influenza A Virus structure and genome.

A Virion Structure



B Genome Organization

	Gene segment	Gene name	Amino acids
	1	PB2	759
	2	PB1	757
	2	PB1-F2	87
	3	PA	716
	3	PA-X	61
	4	HA	550
	5	NP	498
	6	NA	454
	7	M1	252
	7	M2	97
	8	NS1	230
	8	NS2	121

Figure 1.1 Influenza A Virus structure and genome.

The schematic representation illustrates the overall structure of a virion (**A**) and the location of its gene segments and proteins encoded (**B**). The ribonuclear protein (RNP) complex contains the NP and polymerase proteins and surrounds all eight gene segments, which are located in the virion core. The matrix protein gives structural support to the lipid bilayer. The surface glycoproteins are hemagglutinin, neuraminidase and M2. HA is important for attachment and subsequent fusion to host cells and is also the immunodominant protein, targeted by the majority of neutralizing antibody. **B**, Illustrates of the 8 gene segments and the 12 protein products produced from each segment, including their amino acid length of each protein

a lack of preexisting immunity. IAV evolves through two mechanisms, antigenic drift and antigenic shift

IAV has ten internal proteins. The matrix protein (M1) and nucleoprotein (NP) give rigidity to the virion and organize the viral RNA, respectively. The viral polymerase consists of PB1, PB2 and PA proteins. An alternate reading frame on the PB1 gene segment encodes for PB1-F2, which can trigger apoptosis in some cell types. A recently discovered open reading frame resulting from ribosomal frameshifting produces an alternative PA protein, PA-X, which contains the endonuclease domain of PA and a novel C terminal region that suppresses host gene expression (Jagger, Wise et al. 2012). IAV encodes two non-structural proteins (NS), NS1 and NS2 (also known as nuclear export protein, NEP). NS2 is responsible for export of the viral transcripts from the cell nucleus (Robb, Smith et al. 2009). NS1 has several known functions, including blocking host mRNA production, suppression of the interferon response and binding of double-stranded RNA, preventing RNA sensing by cytoplasmic RNA sensors (Lu, Wambach et al. 1995; Fields, Knipe et al. 2013).

Viral binding

Through HA, IAV binds to specific glycosylation motifs with terminal SA linked to the penultimate galactose (Gal) sugar residue. Each host species has different SA-Gal linkages present in their upper airways, and therefore the linkage chemistry determines IAV species specificity. In the human upper airways, glycans that terminate in SA are predominately linked with an α 2-6 linkage to the penultimate sugar, and IAV strains adapted to infect humans bind to this linkage (Ibricevic, Pekosz et al. 2006). Bird upper airway and gut lining have terminally sialylated glycans with α 2-3 linkages, where IAV replicates in birds. Avian-adapted strains of IAV bind to α 2-3 linked SA. Pigs, however, have mixed α 2-3 and α 2-6 linked SA displayed

throughout their airways and are infected by IAV adapted to either host (Fields, Knipe et al. 2013). For this reason the swine population is an especially important reservoir of reassortment and adaptation between birds and humans. Some recent crossover strains are thought to bind to both α 2-3 and α 2-6 linked SA, and further nucleic acid mutations fix the preference for α 2-6 SA in the strain as an outbreak or adaptation continues (Glaser, Stevens et al. 2005). Many cell lines and chicken eggs used to passage IAV in the laboratory contain both SA linkages (Ito, Suzuki et al. 1997) and therefore almost all commonly studied IAV strains, included those used here, are promiscuous binders that can bind and infect cells displaying either α 2-3 or α 2-6 linked SA.

Influenza A virus internalization

Once IAV has bound to surface SA, the virus is internalized through receptor-mediated endocytosis. Entering virus is cycled through the endocytic pathway to the acidic, late endosome phase (Figure 1.2). The low pH of the late endosome enables a conformational change in HA and allows the viral envelope to fuse to the endosomal membrane. The M2 protein is a proton ATPase ion channel, located on the surface of the virion. After the late endosome acidifies, M2 pumps protons across the viral membrane and acidifies the endosome interior, causing the disassociation of M1 from the viral genome (Lakadamyali, Rust et al. 2004). IAV replicates in the cell nucleus, and NP imports the genome via its nuclear localization sequences. Viral proteins are then translated in the cytoplasm, with the major surface proteins shuttling from the endoplasmic reticulum to the plasma membrane, where progeny virion assembly and budding occur. After successful packaging and budding, NA on the progeny virions is required for the final release from an infected cell. IAV NA is an exo- α -sialidase that cleaves terminal α 2-3, α 2-6 and α 2-8 linked SA from host and viral glycoproteins and glycolipids, releasing the mature

Figure 1.2 Infection and replication cycle of IAV and the current drug targets.

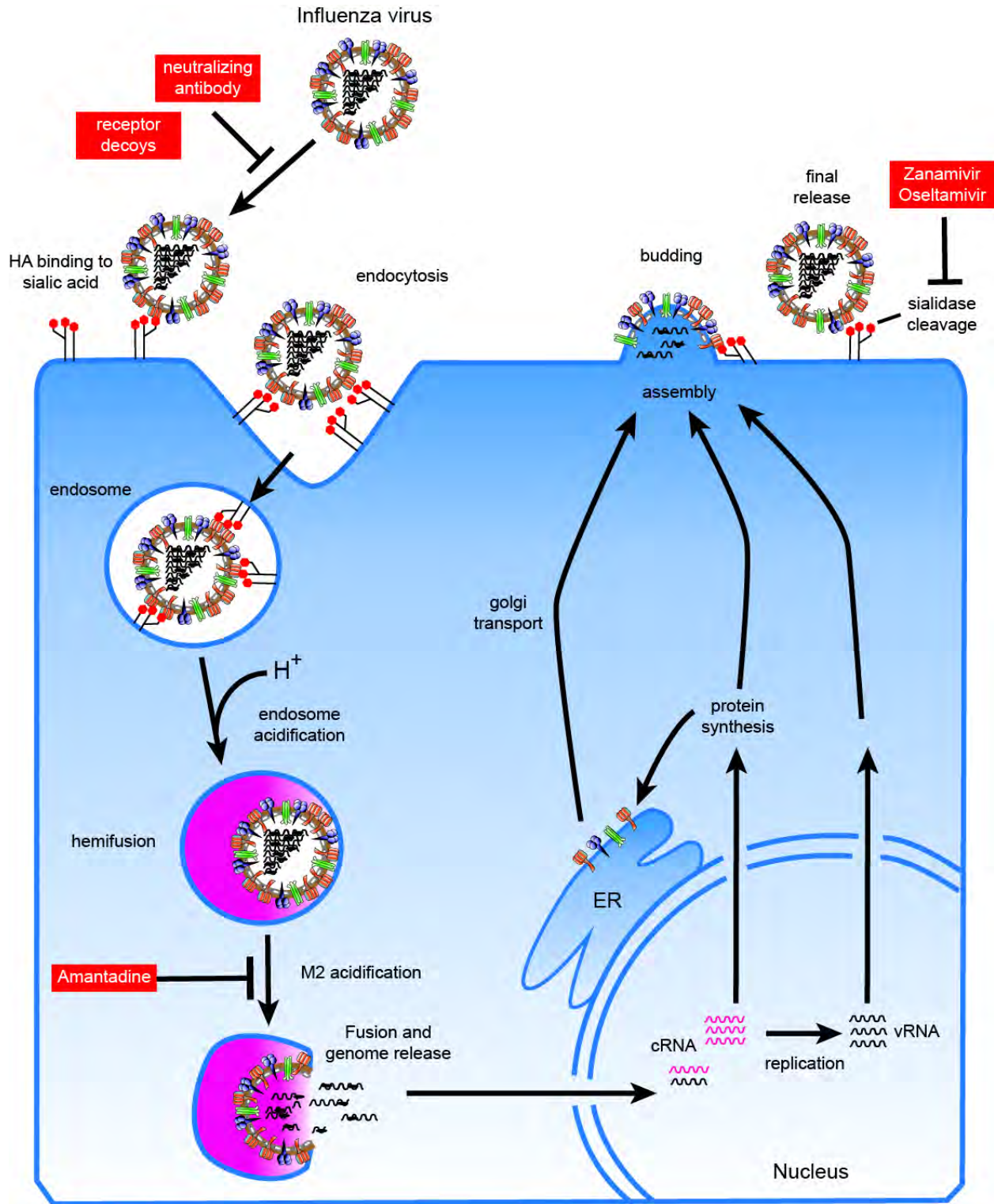


Figure 1.2 Infection and replication cycle of IAV and the current drug targets.

IAV HA binds to sialylated glycolipids and glycoproteins on the cell surface and is internalized by receptor-mediated endocytosis. Binding can be inhibited by neutralizing antibody or receptor decoys. Upon endosome acidification, HA undergoes a conformational change to fuse with the membrane. The M2 ion channel (inhibited by amantadine) acidifies the virion interior and releases M1 from the RNP complex, allowing for genome release into the cell. IAV replication occurs in the nucleus and complementary RNA (cRNA) is translated in the cytoplasm. Surface membrane proteins are inserted into the endoplasmic reticulum (ER) and shuttled to the cell surface via the golgi. IAV's polymerase makes progeny viral RNA (vRNA) and together with de novo protein synthesis, assembly occurs at the apical cell surface. Budding is dependent on NA cleavage of SA on the cell surface as well as on viral proteins (inhibited by Oseltamivir and Zanamivir)

virions and prevents self-aggregation or reattachment to the infected cell surface (Nayak, Hui et al. 2004).

C. The immune response to Influenza A virus

Innate response to IAV

When IAV undergoes a combination of antigenic drift and antigenic shift between human and avian circulating strains, the new IAV strains may not be susceptible to existing antibodies. IAV infection clearance is dependent on an adaptive, sterilizing B-cell mucosal antibody response that typically takes five to seven days to appear in these re-infected patients (Fields, Knipe et al. 2013; Seibert, Rahmat et al. 2013). Conventional human circulating strains and avian circulating strains undergo constant antigenic shift and antigenic drift, creating new virus that is not neutralized by antibodies made during previous infections, and are now susceptible to a new round of infection, although these patients are not completely naïve. The innate immune response is therefore critical to delay viral replication before the adaptive immune response can mature and clear the infection. IAV first infects respiratory epithelial cells in the human upper respiratory tract that express α 2-6 linked SA and from these cells produce large amounts of progeny virus. Infected epithelial cells are also the first cells to mount an innate immune response that is crucial for limiting viral spread. IAV is recognized by a number of innate pattern recognition receptors (PRRs). Toll-like receptors (TLR) 3 recognizes endosomal dsRNA and activates type I interferon (IFN) by the interferon regulatory factors (IRFs). TLR7 recognizes endosomal ssRNA, and activates pro-inflammatory cytokines via NF- κ B. The cytosolic retinoic acid inducible gene-I (RIG-I) recognizes 3' triphosphate RNA generated during viral replication and also signals through the IRFs to produce type I IFN (Fields, Knipe et

al. 2013). Protein kinase R (PKR), another cytosolic viral sensor, is activated by the presence of dsRNA, and is also an IFN-stimulated gene. PKR recognizes IAV dsRNA and phosphorylates eukaryotic translation initiation factor 2a (eIF2a), which in turn halts protein translation. PKR activation also initiates the apoptosis cascade and both mechanisms limit virus replication (Fields, Knipe et al. 2013). IAV, like many other viruses, inhibits PKR activation. IAV NS1 inhibits PKR by blocking IFN production, and therefore limiting the amount of PKR protein produced, by binding to dsRNA, preventing PKR-dsRNA interaction, and by binding directly to the N-terminal region of PKR to prevent activation (Li, Min et al. 2006). Viral RNA and the M2 protein have also been shown to indirectly activate the cytosolic inflammasome receptor, NLRP3 (Allen, Scull et al. 2009; Ichinohe, Pang et al. 2010). TLR activation produces proIL-1 α / β and pro-IL-18, and subsequent NLRP3-dependent caspase activation induces cleavage of these key cytokines into their mature form.

IAV's surface proteins, HA and NA are processed through the Golgi (Figure 1.2) and like other cellular membrane proteins are glycosylated. The lectin receptor family is a group of innate immune sensors that bind to specific glycosylation motifs. Mannose binding protein (MBP) and surfactant protein D (SP-D) both have been shown to recognize IAV. MBP recognizes high-mannose glycosylation and binds to mannose residues on IAV HA, preventing attachment in a similar mechanism as antibody neutralization (Anders, Hartley et al. 1990). IAV can escape from MBP binding by selecting for mutants that lose mannose glycosylation (Hartshorn, Sastry et al. 1993), but removal of a glycosylation site may make these mutants susceptible to circulating antibodies, as addition of a glycosylation site is a common antibody escape mechanism (O'Donnell, Vogel et al. 2012). SP-D also binds to IAV, and research has demonstrated that SP-D agglutinates IAV (Hartshorn, Chang et al. 1996), stimulates neutrophil

binding and respiratory burst (Hartshorn, Crouch et al. 1994), and is important for survival in the mouse after IAV infection (LeVine, Whitsett et al. 2001)

Natural killer (NK) cells have also implicated in killing IAV-infected cells. NK cells are innate cytotoxic cells that do not require previous antigen stimulation to kill infected target cells. Recognition of non-self is, in part, due to the lack of major histocompatibility complex (MHC) class I on an infected cell. MHC class I is down regulated during many infections, including IAV. In addition to the recognition of a lack of MHC class I, the NK cell receptors NKp46 (Mandelboim, Lieberman et al. 2001) and NKp44 (Arnon, Lev et al. 2001) have been shown to bind to IAV HA. However, this recognition is dependent on NK receptor sialylation, and may be an artifact of the experimental setup and not true *in vivo*. NK cells are also susceptible to IAV infection, are permissive for replication and undergo apoptosis after infection (Mao, Tu et al. 2009). Therefore the benefits of NK recruitment during infection remain controversial. Taken together, these initial recognition events are key to establishing an antiviral state with the Type I IFNs, to limit the spread of virus and to recruit additional leukocytes to the infected lung with the proinflammatory cytokines and chemokines. Key cytokines that are induced during IAV infection include IL-1 α/β , IL-6, IL-8 (KC in mice), MCP1, MIP-1 α/β , IP-10 and TNF in both mouse (Wareing, Lyon et al. 2004) and human (Fritz, Hayden et al. 1999) infection.

Innate receptors trigger chemokine production in the IAV infected lung. Patrolling blood neutrophils, mononuclear, and NK cells then infiltrate into the lungs along the chemokine gradients. Infiltrating leukocytes recognize IAV through the same PRRs described above, secrete additional cytokines, phagocytose virus and kill infected cells. They also aid in the maturation of resident dendritic cells (DCs) that, along with leukocyte differentiation cytokines, are the link to the adaptive immune response. DCs express many PRRs, and after encountering

IAV antigens and inflammatory signals, undergo maturation, migrate to the draining lymph nodes and are critical for both proper T- and B-cell maturation (Summerfield and McCullough 2009). As professional antigen presenting cells, DCs can process IAV antigens via both MHC pathways. Phagocytosed IAV antigens are processed in the endosome and loaded onto MHC class II for presentation to CD4 helper T cells, which are crucial for the priming of antigen specific B-cells and for efficient production of neutralizing antibodies (Gerhard, Mozdzanowska et al. 1997). Through the MHC class I pathway, DCs present antigen to CD8 T-cells by transfer of endocytosed antigen to the cytoplasm for cross-presentation on MHC class I molecules. DCs also process antigen when infected by IAV. De novo IAV protein synthesis in the cytoplasm is processed and loaded in class I MHC molecules for presentation to CD8 T-cells. In addition, DCs also aid in the expansion and differentiation of B-cells directly (Douagi, Gujer et al. 2009). With the aid of CD4 helper T-cells, B-cells undergo class-switching, somatic hypermutation and produce neutralizing antibody that clears IAV from the infected lung (Fields, Knipe et al. 2013; Seibert, Rahmat et al. 2013).

Adaptive immune response to IAV

Adaptive immunity consists of two arms, the B-cell humoral response and the cytotoxic T-cell cellular response and is responsible for final clearance of almost all infections. Clearance of IAV is largely dependent on the B-cell neutralizing antibody response. The antibody response appears five days post infection and plateaus two to three weeks post infection (Murphy, Chalhub et al. 1973). The timing of the antibody response is similar during human exposure to avian IAV; neutralizing antibodies appear five days after the onset of symptoms of confirmed H5N1 IAV cases and level off twenty to twenty-five days post first symptoms (Katz, Lim et al. 1999). During IAV infection, B-cells make antibodies to the HA, NA, NP, M1 and M2 proteins.

Antibodies against the surface glycoproteins HA and NA are protective, whereas antibodies against the internal proteins NP and M1 are not (Fields, Knipe et al. 2013). HA and NA are the immunodominant antigens, the majority of all antibodies made target these two proteins, and their presence correlates with resistance to illness and inhibition of IAV replication in humans (Clements, Betts et al. 1986). Anti-HA antibodies act by preventing HA binding to SA on host cells, preventing infection. Anti-NA antibodies act after infection, and prevent progeny IAV release from infected cells, reducing circulating viral titer. Passively transferred antibodies against HA alone can protect against infection, even in SCID mice lacking B- and T-cells (Scherle, Palladino et al. 1992). Anti-HA antibodies are strain-specific, and are therefore susceptible to escape by mutation of the highly variable globular head of HA (van de Sandt, Kreijtz et al. 2012). However, if the HA protein has not changed antigenically, the antibody response is robust and can protect against similar strains many years later. Older patients had partial protection from the 2009 IAV pandemic from cross-reactive antibodies generated from IAV infections in the 1950s (Hancock, Veguilla et al. 2009; Ikonen, Strengell et al. 2010).

Non-neutralizing antibodies generated during IAV infection also play an important role in viral control and protection. Anti-NA antibodies are not neutralizing, but still reduce infectious titer by trapping budding virus onto infected cell surfaces. Non-neutralizing anti-NP antibodies also reduce viral titers (Carragher, Kaminski et al. 2008). The exact mechanism is not fully elucidated, but it may result from antibody-dependent cell cytotoxicity, where antibodies bind to exposed antigens, and the Fc γ RIII on infiltrated NK cells bind to the Fc region of the antibody, resulting in NK-mediated cell lysis.

Cellular immunity is also important during IAV infection. Due to the pervasiveness of influenza and the availability of the vaccine, there are virtually no naïve people in the general

population. When reinfected, a patient will have cross-reactive T-cell responses to conserved internal epitopes to the new IAV strain. In an experimental naïve mouse model, the T-cell response takes typically six to fourteen days to appear, and resolves twenty-one days post infection (Ennis, Rook et al. 1981). There are two major groups of T-cells, CD8⁺, cytotoxic lymphocytes (CTLs) and CD4⁺ helper T-cells. CTLs kill IAV-infected cells displaying a specific antigen on surface MHC class I. CTL epitopes produced during human infection have been map to the HA, M, NP, and PB2 proteins. HA epitopes are generally subtype-specific, while epitopes on the internal proteins are cross-reactive to multiple subtypes (Fleischer, Becht et al. 1985). Unlike antibody, pre-existing memory CD8 T-cell levels do not correlate with protection, but they do correlate with the speed of clearance.

The second major T-cell subsets, CD4⁺ helper T-cells, are important for proper development of antigen specific B-cells during IAV infection. The contribution of helper T-cells to the IAV response have been demonstrated by *in vivo* depletion, resulting in slower IAV clearance (Eichelberger, Wang et al. 1991). CD4⁺ helper T-cells are more important during secondary infection with the same, or similar, IAV strain and quickly produce proinflammatory cytokines and chemokines after infection, resulting in early control of virus (Strutt, McKinstry et al. 2010; Teijaro, Turner et al. 2011).

Pulmonary recovery after IAV infection

The immune system is vital not only in the control and clearance of IAV, but also for the repair of the lung after infection. During infection, there is significant cell death in the lungs, either from lytic viral replication, infected cell death from apoptosis and necrosis, or specific killing by the adaptive immune system. IAV also significantly alters the lung environment after clearance. IAV has been shown to affect pulmonary arterial morphology, PRRs expression, and

T-cell function. These changes leave patients susceptible to secondary bacterial superinfection and other pulmonary disorders (Fields, Knipe et al. 2013; Pociask, Scheller et al. 2013). The repair process after IAV infection is poorly understood, but two cytokines, IL-4 and IL-22, have been demonstrated to be key to rebuilding the lung architecture and shutting off the immune response. The anti-inflammatory cytokine IL-4 accumulates late in infection, in mice IL-4 levels increase at 8 days post infection (Gowdy, Krantz et al. 2010). IL-4 has been shown to blunt CTL primary (Aung, Tang et al. 1999) and memory (Bot, Holz et al. 2000) responses to RSV and IAV, respectively. Along with TGF β , IL-4 has been shown to help CD8⁺ T-cells develop into IL-10 producing, inefficient cytotoxic effectors (Visekruna, Ritter et al. 2013). IL-4 also drives differentiation of macrophages into alternatively activated (M2) macrophages (Gowdy, Krantz et al. 2010). M2 macrophages reduce inflammation by producing the potent anti-inflammatory cytokine IL-10, and low levels of IL-12, a key proinflammatory cytokine important in T-cell survival and function.

IL-22 is another important repair cytokine that has recently been shown to be important in the recovery to IAV infection (Pociask, Scheller et al. 2013) and in other models (Sugimoto, Ogawa et al. 2008; Schnyder, Lima et al. 2010). Mice lacking IL-22 had significantly slower and less overall repair of the lung epithelium than wild-type mice after IAV infection. IL-22^{-/-} mice also had more lung stiffness and less lung function following IAV infection. And IL-22^{-/-} mice had dysregulated epithelial repair and development genes in the lung, such as secretoglobin family 1A, which is important for Clara cell development, and caveolin 1, which is important for alveolar type I and endothelial cells (Pociask, Scheller et al. 2013). The immune system is vital for control, elimination and recovery from influenza with the two arms of the immune system,

the innate and adaptive immune responses, resulting in a non-lethal, limited infection in the majority of exposed patients.

D. Combating influenza – chasing a moving target

While IAV is a major public health concern, the current therapeutic options are limited, with vaccination being the most effective tool against the disease. The IAV vaccine is a yearly, trivalent inactivated vaccine, formulated at least six months before the next annual IAV season. The current vaccine consists of H3N2, H1N1 and influenza B virus isolates that are predicted to dominate the upcoming season. Vaccine production starts in January with the FDA's strain selection, commercial production beginning in January and February, shipping in September and product release around October (Gerdil 2003). Thus the lead-time from beginning to end for the IAV vaccine is about nine months, and if the circulating strain drifts or the chosen strains do not dominate the flu season, the vaccine offers little protection (Potter 2001). Osterholm *et al.* (2012) reviewed 31 IAV vaccine studies and found that the typical trivalent inactivated vaccine was only 59% protective in adults (Osterholm, Kelley *et al.* 2012). Furthermore, in pandemic outbreaks, vaccines cannot be generated and delivered at the required speed or dosage level, due to the long lead-time of vaccine production (Moscona 2005).

Small molecule inhibitors

Therapeutic treatments for IAV include small-molecule inhibitors such as M2 ion channel blockers, amantadine and rimantadine, and neuraminidase inhibitors, including oseltamivir and zanamivir. Amantadine works by binding to the pore opening of the M2 ion channel (Figure 1.2), blocking acidification of the endosome-virion interior, the M1-genome interaction is not weakened, and prevents genome release into the host cell cytoplasm (Jing, Ma *et al.* 2008). Oseltamivir and zanamivir target NA by binding the deep, conserved enzymatic

pocket responsible for cleaving SA from HA on budding virus, thus preventing mature virion release from infected cells. These and other potent NA inhibitors were designed to fit into this pocket as observed in the crystal structure of NA (von Itzstein, Wu et al. 1993).

In the past decade, resistance to the amantadines has increased dramatically, restricting their utility (Potter 2001). Historically, clinical isolates have had resistance rates of 1-3%, but during the 2003 flu season, resistant H3N2 isolates from China and Hong Kong emerged and quickly spread worldwide. During the 2005-2006 flu season H3N2 resistance rates for China were near 100%, greater than 90% in America, 50% in Europe and averaged 90% worldwide (Deyde, Xu et al. 2007; Hayden 2009). Resistance has also arisen in H1N1 isolates, which make up a smaller percentage of clinical cases, ranging from 71% resistance in China to about 5% in America, and 15% worldwide during the 2006-2007 season (Deyde, Xu et al. 2007). H1N1 amantadine resistance has also become fixed, albeit slower than H3N2 resistance, climbing to 100% resistance in a survey of clinical cases in Hong Kong in 2008 and 2009 (Cheng, To et al. 2010). The 2009 triple reassortment pandemic strain is also amantadine resistant; Gubareva *et al.* (2010) found that greater than 99% (3,359 out of 3,362) of isolates tested were resistant to amantadine (Gubareva, Trujillo et al. 2010).

Resistance to the NA inhibitor oseltamivir has also rapidly increased: only 12.3% of H1N1 viruses tested were oseltamivir-resistant in the 2007-2008 season, but this number escalated to 98.5% in the 2008-2009 season (Dharan, Gubareva et al. 2009). Resistant viruses have a mutation in the hydrophobic active site of NA that prevents oseltamivir binding, but does not affect zanamivir binding. Therefore, the frequency of zanamivir resistant isolates is markedly lower, but the same escape mechanism is also a danger for acquiring zanamivir resistance (Collins, Haire et al. 2008). Another drawback of NA inhibitors is that they must be

used early in the course of an infection to be fully effective (Govorkova, Baranovich et al. 2013). If resistance to either of these drugs becomes fixed in the IAV population, then a significant amount of available IAV therapeutics would be rendered ineffective. Clearly, alternative treatment options are needed, as resistance becomes an increasing threat.

Antibody therapeutics

Antibody treatment as a therapeutic has a long history, beginning before the 1900s with Emil von Behring's Nobel winning anti-diphtheria serum, a crude horse sera used to treat multiple diseases before the advent of modern antibiotics (Lachmann 2009). In the intervening years, the use of therapeutic antibodies have evolved to be safe, with pure monoclonal antibodies that are very effective at treating severe clinical cases, with little side effects. The majority of neutralizing antibodies generated during an IAV infection are against the globular head of HA. Neutralizing monoclonal antibodies (mAbs) have been shown to block HA by binding around the edge of the receptor-binding domain to create steric hindrance and prevent SA from entering the HA binding groove (Krause, Tsibane et al. 2012; Ohkura, Kikuchi et al. 2012). Broadly neutralizing mAbs have been found that bind to multiple HA subtypes. These mAbs, including the F16 antibody, which binds to all 16 HA subtypes (Corti, Voss et al. 2011), have been hyped as the next generation of therapeutics; however mAbs have major drawbacks that limit their use as therapeutic agents. Most anti-HA mAbs bind around the receptor-binding site (T) to one of the five HA antigenic sites. Escape mutants can rapidly appear in and around these highly variable regions, preventing antibody binding and producing an escape variant (Krause, Tsibane et al. 2012; Rudneva, Ignatieva et al. 2012). Escape mutants can be generated *in vitro* or *in vivo* in the presence of neutralizing mAbs. Mutations on HA include the addition or removal of a charged

amino acid residue, additional N-glycosylation sites, or simple steric changes (Hensley, Das et al. 2009; O'Donnell, Vogel et al. 2012).

Neutralizing mAbs as therapeutics also suffer other, more practical issues. mAbs are large, complex molecules that require sophisticated culturing and purification systems. mAbs' size also reduces the rate of tissue penetration. In addition, studies have demonstrated that in order to achieve clinical efficacy, large doses of antibody are required, driving up production costs (Chames, Van Regenmortel et al. 2009). All of these properties and requirements as well as high production costs and significant lead-time make mAbs unsuited for use as a common therapeutic.

Decoy receptors

An alternative therapeutic strategy is to target the attachment and fusion of IAV particles to host cells, specifically the RBS on HA. A drug targeting the RBS mimics the pathogen's natural ligand on a host cell and therefore is referred to as a receptor decoy. The principle of receptor decoys as therapeutics is wide-ranging; Dennehy *et al.* (2007) dramatically inhibited bacterial phage growth when decoy cells – bacteria susceptible to infection but not permissive to phage replication – were mixed into a population of phage permissive bacteria. Human pathogens are also susceptible to decoy therapeutics. Asher *et al.* (2005) created transgenic mice with coxsackievirus B receptor expressed on erythrocytes, creating a decoy cell that bound virus but did not allow for replication. The recombinant decoy mice had reduced viral load and less mortality after coxsackievirus infection. Ziebert *et al.* (1992) blocked poliovirus infectivity using a soluble form of the receptor's ligand as a decoy. For IAV, and other viruses that bind to SA, it is possible that sialylated glycans in breast milk may act as natural receptor decoys for newborns (Martin-Sosa, Martin et al. 2003).

Influenza virus decoy receptors

The receptor decoy approach has also been used to combat IAV. Like all RNA viruses, the IAV polymerase is error prone and the antigenic sites on the immunodominant proteins rapidly change. However, regions critical for IAV function, such as the RBS of HA, are well conserved (Suwannakarn, Chieochansin et al. 2010) and therefore make ideal drug targets. While SA is the key monosaccharide on the host-glycan that interacts with HA, the monovalent HA-SA interaction is weak. Several groups have tested different monovalent SA-containing molecules and found that they bind and inactivate IAV, but the 50% inhibitory concentration (IC_{50}) of these SA analogs for IAV attachment varies from the millimolar (Sauter, Bednarski et al. 1989; Glick, Toogood et al. 1991; Matrosovich, Gambaryan et al. 1993) to the micromolar range (Weinhold and Knowles 1992). IAV attachment involves many individually weak HA-SA binding events. Combining many weak HS-SA interactions creates a strong, multivalent link, a process utilized by many viruses (Kiessling and Pohl 1996). Synthetic multimers of SA can recreate a multivalent bond between virus and receptor decoy. Building on the findings from monovalent SA analogs, Glick *et al.* (1991) created SA-containing dimers, doubling the number of SA residues available on each molecule for binding HA, and presumably increasing binding affinity. SA dimers do have stronger affinities than monovalent SA, but they are still in the same $\log IC_{50}$ range (Glick, Toogood et al. 1991). In order to increase the SA decoy attachment IC_{50} by any significant amount, SA oligomerization is required.

Oligomerization of sialosides greatly increases the apparent affinity for HA, making them strong inhibitors. Several groups have made multivalent SA molecules either by linking SA into a dendrimer structure (Reuter, Myc et al. 1999), or by linking SA to one of several polymer backbones (Spaltenstein and Whitesides 1991; Lees, Spaltenstein et al. 1994; Mochalova, Tuzikov et al. 1994; Mammen, Dahmann et al. 1995; Gambaryan, Tuzikov et al. 2002). When

complexed into a polymer backbone, SA forms multivalent interactions with many HA trimers on a single IAV virion, and possibly on multiple virus particles, creating larger complexes ideal for immune surveillance. Polymerized receptor decoys also suffer from several critical defects. One major drawback to these polymers is that some backbones are cytotoxic. Most SA polymers above are built with backbones of polyacrylamide derivatives, and the breakdown monomer of polyacrylamide is a potent human neurotoxin and carcinogen. Polymerized SA decoys have rigid backbones, with fixed spacing of SA. This fixed spacing could prevent maximal binding of SA to HA, limiting the binding strength. Polymers are also often partially insoluble and antigenic, making them less than ideal for *in vivo* use.

Sialylated decoy liposomes

An alternative method for generating multivalent, polymer-like molecules is to create sialylated liposomes. Liposomes, first described in the 1950s, are synthetic vesicles produced from purified phospholipids, which consist of a hydrophilic lipid bilayer that surrounds an aqueous interior. Liposomes are especially suited for creating polymer-like functional groups because the lipid bilayer is fluid, allowing for lipid-conjugated functional groups to diffuse across the surface (Baumgart, Hess et al. 2003). Using naturally occurring lipids and other components, such as cholesterol, liposomes are not immunogenic and have long *in vivo* half-lives (Immordino, Dosio et al. 2006). Additionally, many changes can be made to the basic formulation, such as inclusion of charged lipids, lipids with different acyl chemistries, and drug loading into the liposome interior.

The data presented in this dissertation demonstrates that SA-containing liposomes are effective inhibitors of IAV infection. Previously, several groups have created SA-containing decoy liposomes that were capable of inhibiting IAV hemagglutination better than the

monovalent building blocks and on par with other SA-polymer decoys. These studies show that liposomes can be used to create polymer-like multivalency of SA, but they were limited in scope. The majority only tested binding by the HAI assay (Kingerywood, Williams et al. 1992; Sun, Kanie et al. 2000). The two studies that tested infectivity inhibition also had major flaws; Spevak *et al.*, (Spevak, Nagy et al.) had a disconnect between their HAI and infectivity results when they used liposomes with different mole percentages of SA. Decoy liposomes created by Guo *et al.*, (Guo, Sun et al.) inhibited H3N2 IAV but were ineffective against H1N1 IAV. These previous decoy liposome studies have a few notable differences from the data presented in this dissertation. First, each study used a single SA residue attached directly to the phospholipid or steric linker. IAV will bind to a single SA residue linked in either a α 2-3 or α 2-6 bond directly to the lipid backbone, but longer glycan chains allow for optimal presentation of the terminal SA for different subtypes of IAV. LSTc is a long glycan, and it adopts an umbrella-shaped conformation when bound to human-adapted HA while LSTa forms a conical conformation when bound to avian-adapted HA (Xu, Newhouse et al. 2009) and LSTc and LSTa have been shown to bind to several HA subtypes (Chandrasekaran, Srinivasan et al. 2008). The liposomes presented in this study contain a two acyl, unsaturated phospholipid with a low melting temperature, meaning that the decoy liposomes will be fluid at body temperature, whereas the lipids used in previous studies have had higher melting temperatures, possibly reducing the bioavailability of liposomal SA and reducing efficacy. The changes our group have made in the decoy liposome formulations represent a new generation of state-of-the-art decoy liposomes capable of inhibiting multiple IAV subtypes' infectivity as well as other pathogens when decoy liposomes are created with the corresponding decoy glycolipid

E. Model systems for studying Influenza

Our receptor decoy liposomes target IAV via its receptor protein HA, by providing the virus with higher affinity α 2-6 linked SA analogs. There are many methods that can be used to measure the effectiveness of these decoy liposomes to bind and inactivate IAV. One proven method for rapid screening for competitive binding is the hemagglutination inhibition assay, or HAI. IAV binds to SA on the surface of red blood cells (RBCs), which contain both α 2-6 and α 2-3 linked SA, causing hemagglutination. A constant amount of virus that will agglutinate RBCs is tested against candidate drugs, diluted serially two-fold. Here SA-containing decoy liposomes are challenged with a constant amount of IAV. If the drug is present in sufficient quantities, then hemagglutination will be inhibited. Once diluted past the inhibitory concentration of drug, IAV will agglutinate, and an inhibitory concentration of the drug can be calculated. In our studies, decoy liposomes or control liposomes are serially diluted and mixed with four HA units of one of several IAV strains. The reciprocal of the last dilution of decoy liposome that inhibits agglutination is the HAI titer, and the inhibitory concentration (IC_{90}) molarity of SA can be calculated for that dilution. Because the assay can be completed in about two hours, many IAV strains and decoy liposome formulations can be screened for competitive binding in a rapid manner, and this assay serves as an initial test of decoy effectiveness.

Decoy-virus binding can also be directly visualized with microscopy. Binding, in the form of colocalization, can be detected with adhered virus and decoys in solution. By using fluorescent tags added onto IAV and distinct tags incorporated into liposomes, specific colocalization can be measured by confocal microscopy after washing away unbound decoy or control liposomes. This model allows us to directly visualize binding and with powerful colocalization analysis calculations, (Bolte and Cordelieres 2006) determine if the data is biologically significant. Flow cytometry can also be used to measure binding. IAV will adhere

to cells displaying surface SA and decoy inhibition of decoy binding can be measured by fluorometric analysis of labeled virus. IAV can be labeled either by covalent Alexa Fluor labeling or by anti-IAV antibody staining. Binding of labeled virus is measured in the presence or absence of an anti-viral drug. Flow cytometry has the advantage of using relevant target cells, e.g., the human lung epithelial cell line A549, to demonstrate decoy liposome-dependent binding inhibition.

Whereas competitive binding indicates that a drug would neutralize the virus and prevent infection, direct measurement of infectivity is required for verification. The Madin-Darby Canine Kidney (MDCK) cell is the standard cell line used to test IAV replication. Used widely as a model epithelial cell line, MDCK cells have both α 2-6 and α 2-3 linked SA and are permissive to IAV. To measure infectivity inhibition, decoy or control liposomes are mixed with a fixed amount of virus before addition to MDCK cells. In this experimental setup, viral particles are expected to bind to native SA on MDCK cells only when not competitively bound to decoy liposomes. Viral particles bound to decoy liposomes are unable to attach to the MDCK cells and thus would be inhibited. In this assay, unbound virus and decoys are washed out after a one-hour infection, and agar is added on top of the cell monolayer. Internalized virus is allowed to grow in the MDCK monolayers, viral spread is prevented by the agar, and distinct plaques form where one infectious particle originally infected the MDCK monolayer.

The plaque inhibition model assays the decoy liposome's ability to block initial binding and infectivity, and with serial dilutions of liposomes, can quickly generate dose response data from which a 50% inhibitory concentration (IC_{50}) of each liposome formulation can be calculated. An advantage of this system is that MDCK cells present both α 2-6 and α 2-3 SA linkages, allowing IAV isolates that bind to either or both to be tested against our decoy

liposomes. When tested with only α 2-6 linked SA containing liposomes, these cells present a higher bar to inhibition if the IAV isolate can bind to both α 2-6 and α 2-3 linked SA.

The MDCK infectivity model can be expanded to assay viral growth over several replication cycles. The IAV growth model is a similar assay, but after the initial one-hour infection, IAV growth media is added with decoy or control liposomes and replication is allowed to continue. In this model, the amount of virus that is challenged with decoy liposomes is several logs higher than in the MDCK infectivity assay above. This model is well suited to fully test the log scale of inhibition from decoy liposomes. However, this system is more cumbersome and time-consuming and is therefore not useful for screening small formulation changes to the liposome platform.

Of the several *in vivo* model systems for IAV infection, the pulmonary mouse infection is the most applicable for testing our decoy liposomes. The mouse system benefits from a plethora of species-specific molecular and genetic tools. IAV infection in mice is dose-dependently lethal, with predictable weight loss kinetics that can be used as a proxy for successful inoculation of virus, with higher doses resulting in faster and greater weight loss (Powell, Dwyer et al. 2006). IAV infection in mice results in cytokine and type I IFN production in the lungs, followed by leukocyte infiltration. Viral titers peak 4 to 7 days post infection and clearance is dependent on B-cells (Graham and Braciale 1997), as is also true in humans. The major difference between the mouse model and humans is that the human upper airways mainly contain α 2-6 linked SA, and lower airways have both α 2-6 and α 2-3 linked SA, while mice have an even distribution of α 2-6 and α 2-3 linked SA throughout their airways (Fields, Knipe et al. 2013). Due to this disparity, some mouse-adapted IAV strains bind α 2-3 linked SA more than when first isolated

from humans, but a decoy that uses α 2-6 SA to inhibit mouse pathogenesis is predicted to also work on α 2-6-adapted virus when α 2-3 linked SA is not present.

F. Thesis objectives

IAV is an important public health threat. It evolves rapidly by a combination of antigenic shift and antigenic drift, limiting the effectiveness of the current therapeutics. The current vaccine must be reformatted yearly and, due to lead-time, may not fully protect the recipients. In addition, IAV has rapidly developed resistance to several small molecule inhibitors, and resistance remains a threat for the few remaining clinical inhibitors available. To be successful, an inhibitor of IAV must target a highly conserved region of the virus. The SA receptor binding site, or RBS, is highly conserved between IAV subtypes. A receptor decoy that binds strongly to the RBS would bind and inactivate multiple strains of IAV and resist escape mutations.

In this dissertation, I will examine the use of decoy receptor liposomes as a method of creating strong, neutralizing interactions with IAV as a potential therapeutic. The specific aims of this dissertation are as follows:

1. Characterize novel LSTc-containing decoy receptor liposomes as an IAV therapeutic
 - Investigate the mechanism by which decoy liposomes neutralize IAV
 - Establish the degree of inhibition of a number of IAV H1 and H3 subtypes
 - Characterize an *in vivo* mouse model of protection with decoy liposomes
2. Optimize the decoy liposome platform
 - Test additions and modifications of the liposome formulation in order to improve IAV inhibition

- Exchange the decoy receptor glycolipid with LSTa and characterize the inhibitory properties against IAV and
3. Create decoy liposomes that target the heparan sulfate binding viruses
- Generate heparin octasaccharide glycolipid-containing decoy liposomes and characterize the inhibitory properties against herpes simplex virus, respiratory syncytial virus and human parainfluenza virus 3.

Chapter II

Materials and Methods

Purification of LSTc and LSTa – LSTc and LSTa were either obtained from a commercial source (Dextra, Reading, UK) or purified from milk. Frozen bovine milk was thawed and centrifuged at 4,000 x g for 10 min at 4°C. The upper fatty layer was discarded and the lower aqueous layer was mixed with 2 volumes of ethanol and kept at 4°C overnight. Precipitate was removed by centrifugation at 12,000 x g for 10 min at 4°C; the supernatant, consisting primarily of oligosaccharides and lactose, was dried under nitrogen at room temperature and then reconstituted with 0.2 volumes of fresh 20% methanol and stored at -20°C until use. To separate LSTc or LSTa from other oligosaccharides, the reconstituted solution was subjected to dual stage purification, using size exclusion as the first step to remove high molecular weight material and to exchange the sample into a suitable buffer. As the second step, weak anion exchange purification was performed using ammonium formate as the eluting agent. Fractions were monitored by mass spectrometry, pooled and lyophilized. Purity of sample was assessed using capillary electrophoresis.

Purification of HS-octa – Full length heparin was purchased from a commercial source, and cleaved into oligosaccharides with heparinase. To separate octasaccharide from other oligosaccharides, the reconstituted solution was subjected to dual stage purification, using size exclusion as the first step to remove high molecular weight material and to exchange the sample into a suitable buffer. As the second step, weak anion exchange purification. Fractions were

monitored by mass spectrometry, pooled and lyophilized. Purity of sample was assessed using capillary electrophoresis.

Glycolipid synthesis – 1,2-dioleoyl-*sn*-glycero-3-phosphoethanolamine (DOPE) (Avanti Polar Lipids, Alabaster, AL) and N-(FMoc-13-amino-4,7,10-trioxa-tridecyl)succinamic acid (FMOC) (Polypeptide Laboratories, San Diego, CA) were purchased from commercial sources and used without further purification. Ethyl-3-[3-dimethylaminopropyl] carbodiimide hydrochloride (EDC) was purchased from Sigma-Aldrich (St. Louis, MO). Thin layer chromatography (TLC) was performed on silica-coated glass plates. Column chromatography was performed using silica gel 60 Å. Mass spectrometry was performed using 4800 MALDI-MS and MALDI-TOF instruments (Voyager DE-STR, Applied Biosystems, Carlsbad, CA). Solvent evaporation was performed on a rotary evaporator under reduced pressure at 30-35°C. All other synthetic lipids were purchased as solutions in chloroform (Avanti Polar Lipids, Alabaster, AL) including: DOPC (1, 2-dioleoyl-*sn*-glycero-3-phosphocholine), DOPG (1, 2-dioleoyl-*sn*-glycero-3-[phospho-*rac*-(1-glycerol)] (sodium salt)), and DOPE-NBD (1, 2-dioleoyl-*sn*-glycero-3-phosphoethanolamine-N-(7-nitro-2-1,3-benzoxadiazol-4-yl) (ammonium salt)). Cholesterol (purity \leq 99%, MW 386.65) was purchased dry (Sigma-Aldrich, St. Louis, MO) and dissolved in chloroform. Chloroform was >99.8% pure, stabilized with ethanol (Acros Organics, Morris Plains, NJ), ethanol was 200 proof (Goldshield Chemical Co., Hayward, CA), hydrochloric acid was certified ACS plus (Fisher Scientific, Pittsburgh, PA), and all water used was ultra-purified (MilliQ A10, Millipore, Billerica, MA).

DMB-HPLC quantification – LSTc incorporation into glycolipid was quantified by HPLC as described by Klein *et al.* (Klein, Veenstra *et al.* 1997); briefly, glycolipid or standard was treated with 2N glacial acetic acid at 80°C for 5 h and then dried by centrifugal evaporation. Samples were treated with 30 µL 1,2-diamino-4,5-methylene dioxybenzene (DMB) labeling mixture (1.6 mg 1,2-diamino-4,5-methylenedioxybenzene dihydrochloride, 3.1 mg sodium hydrosulfite, 58 µl β-mercaptoethanol, 82 µL glacial acetic acid per mL) at 50°C for 2.5 h in the dark. Samples were diluted with 20 µL ddH₂O, and analyzed by reverse phase HPLC using a TSKgel ODS-120T column (Tosoh Corp., South San Francisco, CA) running 7% methanol in water. Fluorescence of the DMB-SA complex is detected at ex373/em448.

Liposome Preparation – Gas-tight syringes (Hamilton Co., Reno, NV) and 4 mL borosilicate glass vials with Teflon-lined caps (National Scientific, Rockwood, TN) were thoroughly cleaned before use. Syringes were rinsed 10x with 100% ethanol and then 10x with chloroform. Vials were soaked in 300 mM HCl for 1.5 h, and then rinsed thoroughly with water, 3x with ethanol and 3x with chloroform. Residual solvent was evaporated under a filtered stream of dry nitrogen gas.

Lipids were mixed and deposited in clean vials using clean syringes. Solvent was evaporated under a filtered stream of dry nitrogen gas while manually rotating the vial until only a thin layer of lipid remained on the inner walls. Residual solvent was removed by placing uncapped vials in a desiccator (Dry Seal; Wheaton, Millville, NJ) followed by application of reduced pressure for 24 h using an oil-free diaphragm vacuum pump (Gast, Benton Harbor, MI).

Aqueous lipid solutions were made by hydrating lipid films in 150 mM phosphate buffered saline (PBS) (140 mM NaCl, 8.5 mM NaH₂PO₄, 1.5 mM Na₂HPO₄, pH 7.4) and

vortexing for 2 min in 30 s intervals. Lipid solutions were then subjected to 10 rapid cycles of freeze-thawing by submersion in liquid nitrogen and 70°C water, respectively, to break apart multi-lamellar structures, and then extruded through 200 nm pores. Extrusion consisted of either 10 passes through an aluminum oxide membrane using a Lipex Thermobarrel Extruder (Northern Lipids, Burnaby, BC, Canada) or 21 passes through a polycarbonate membrane using a LiposoFast-Basic Extruder (Avestin; Ottawa, ON, Canada). Extruders were thoroughly cleaned and primed with buffer before use. After the final pass, samples were collected in a clean vial, sealed with a Teflon-lined cap and stored at 4°C until use.

Lipid concentration post-extrusion relative to pre-extrusion was determined by fluorimetry. Typical recoveries were ~50% with the Lipex Thermobarrel Extruder and ~80% with the LiposoFast-Basic Extruder. The concentration of lipid in a final solution made from a stock mixture of 3 mol% DOPE-NBD and 97 mol% DOPC was determined colorimetrically, as described (Weirich, Israelachvili et al. 2010) and served as a reference for fluorimetric measurements on solutions made from the same lipid stock. Results were consistent with concentrations estimated based on mass lipid deposited and volume hydrated. Samples containing DOPE-NBD or DOPE-Rh were hydrated to an estimated concentration of 7.7 mM total lipid.

Liposome modifications – The decoy liposome formulation described above was modified to include the following additions. The construction process for each modification was the same as above, except where noted, all changes were made to both control and LSTc-containing decoy liposomes. Size changes: liposomes were extruded through either a 20 or 200 nm pore during the passes through the extruder membrane. Liposomes with cholesterol: 30 mol% of cholesterol was

added to the lipid mix, and the amount of DOPC used was decreased by 30 mol%. Osmotic crushed liposomes: control and decoy liposomes were extruded into a buffer containing 15 mM PBS. The liposomes remained in this buffer till immediately before testing, when they were diluted to the desired concentration of SA in 150 mM PBS, causing water outflux from the liposome interior. PEGylated liposomes were created by adding 10 mol% PEG-1000–DOPE (Avanti Polar Lipids) to the lipid mix and decreasing the DOPC amount used by the same amount. Liposomes with 15 mol% negative charge were created by either (i) increasing DOPG lipid by 7.5 mol%, or (ii) increasing LSTc-DOPE glycolipid by 7.5 mol% and decreasing DOPC lipid by the same extent in both methods.

Liposome Characterization – Diameter and polydispersity of liposomes were determined by dynamic light scattering (Zetasizer Nano; Malvern Instruments, Worcestershire, UK) specifying a lipid refractive index of 1.480 and a dispersant (150 mM PBS) refractive index of 1.332. Measurements were taken using 40 µL disposable cuvettes at room temperature (20°C) and a backscattering angle of 173 degrees. Data are reported as the average of five measurements separated by 15 s. Decoy liposomes were stored at 4°C for 12 months and were stable over this period, retaining their anti-IAV properties.

Viral strains – Influenza A/Puerto Rico/8/34 virus (PR/8, H1N1) was generously provided by Susan Swain (University of Massachusetts, Worcester, MA). Influenza A/Philippines X-79 (H3N2) was provided by Richard Dutton (University of Massachusetts, Worcester, MA). Influenza A/Aichi/68 (X-31, H3N2) and Sendai virus (Cantell Strain) were purchased from Charles River Laboratories (North Franklin, CT). Influenza A/Beijing/262/95 (H1N1) was

purchased from Meridian Life Science (Saco, ME). HSV-1 kos was generated in the laboratory of Dr. David Knipe (Harvard Medical School). Influenza viruses and Sendai virus were originally grown in the allantoic cavity of embryonated chicken eggs. Influenza viruses were stored at -80°C prior to use and titrated on Madin-Darby canine kidney (MDCK) cells. Respiratory syncytial virus (RSV) strain A2 was grown in Vero cells in 5% fetal bovine serum (FBS), cell debris was frozen at -80°C and subsequently titrated on Vero cells. Recombinant influenza A/WSN/33 with AlexaFluor 647 covalently attached to the HA protein via sortase (WSN HA-647) was prepared as described (Popp, Karssemeijer et al. 2012) and stored at 4°C prior to use.

Cell lines – MDCK cells were obtained from the American Type Culture Collection (ATCC, Manassas, VA) and were cultured in Eagle’s minimal essential medium (MEM) with 10% fetal bovine serum (FBS), 2 mM L-glutamine, 2 mM Penicillin/Streptomycin (Pen/Strep), 0.1 mM non-essential amino acids and 1 mM sodium pyruvate. A549 cells were obtained from ATCC and cultured in Dulbecco’s modified Eagle’s medium (DMEM) with 10% FBS and 2 mM Pen/Strep. Vero cells were obtained from ATCC and cultured in DMEM with 10% FBS and 2 mM Pen/Strep.

Mouse infection studies – Female C57BL/6 wild-type mice were purchased from the Jackson Laboratory (Bar Harbor, ME). Mice were 8 to 10 weeks of age at the time of infection. IAV (1,000 plaque forming units or PFU) was combined with LSTc decoy liposomes (170 µM SA) or the equivalent amount of control liposomes in a final volume of 30 µL and incubated at 37°C for 30 min. Samples were stored on ice until use. Mice were infected intratracheally with 30 µL of

sample and monitored daily. Mice were scored as deceased when found dead or were clearly imminently moribund, in which case they were euthanized. The University of Massachusetts Medical School Institutional Animal Care and Use Committee approved all experimental protocols.

Mice infected for lungs harvests were infected as described above, except as noted. Mice infected with 350 PFU of IAV were given an overdose of anesthesia, lungs were removed, and stored in 300 μ L ice-cold PBS. Lungs were stored at -80°C prior to use. Lung samples were thawed on ice, homogenized and clarified. IAV viral titer were tested by serial dilution of samples in PBS-1% BSA and plaqued on MDCK cells as described below. Lung IL-1 β levels were measured from lung samples by EILSA (BD Biosciences, San Jose, CA).

Mice infected before decoy liposome treatment were given 350 PFU of IAV diluted into sterile saline in a final volume of 30 μ L and incubated at 37°C for 30 min and stored on ice prior to use. Mice were anesthetized, infected intratracheally with 30 μ L of virus, and rested for 30 min before being anesthetized again and treated intratracheally with LSTc decoy liposomes (170 μ M SA) or the equivalent amount of control liposomes diluted in sterile saline in a final volume of 30 μ L (stored on ice). Mock treatment mice were anesthetized and given 30 μ L of ice-cold saline. Mice infected after decoy liposome treatments were treated in a similar fashion but with the regimen reversed, and they received 1,000 PFU of PR/8. All mice were followed as described above.

Hemagglutination inhibition assay – Red blood cells (RBCs) were isolated from normal human peripheral blood, blood type O. Whole blood was washed in sterile PBS three times to remove serum. Packed RBCs were diluted 1:30 in sterile PBS and stored at 4°C prior to use. All

procedures involving human subjects were approved by the University of Massachusetts Medical School Committee for the Protection of Human Subjects in Research and in accordance with the Declaration of Helsinki.

HA titers for each virus were determined on RBCs prior to inhibition studies per standard protocol (Choi, Mammen et al. 1996). For hemagglutination inhibition (HAI) assays, liposome samples were diluted two-fold in PBS. Four HA units of virus in 25 L of PBS were added to all dilutions. Samples were incubated for 30 min at room temperature. 50 L of diluted RBCs were added to the wells and incubated for an additional hour at room temperature to allow agglutination. The HAI titer is the reciprocal of the last dilution of liposomes that results in non-agglutinated RBCs.

Plaque assay with immunostaining – MDCK cells were seeded into 12-well plates and incubated at 37°C for 24 hours to form monolayers. Liposome samples were diluted to the desired concentration in sterile PBS-1% bovine serum albumin (BSA, Sigma-Aldrich, St. Louis, MO) in a final volume of 225 l. IAV was diluted to 300 PFU/mL and mixed 1:1 (v/v) with liposome samples and incubated at 37°C for 30 min. MDCK cells were washed twice with PBS-1% BSA and samples were added to wells in duplicate (200 µL per well). Samples were incubated at 37°C for 1 hour on MDCK cells. Cells were washed with PBS-1% BSA and overlaid with freshly prepared 0.5% agar in DMEM-F12 and incubated at 37°C for 48 hours. Cells were fixed and stained with anti-hemagglutinin antibody MAB8261 (Millipore, Billerica, MA). Plaques were visualized with anti-mouse horseradish peroxidase–conjugated secondary antibody (BD Biosciences, San Jose, CA) and developed with peroxidase substrate kit (Vector Laboratories,

Burlingame, CA). Viral plaques in the MDCK monolayer were counted and the PFU/mL was determined.

For some experiments, RSV was used in a similar fashion, except as noted. Vero cells were grown to confluency in 24-well plates. Liposome samples, heparin or HS-octa in solution, were diluted to the desired concentration in serum-free DMEM in a final volume of 130 μ L. RSV was diluted to 1,000 PFU/mL and mixed 1:1 (v/v) with treatment samples and incubated at 37°C for 30 minutes. Vero cells were prewashed in serum-free DMEM before addition of 100 μ L of sample, in duplicate. After one hour of infection, cells were washed with DMEM-10% FBS and incubated in DMEM-10% FBS and 2 mM Pen/Strep for three days at 37°C. Cells were fixed with 80/20 (v/v) acetone/PBS and stained with anti-F and anti-G glycoprotein antibodies (MAB8599 and MAB858, respectively; 1:1000 dilution, Millipore, Billerica, MA). RSV plaques were visualized and quantified as for IAV.

HSV Plaque assay – HSV-1 plaque assays were done in a similar fashion to RSV plaque assays, except as noted. After the one hour infection, cells were washed with PBS and incubated in DMEM with 1% FBS and 0.165 mg/ml of Human IgG (Innovative Research, Novi, MI) for two days at 37°C. Cells were fixed and stained with 20% ethanol, 0.5% crystal violet.

Lactate dehydrogenase release – MDCK cells were plated into a 96 well plate at 2.5×10^4 cells per well and allowed to become adherent. Cells were washed with PBS-1% BSA and treated with decoy liposomes ranging in concentration from 164 to 2,625 nM LSTc (2 fold increments) or control liposomes at lipid concentrations equivalent to the 2,625 nM LSTc decoy liposome treatment, for 1 hour at 37°C. Cells treated with Triton X-100 were used at 100% lysis controls

and cells treated with PBS-1% BSA were used as no lysis controls, both in done duplicate. Cells were spun at 250 G for 10 min at 4°C and 100 µl of supernatants were tested with a colorimetric LDH release kit (Roche, Mannheim, Germany).

Inhibition of IAV growth – MDCK cells were seeded into 24-well plates and allowed to grow to confluency overnight at 37°C. MDCK monolayers were washed with PBS-1% BSA, and treated with decoy liposomes ranging in concentration from 1 to 1,000 nM SA LSTc or control liposomes, at lipid concentrations equivalent to the 1,000 nM SA LSTc decoy liposome treatment, for 30 min at 37°C. Treated MDCK cells were then infected at a multiplicity of infection (MOI) of 0.01 or 0.001 of PR/8 diluted in PBS-1% BSA without removal of liposome solution. After an infection period of one hour at 37°C, the inocula were removed and MDCK cells were washed with PBS-1% BSA. Viral growth medium (0.5 mL) with identical liposome treatment as during the infection step was added. After 24 hours, supernatants were taken and virus growth was measured by plaque assay

Inhibition of RSV growth – Vero cells were seeded into 24-well plates and allowed to grow to confluency overnight at 37°C. Vero cells were washed with serum free DMEM. RSV was either (i) co-incubated with liposome treatments for 30 minutes at 37°C before infection or where indicated (ii) added to Vero cell monolayers 15 minutes at 37°C before liposome treatment. Decoy liposomes were use at concentrations ranging from 0.01 to 10µM HS-octa decoy liposomes containing either 10 or 30 mol% HS-octa or control liposomes, at lipid concentrations equivalent to the highest concentration decoy liposomes. After an infection period of one hour at 37°C, the inocula were removed and Vero cells were washed with serum free media. Viral

growth medium (0.5 mL) with identical liposome treatment as during the infection step was added. After 24 hours, supernatants were taken and virus growth was measured by plaque assay.

Inhibition of HSV growth – Vero cells were seeded into 24-well plates and allowed to grow to confluency overnight at 37°C. Vero cells were washed with serum free DMEM. HSV was co-incubated with liposome treatments ranging from 10⁻⁴ to 10 µM HS-octa decoy liposomes or control liposomes, at lipid concentrations equivalent to the highest concentration decoy liposomes, for 30 minutes at 37°C before infection. After an infection period of one hour at 37°C, the inocula were removed and Vero cells were washed with serum free media. Viral growth medium (0.5 mL) with identical liposome treatment as during the infection step was added. After 48 hours, cells were fixed and stained with 20% ethanol, 0.5% crystal violet and evaluated for monolayer loss.

Flow cytometry – Adherent A549 cells were detached with 0.25% Trypsin/2.21 mM EDTA. Cells were washed twice with PBS, enumerated using a hemocytometer, and transferred to 96-well round-bottom plate (Costar, Washington DC) at 50,000 cells per well. Alexa Fluor labeled IAV (WSN HA-647) and decoy liposomes were co-incubated for 30 min. WSN HA-647 was tested at 1.3, 6.5 and 13 HA units with 1000 nM, 7.5 mol% LSTc decoy liposomes, diluted in PBS-1% BSA in a final volume of 50 µl. Control liposomes without LSTc were diluted to the same lipid concentration as decoy liposomes. Cells were treated with virus/decoy mixtures for 15 min at 37°C before being fixed with formalin (final concentration 1%). Cells were analyzed using a BD LSR II flow cytometer and FlowJo version 9.4.11 (TreeStar software).

Confocal microscopy – 30 HA units of WSN HA-647 were absorbed onto glass coverslips overnight, then treated with either 7.5 mol% LSTc decoy liposomes or control liposomes, both containing NBD-labeled lipids. Decoy liposomes were diluted to 1,000 nM LSTc in a final volume of 50 μ L; control liposomes were diluted to the same lipid concentration as the decoy liposomes. Decoy or control liposomes were incubated on the WSN HA-647 coverslips for 30 min at 4°C and washed three times with PBS-1% BSA before imaging. For experiments involved decoy liposomes binding to cell surfaces, A549 cells were grown overnight on glass coverslips and infected the next day with PR/8 IAV at a MOI of 1, diluted in PBS-1% BSA. After an infection period of one hour at 37°C, the inoculate was removed and A549 cells were washed with PBS-1% BSA. A549 cells were incubated overnight in viral growth medium at 37°C. Cells were then washed with PBS-1% BSA and mixed with decoy or control liposomes, diluted as described above for 30 minutes, at 37°C. Cells were fixed and stained for anti-neuraminidase (ab21305; 1:50 dilution, Abcam, Cambridge, MA) and visualized with anti-rabbit IgG Alexa-594 conjugated secondary antibody (A11012, Invitrogen) and Hoechst 34580 (diluted to 5 μ g/ml; Invitrogen). For all experiments, images were taken on a Leica SP2 AOBS confocal laser-scanning microscope with a 63X objective using the Leica Confocal Software (version 2.6.1). Multichannel images were obtained by sequential scanning with only one laser active for each scan to avoid cross-excitation. Overall brightness and contrast of images were optimized using Image J (Schneider, Rasband et al. 2012).

Statistics – Statistical analysis was performed using the unpaired, two-tailed Student's t-test. Values of $p \leq 0.05$ were considered significant. Error bars are \pm standard deviation or \pm standard error of the mean (SEM), as listed in each figure legend. For survival analysis, the Mantel-Cox

Log-rank test was performed. Statistics were calculated using Prism Version 6.0 (GraphPad Software).

Chapter III

Use of sialic acid containing decoy liposomes to prevent influenza A virus infection

Preface

This chapter contains information dealing with the construction, characterization and quantification of LSTc-containing and control liposomes and their use as a therapeutic against IAV infection. The entire process would not have been possible without the collaboration of the following labs, Dr. Zachary Shriver's laboratory at the Massachusetts Institute of Technology purified LSTc glycans and constructed glycolipids to form the building blocks of the LSTc-containing liposomes; Dr. Deborah Fygenon's laboratory, especially Dr. Kim Weirich and Lourdes Velazquez, at the University of California at Santa Barbra constructed and characterized all liposomes, including the many modified liposomes that were perfected over the span of this dissertation; Dr. Hidde Plough and Dr. Joe Ashour at the Whitehead Institute provided the Alexa Fluor-labeled recombinant sortase IAV and assisted with manuscript preparation. I tested the liposomes in all experiments described below, including HAI assays, confocal and flow cytometry to test Alexa Fluor-labeled IAV binding, infectivity assays and growth inhibition studies, mouse infections and analysis, statistical analysis and manuscript preparation for publication.

Introduction

Influenza poses a significant and on-going public health risk, even with the licensed vaccine. The yearly reformatted vaccine has the potential to be made against a strain that does not become one of the dominate circulating strains in the following the flu season, and therefore can fail to provide adequate protection. Likewise the vaccine will not protect against newly emerged, potentially pandemic IAV strains. For these situations, anti-IAV therapeutics must be used in life-threatening cases. Several small molecule inhibitors and commercial neutralizing mAbs are available for patients; however, circulating strains of IAV have shown an alarming ability to develop resistance to these drugs, so much so that use of some for example, amantadine, are no longer used clinically. In this chapter I will describe a novel approach to create a potential therapeutic for IAV that combines the use of receptor decoy and liposomal delivery technologies. By taking advantage of the virus' own receptor and need to bind sialic acid in order to infect a target cells, our collaborators constructed lipid bi-layer liposomes functionalized with a sialic acid containing molecule to bind to IAV HA. The use of liposomes as a scaffold for SA allows for optimal presentation to HA, and formation of multivalent interactions between decoy and virus. The data described in this chapter demonstrate that sialic acid functionalized liposomes can bind to and inhibit IAV both *in vitro* and *in vivo*, and they may be a promising human therapeutic.

Use of sialic acid containing decoy liposomes to prevent influenza A virus infection

Results

Generation of decoy liposomes containing the sialic acid moiety LSTc or LSTa

We chose a lipid backbone for our decoys to promote LSTc flexibility and permit multivalent binding to IAV HA trimers. Our collaborators formulated decoy liposomes from a mixture of phospholipids with two 18:1 fatty acyl chains such as DOPC, a principal component of mammalian membranes (Figure 3.1A). DOPC has a low gel transition temperature, which allows it to form relatively disordered membranes that remain fluid. Into this background they incorporated LSTc-DOPE. DOPE carries a primary amine that is easily linked to LSTc, and that allows controlled addition of SA moieties with distinct linker chemistries and of defined stoichiometry. This allows optimal presentation of the decoys to IAV HA. The DOPE primary amine also enables ready modification with the fluorescent dye NBD or rhodamine, a marker to assist with tracking and quantification. They added DOPG in some formulations to compensate for the net negative charge imparted by LSTc-DOPE.

Previous studies using glycan-specific lectins in histological analysis of tissue sections of the human respiratory tract demonstrated that the upper respiratory tract predominately contains glycans with α 2-6 linked SA, while alveolar cells of the deep lung are dominated by glycans bearing α 2-3 linked SA. Further, solid phase glycan array analysis of human-adapted IAV from H1N1, H2N2 and H3N2 subtypes has revealed a high affinity

Figure 3.1 Summary of decoy liposome construction.

A

Compound	Full Name	Purpose
LSTc-DOPE	LSTc-1,2-dioleoyl-sn-glycero-3-phosphoethanolamine	Glycolipid. Mimics the influenza receptor
DOPE-NBD or -Rh	1,2-dioleoyl-sn-glycero-3-phosphoethanolamine-N-(7-nitro-2-1,3-benzoxadiazol-4-yl) or -rhodamine	Fluorescent lipid. Enables quantification and tracking of decoys
DOPG	1, 2-dioleoyl-sn-glycero-3-[phospho-rac-(1-glycerol)]	Negatively charged lipid. Maintains decoy charge when varying mol% LSTc-DOPE
DOPC	1, 2-dioleoyl-sn-glycero-3-phosphocholine	Neutral lipid. Constitutes majority of decoy

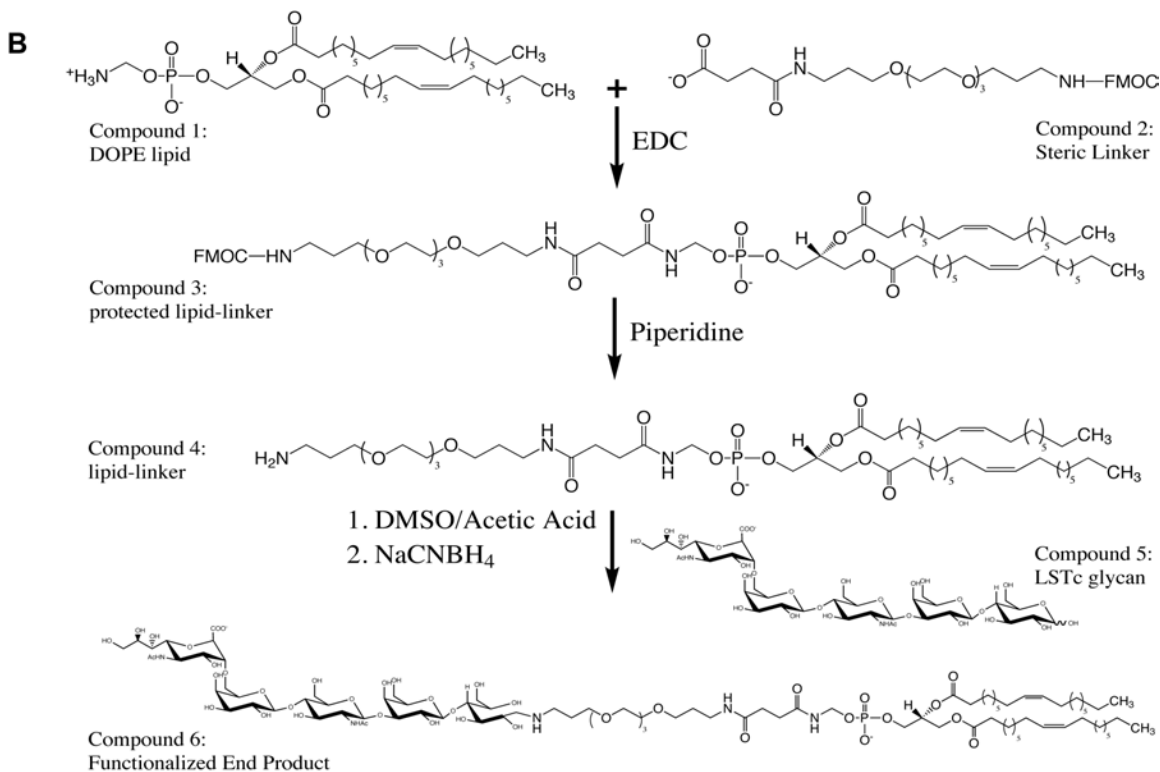


Figure 3.1 Summary of decoy liposome construction.

A, The different components of decoy liposomes are described. **B**, The chemical synthesis of LSTc-DOPE is outlined in the diagram. Additional details are described in the accompanying text. **Rh**, rhodamine; **EDC**, ethyl-3-[3-dimethylaminopropyl] carbodiimide hydrochloride; **NaCNBH₃**, sodium cyanoborohydride; **DMSO**, dimethyl sulfoxide.

binding to long (tetrasaccharide or longer) α 2-6 linked sialylated glycans as a key common feature (Chandrasekaran, Srinivasan et al. 2008; Xu, Newhouse et al. 2009). Therefore, a readily available 'long' α 2-6 sialylated glycan LSTc (Neu5Aca2-6Galb1-4GlcNAcb1-3Galb1-4Glc) was selected for use in decoy liposomes for human-adapted IAV. In order to study promiscuous binding and mouse-adapted IAV strains, the related sialylated glycan with the α 2-3 SA linkage, LSTa (Neu5Aca2-6Galb1-4GlcNAcb1-3Galb1-4Glc), was also selected for incorporation into decoy liposomes. LSTc and LSTa are also ideal sialylated glycans due to their ability to bind to multiple HA subtypes, a feature not true for all sialylated glycans (Ha, Stevens et al. 2001; Russell, Stevens et al. 2006; Xu, Newhouse et al. 2009); the chemistry for LSTa was the same as LSTc incorporation.

Glycolipid synthesis is schematically represented in Figure 3.1B. Our collaborators attached DOPE, a commercially available amine-linked unsaturated phospholipid (Figure 3.1B, compound 1) to an Fmoc-protected linker acid (compound 2) using carbodiimide coupling. They obtained compound 3 by purification of the crude product by silica gel column chromatography and used piperidine to deprotect the FMOC-modified lipid-linker conjugate (compound 3) and monitored the reaction by TLC. The crude amine (compound 4) was purified by column chromatography and eluted in organic solvent. The free amine of compound 4 is available for coupling to the sugar aldehyde (reducing end). Conjugation with the free non-reducing sugar aldehyde of LSTc was achieved via reductive-elimination. LSTc (compound 5) and compound 4 were conjugated at 60°C in minimal acid to minimize hydrolysis (desialylation) of LSTc. The final product (compound 6) was partially purified using flash chromatography and further purified by HPLC to obtain LSTc-containing

glycolipids. The final LSTc-DOPE product was assessed by DMB-HPLC to confirm the presence of SA in the glycolipid and was characterized the purified product by MALDI-MS and found the final glycolipid had $m/z = 2029-2031$ Da, expected $m/z = 2032$ Da (data not shown).

Our collaborators generated decoy liposomes with variable amounts of LSTc to determine the optimal amount of SA required for efficacy. The LSTc glycan is negatively charged and all decoys containing less than 7.5 mol% LSTc were made with DOPG as needed to generate decoy liposomes with the same net negative charge (Figure 3.1A). SA concentrations for each preparation were estimated based on the percent of input LSTc-DOPE and by the nanomolar concentration of total lipid. Liposomes with 0 mol% LSTc (and 7.5 mol% DOPG) were used as control liposomes. Our collaborators used extrusion through 200 nm pores to create the liposomes and measured their average size and polydispersity index using dynamic light scattering.

Decoy liposomes containing LSTc bind to different strains of IAV

I used a standard hemagglutination inhibition (HAI) assay to assess binding of decoy liposomes to influenza A/Puerto Rico/8/34 (PR/8, H1N1). The indicated percentage of sialoside at the liposome surface represents the mole percentage of lipid monomers used in the liposome synthesis reaction. IAV binds to SA on the surface of RBCs, causing hemagglutination. LSTc decoy liposomes provide an alternative SA binding option for IAV and will inhibit hemagglutination when present in sufficient quantity. The ability of liposomes to inhibit hemagglutination can be expressed either as the HAI titer (i.e., the

reciprocal of the last dilution of liposomes required to inhibit hemagglutination) or as the concentration (molarity of SA) that results in 90% inhibition (IC_{90}). For PR/8, decoy liposomes with 7.5 mol% LSTc had HAI titers of 256 and an IC_{90} of 0.041 μ M SA, and decoy liposomes with 5 mol% LSTc had HAI titers of 128 and an IC_{90} of 0.04 μ M SA (Table 3.1). Decoy liposomes containing 1 mol% LSTc did not inhibit hemagglutination at the highest concentration tested, 0.52 μ M SA. Control liposomes, used at similar lipid concentrations as the LSTc decoy liposomes, did not inhibit hemagglutination. Monovalent LSTc used at 5×10^5 M did not inhibit hemagglutination (Table 3.1). I also tested the activity of decoy liposomes containing either 10, 20 or 30 mol% LSTc by HAI against various strains of IAV, but did not see any significant increase in HAI titers compared to liposomes containing 7.5 mol% LSTc (data not shown).

To test the specificity of our decoy liposomes, I performed the HAI assay with several additional strains of IAV as well as another RNA virus, Sendai virus (SeV). SeV is a paramyxoviridae family virus that binds specifically to α 2-3 linked SA (Markwell and Paulson 1980), which is not present in our LSTc decoy liposomes. Decoy liposomes containing 7.5 mol% LSTc inhibited all strains of IAV tested: A/Philippines/2/82/X-79 (Philippines, H3N2) with an HAI titer of 16 (IC_{90} = 0.98 SA), X-31 (A/Aichi/68, H3N2) with an HAI titer of 32 (IC_{90} = 0.26 μ M SA), and A/Beijing/262/68 (Beijing, H1N1) with an HAI titer of 64 (IC_{90} = 0.11 μ M SA) (Table 3.2). However, 7.5 mol% LSTc decoy liposomes did not inhibit SeV agglutination (Table 3.2), demonstrating that the observed binding is specific for α 2-6 linked SA binding rather than a non-specific binding event.

Table 3.1 Assessment of different decoy liposome formulations by hemagglutination inhibition assay.

Mol% LSTc on liposomes	HAI Titer	IC₉₀ (μM SA)
0	No inhibition	N /A
1	No inhibition	> 0.52
5	128	0.04
7.5	256	0.041
Monovalent LSTc	No inhibition	> 500,000

Table 3.1 Assessment of different decoy liposome formulations by hemagglutination inhibition assay.

LSTc-containing decoy liposomes competitively bind to A/PR/8 (H1N1). Several different liposome formulations were assessed. Decoy liposomes containing 0, 1, 5, or 7.5 mol% LSTc were effectively inhibited hemagglutination of PR/8 IAV. Monovalent LSTc did not inhibit PR/8. “No inhibition” indicates that no inhibition was observed at the highest concentration tested. IC₉₀ values are shown as molarity of sialic acid.

Table 3.2 Assessment of 7.5 mol% LSTc decoy liposomes by hemagglutination inhibition assay of multiple strains of influenza A virus and sendai virus.

Virus	HAI Titer	IC₉₀ (μM SA)
Philippines H3N2	16	0.98
X-31 H3N2	32	0.26
Beijing H3N2	64	0.11
PR/8 H1N1	256	0.041
Sendai	No inhibition	> 84

Table 3.2 Assessment of 7.5 mol% LSTc decoy liposomes by hemagglutination inhibition assay of multiple strains of influenza A virus and sendai virus.

Decoy liposomes competitively bind to several strains of IAV. Decoy liposomes containing 7.5 mol% LSTc are effective at inhibiting hemagglutination of Philippines, X-31, Beijing, and PR/8 IAV strains. IC₉₀ values are shown as molarity of sialic acid. Hemagglutination of Sendai virus is not inhibited by 7.5 mol% decoy liposomes at the highest concentration tested.

Decoy liposomes containing LSTc co-localize with IAV and inhibit binding of IAV at the surface of A549 human lung epithelial cells

I surmised that inhibition of hemagglutination results from the direct binding of SA on LSTc decoy liposomes to hemagglutinin. To directly observe contact between decoy and IAV, I took advantage of a method for enzymatically attaching a fluorophore onto viral particles for single virion tracking (Popp, Karssemeijer et al. 2012). WSN HA-647, generated by the Plough laboratory, was absorbed onto glass coverslips, then treated with either decoy or control liposomes containing NBD-labeled lipids. WSN HA-647, decoy and control liposomes were each readily visible by confocal microscopy when fixed to glass coverslips (data not shown). I observed significant co-localization when WSN HA-647 was treated with 1,000 nM SA decoy liposomes with 7.5 mol% LSTc (Figure 3.2 A, C, Pearson's correlation coefficient: $r = 0.423$, $p \leq 0.01$). Control liposomes did not co-localize with adhered virus (Figure 3.2 B, D, Pearson's correlation coefficient $r = 0.023$, $p = 0.87$). I used cross-correlation analysis to validate the association of virus and decoy liposomes. The cross-correlation function (CCF) establishes whether there is a relationship between two channels of a complex 3-D stacked image (van Steensel, van Binnendijk et al. 1996). Figure 3.2 E shows the CCF of WSN HA-647 treated with decoy or control liposomes. The maximum CCF for LSTc decoy liposomes is at 0 x-voxel displacement and follows the standard decay curve for x shift in both positive and negative directions. The distribution of LSTc decoy liposomes and virus have significantly more overlap than control liposomes and virus, where the CCF does not peak at 0 x-voxel displacement, but peaks at 20 x-voxel shift with an $r = 0.023$ and has a flat distribution of CCF throughout the x-voxel shift.

Figure 3.2 LSTc decoy liposomes bind directly to influenza A virus.

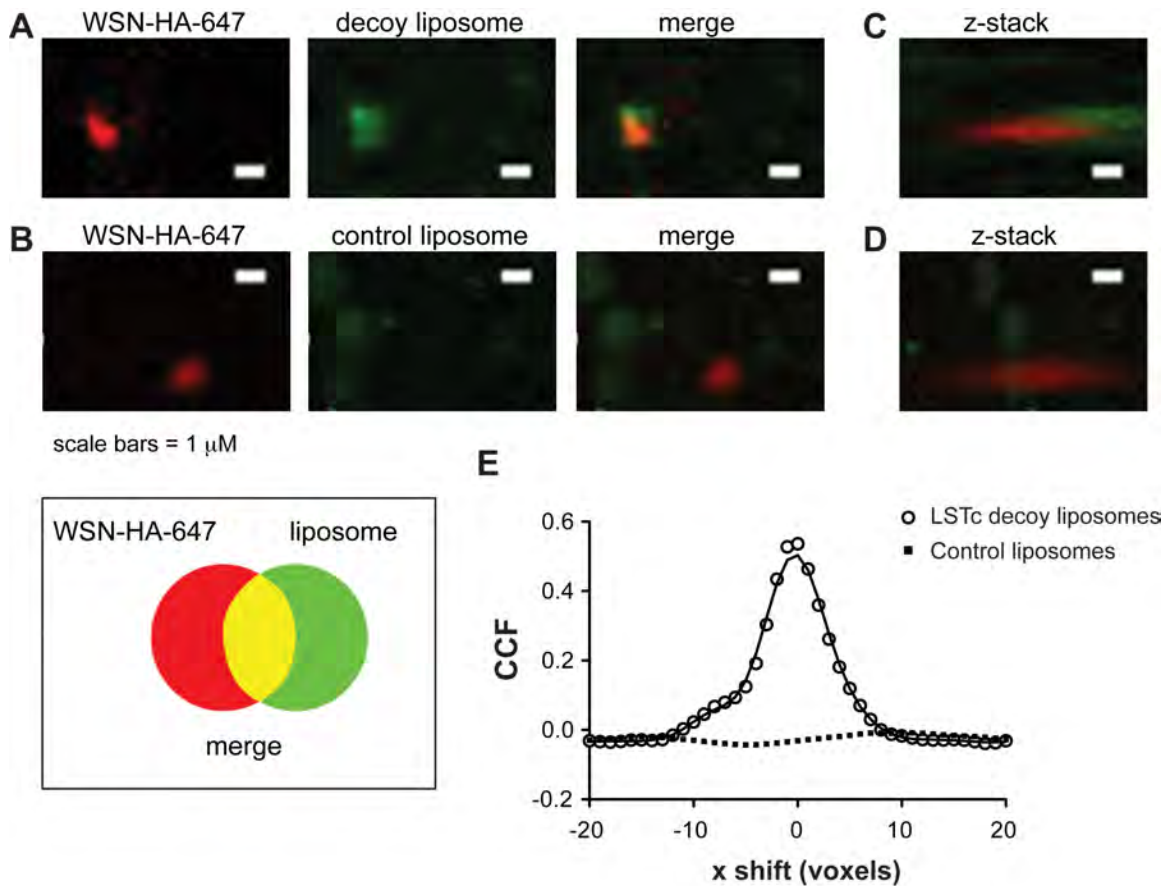


Figure 3.2 LSTc decoy liposomes bind directly to influenza A virus.

Immunofluorescent z-stack images were obtained of WSN HA-647 and fluorescent liposomes, viewed from above (**A** and **B**) or rotated 37 degrees (**C** and **D**). **A** and **C**, LSTc decoy liposomes, which contain NBD (**green**) bound specifically to WSN HA-647 (**red**) can be seen binding to the apical portion of virus foci when the field of view is rotated 37 degrees. **B** and **D**, control liposomes do not show significant co-localization with WSN HA-647. **Scale bar**, 1 μ m. **E**, Van Steensel's CCF coefficient analysis of images **A** and **B**. The CCF is the Pearson coefficient of WSN HA-647 and liposomes at each pixel shift in the x dimension; this calculation is based on a representative field of 45 by 45 μ m. Decoy liposomes (**open circles**) significantly correlate to WSN HA-647 ($p < 0.001$), whereas control liposomes (**black squares**) do not ($p = 0.21$).

To further test the competitiveness of LSTc decoy liposomes for IAV, I challenged human alveolar basal epithelial cells (A549 cells) with three different doses of WSN HA-647 combined with either LSTc-bearing decoy liposomes or control liposomes. Mixtures of virus and liposome were added to A549 cells where free virus would bind to cells. Binding of virus at the single cell level was assessed by detection of WSN HA-647 by flow cytometry. WSN HA-647 in combination with control liposomes allowed a high degree of binding to A549 cells (Figure 3.3A, gray lines). No significant shifts were noted for A549 cells challenged with control liposomes mixed with 1.3, 6.5, or 13 HA units of WSN-HA-647 (Figure 3.3A, left, middle, and right panels). However, decoy liposomes at 7.5 mol% LSTc reduced viral binding when challenged with WSN HA-647 (Figure 3.3A, black lines). Decoy liposomes decreased 75%, 79% and 54% of binding when challenged with 1.3, 6.5, or 13 HA units of WSN HA-647 (Figure 3.4A, left, middle, and right panels, respectively). At the 1.3 HA unit dose of WSN HA-647, the mean fluorescence intensities (MFI) \pm S.E.M. for control liposomes and decoy liposomes were 369 (\pm 158) and 89 (\pm 88) ($p = 0.11$) (Figure 3.3B). The MFIs for 6.5 HA unit dose of WSN HA-647 were 1071 (\pm 145) and 223 (\pm 86) ($p \leq 0.001$) and for 13 HA unit dose of WSN HA-647, 1142 (\pm 113) and 522 (\pm 89) ($p \leq 0.001$) (Figure 3.3B). Together these data demonstrate that the LSTc-containing decoy liposomes competitively bind to IAV and block its adhesion to SA on uninfected cells, suggesting a block of infection.

Figure 3.3 LSTc-containing decoy liposomes inhibit binding of influenza A virus to A549 cells.

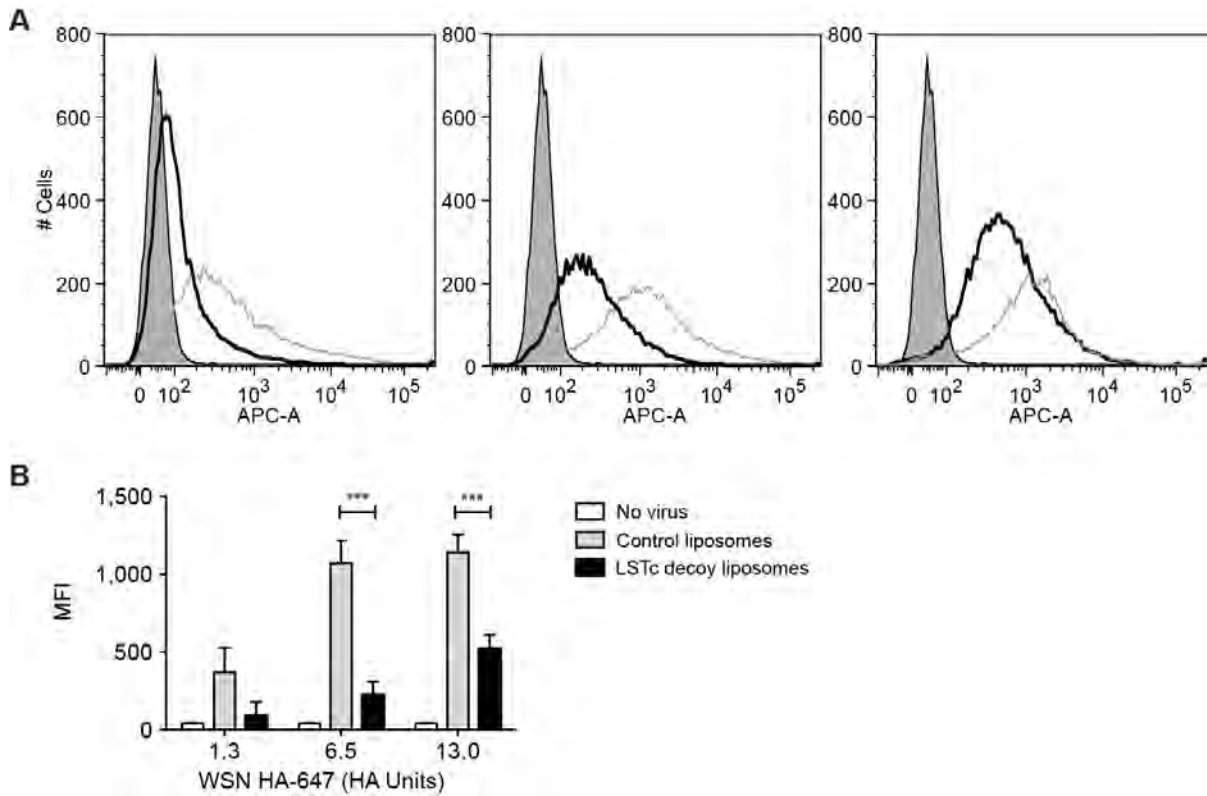


Figure 3.3 LSTc-containing decoy liposomes inhibit binding of influenza A virus to A549 cells.

A, Representative flow cytometry plots of A549 cells treated with control liposomes (**gray lines**) combined with WSN HA-647 (1.3 HA units (**left panel**), 6.5 HA units (**middle panel**), and 13 HA units (**right panel**)), LSTc-containing decoy liposomes combined WSN HA-647 (**black lines**), or A549 cells without virus (**gray-shaded**). LSTc-decoy liposomes contained 7.5 mol% LSTc. **B**, shown is mean fluorescence intensity (**MFI**) quantification of data in **A**; data are presented as the mean \pm S.E. ***, $p \leq 0.001$ decoy liposomes *versus* control liposomes.

LSTc decoy liposomes co-localize specifically to IAV infected A549 cells

The data above demonstrate that the decoy liposomes bind to mature virions and can prevent binding to cell surfaces. To further examine the utility of our LSTc decoy liposomes, I measured their ability to bind to budding virus on infected cell surfaces. I observed decoy liposome binding with fluorescent co-localization microscopy. I infected adhered A549 cells on glass coverslips, treated with either control or decoy liposomes containing NBD-labeled lipids, and washed to remove unbound liposomes before immunostaining for IAV NA. There was significant co-localization when PR/8 infected A549 cells were treated with LSTc-containing decoy liposomes (Figure 3.4A, Pearson's correlation coefficient $r = 0.629$, $p \leq 0.001$). Control liposomes did not bind to PR/8 infected cells (Figure 3.4B Pearson's correlation coefficient $r = 0.046$, $p = 0.78$). Co-localization was dependent on infection; LSTc-containing decoy liposomes did not bind to uninfected A549 cells (Figure 3.4C Pearson's correlation coefficient $r = 0.027$, $p = 0.87$). Cross-correlation analysis reveals a CCF peak at 0 x-voxel shift for LSTc decoy liposomes and standard decay curve in both the positive and negative x-voxel shifts (Figure 3.4D) indicating that decoy liposomes and NA staining have significant co-localization. The CCF for infected A549 cells treated with control liposomes and uninfected cells treated with decoy liposomes peaked significantly lower, had flatter decay curves, and overall lower pixel intensity staining for liposomes (Figure 3.4D). Taken together, these binding data demonstrate that the decoy liposomes bind to IAV in many environments, bind directly in a cell system, block IAV adhesion to sialylated cells and bind to virus budding from infected cells.

Figure 3.4 LSTc-containing decoy liposomes bind to PR/8 infected A549 cells.

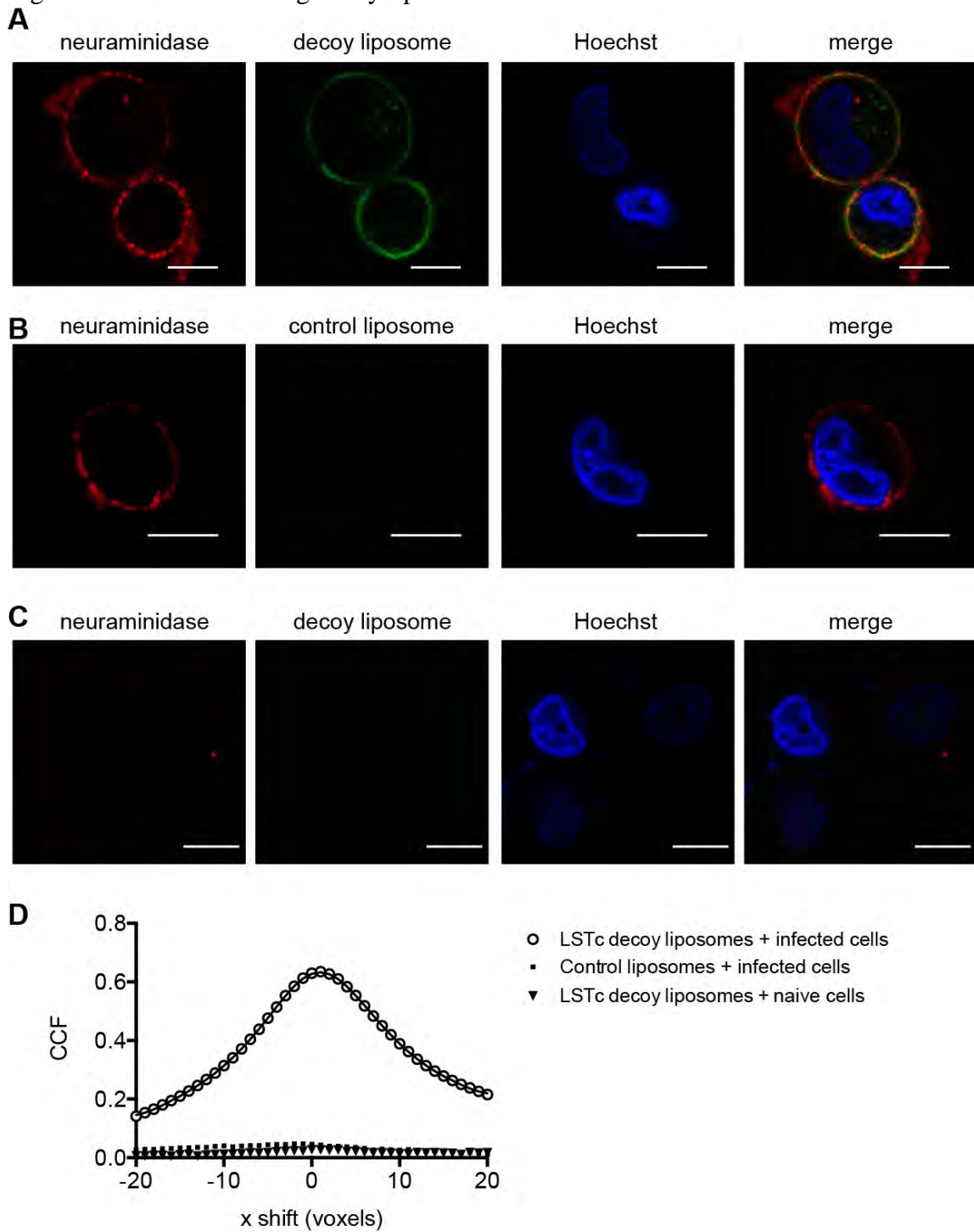


Figure 3.4 LSTc-containing decoy liposomes bind to PR/8 infected A549 cells.

Immunofluorescent images were obtained of IAV neuraminidase expression on A549 cells infected with PR/8 IAV (**A and B**) or mock infected (**C**) and fluorescent liposomes. **A**, LSTc decoy liposomes, which contain NBD (**green**), bound specifically to infected A549 cells expressing NA (**red**) **B**, control liposomes do not show significant co-localization with NA on infected A549 cells. **C**, LSTc decoy liposomes do not bind to mock infected A549 cells. **Scale bar**, 10 μm . **D**, Van Steensel's CCF coefficient analysis of merged images in **A**, **B** and **C**. The CCF is the Pearson coefficient of IAV neuraminidase and liposomes at each pixel shift in the x dimension; this calculation is based on a representative field of 45 by 45 μm . Decoy liposomes significantly correlate to infected A549 cells (**open circles**), whereas neither control liposomes with infected A549 cells (**black squares**) or decoy liposomes with uninfected A549 cells (**black triangles**) correlated. Data are representative of a single independent experiment repeated twice, both having similar results.

Decoy liposomes containing LSTc prevent IAV infection of MDCK cells

To investigate the impact of decoy liposomes on IAV infectivity, I co-incubated PR/8 with either LSTc-containing decoy liposomes or control liposomes prior to infection of MDCK cell monolayers. In this experiment, viral particles are expected to bind to native SA on MDCK cells only when not competitively bound to decoy liposomes. Increasing concentrations of LSTc decoy liposomes inhibited infectivity of PR/8 (Figure 3.5A) in these cells, while control liposomes did not inhibit infection. The molarity of SA in the solution was calculated by multiplying the mole percent input of LSTc-DOPE glycolipids by the total lipid concentration. At 1 nM SA, all decoy liposomes displayed weak inhibition. As the total concentration of SA increased, each series with different mole percentages of LSTc on the liposome surface inhibited more PR/8. Decoy liposomes with 1 mol% LSTc inhibited weakly, blocking only $22 \pm 5.6\%$ of PR/8 at 515 nM SA. LSTc decoy liposomes at 5 mol% inhibited weakly at low concentrations of LSTc, but increasing the concentration of these decoys had a more pronounced inhibitory effect, inhibiting $73 \pm 10\%$ of PR/8 at 1,000 nM SA. LSTc decoy liposomes at 7.5 mol% blocked PR/8 infection to the largest extent, inhibiting PR/8 almost completely at 1,000 nM SA, $93.8 \pm 1.3\%$ compared to control liposomes (Figure 3.5A).

These data show not only a dose-dependent response of LSTc in the medium on IAV inhibition, but also that the density of LSTc displayed on the surface of each liposome at a given concentration of LSTc affects the extent of viral inhibition. For example, when each series of LSTc decoy liposomes was diluted to 100 nM of total SA and challenged with PR/8, 7.5 mol% LSTc decoy liposomes inhibit to a greater degree than decoy liposomes with either 5 or 1 mol% LSTc (Figure 3.5A). This inhibition occurs despite the fact that decoy

Figure 3.5 LSTc decoy liposomes selectively inhibit influenza A virus infection of MDCK cells.

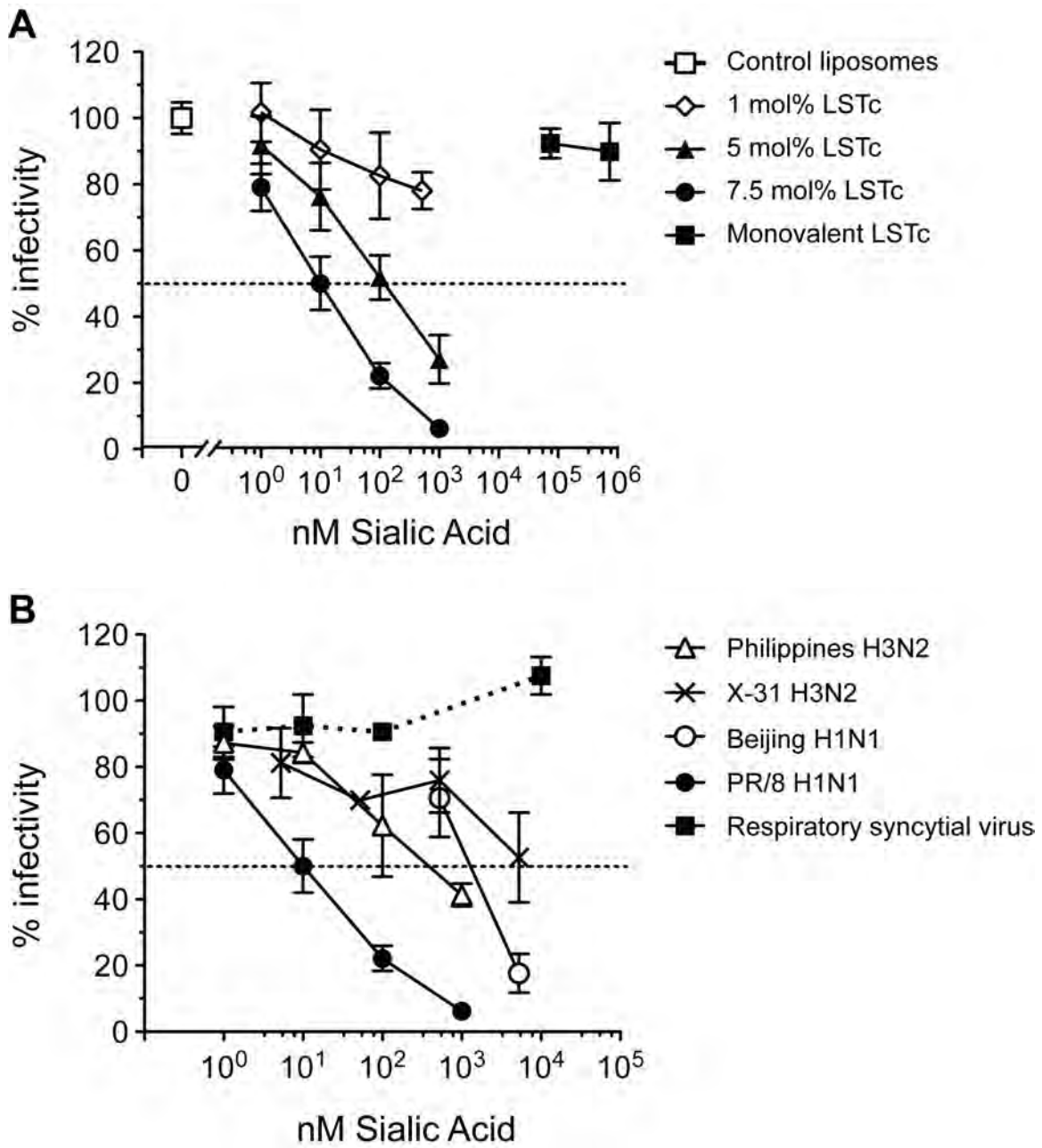


Figure 3.5 LSTc decoy liposomes selectively inhibit influenza A virus infection of MDCK cells.

A, PR/8 (50 PFU/well) was incubated with control liposomes, LSTc-containing decoy liposomes, or monovalent LSTc before addition to MDCK cells. Plaques per well of virus treated with control liposomes (0 mol% LSTc) are defined as 100% infectivity (**open square**), and virus treated with different liposome formulations are expressed as the percent reduction from its respective control. Decoy liposomes with 7.5 mol% LSTc (**circles**) inhibited PR/8 to the greatest extent. Decoy liposomes with 5mol%LSTc (**triangles**) also significantly inhibited infection; however, decoy liposomes with 1 mol% LSTc (**open diamonds**) poorly inhibited infection. **B**, decoy liposomes containing 7.5 mol% LSTc inhibit multiple strains of IAV. Decoy liposomes inhibited Philippines (**open triangles**, 50 PFU/well), X-31 (**crosses**, 50 PFU/well), Beijing (**open circles**, 15 PFU/well), and PR/8 (**filled circles**, 50 PFU/well) strains of IAV. LSTc decoy liposomes did not inhibit RSV (**filled squares**, 50 PFU/well). The data represent the average \pm S.E. of three experiments for PR/8 and two experiments for Philippines, X-31, Beijing, and RSV.

preparations with a higher density of LSTc per liposome have fewer liposomes in solution at equimolar concentrations of LSTc. Decoy liposomes with denser LSTc are therefore more efficient at inhibiting IAV. I also tested the infectivity inhibition of decoy liposomes containing more than 7.5 mol% LSTc and saw no significant increase of inhibition from liposomes with up to 30 mol% LSTc (data not shown). These results were similar to the finding that decoy liposomes with more than 7.5 mol% did not increase HAI titers of IAV.

Next, I tested our decoy liposomes at 7.5 mol% LSTc on several additional IAV strains. Decoy liposomes at 7.5 mol% inhibited all IAV strains in a dose-dependent manner. Decoy liposomes inhibited Philippines up to $58.3 \pm 3.4\%$ at 1,000 nM SA. At 5,250 nM SA, decoy liposomes at 7.5 mol% inhibited infectivity of X31 by $47.3 \pm 13.5\%$ and infectivity of Beijing by $82.3 \pm 5.9\%$. Control liposomes lacking LSTc did not inhibit any of these strains. Decoy liposomes displayed high avidity for IAV in both the HAI and infectivity assays. I also compared LSTc-containing decoy liposomes with monovalent LSTc at SA concentrations well in excess of the estimated SA concentrations for LSTc-containing liposomes. However, 74,000 nM monovalent LSTc did not inhibit the infectivity of either PR/8 (Figure 3.5) or Philippines (data not shown). At this high concentration, monovalent LSTc would be expected to bind to both PR/8 and Philippines HA during the pre-incubation period. Given that infection was not inhibited, monovalent LSTc did not make multivalent, high avidity interactions with IAV, while LSTc complexed in liposomes can make multivalent, high avidity interactions with IAV.

Decoy liposomes containing LSTc do not prevent infection of respiratory syncytial virus in Vero cells

To test the specificity of LSTc-containing decoy liposomes, I assessed whether decoy liposomes would affect RSV infection of Vero cells. RSV interacts with cellular heparan sulfate for attachment and infectivity (Feldman, Audet et al. 2000) and has not been reported to interact with SA receptors. I co-incubated 7.5 mol% LSTc decoy liposomes or control liposomes with RSV prior to infection of Vero cells. LSTc-containing liposomes did not affect RSV infectivity (Figure 3.5B), even at a SA concentration of 10,000 nM SA, an amount that inhibits nearly 100% of PR/8. This lack of inhibition, along with the lack of hemagglutination inhibition of SeV, demonstrates that our LSTc-decoy liposomes specifically inhibit via α 2-6 linked SA.

Functionalized decoy liposomes are not toxic *in vitro* or *in vivo*

Liposome components are non-toxic, and they were chosen in part for their similarity to biological molecules. The backbone lipid, DOPC, which comprises over 90% of each liposome, is a non-toxic synthetic derivative of phosphatidylcholine (PC), which makes up a large percentage of mammalian cell membranes (Kaneko, Baba et al. 1996). Likewise, the LSTc glycolipid, a four-residue sugar purified from cow's milk, is regularly consumed by the general public and is therefore thought to be non-toxic. In addition, similar FDA-approved liposome drug carriers, which undergo extensive toxicity evaluation, are non-toxic (Hiemenz and Walsh 1996).

To measure toxicity, I tested cells for lactate dehydrogenase (LDH) release, a marker of cell death, after incubation with our liposomes. I incubated control and LSTc-containing decoy liposomes with MDCK cells in the infection buffer for one hour and compared LDH release to cells treated with assay media alone or Triton X-100. Addition of Triton X-100 resulted in 100% cell death and an LDH release of 1.820 ± 0.078 OD, while no cell death (assay media alone) had background levels of 0.309 ± 0.01 OD (Figure 3.6A). Neither LSTc-containing decoy liposomes nor control liposomes resulted in significant LDH release. When diluted in two-fold serial dilutions, decoy liposomes with 7.5 mol% LSTc resulted in an average of 0.309 ± 0.02 OD LDH release from MDCK cells, even at the highest concentration tested, 5,250 nM SA, a concentration higher than necessary for complete inhibition. Control liposomes, which are similar except they containing DOPG lipid in place of LSTc glycolipid, resulted in an average of 0.358 ± 0.03 OD LDH release from MDCK cells (Figure 3.6A).

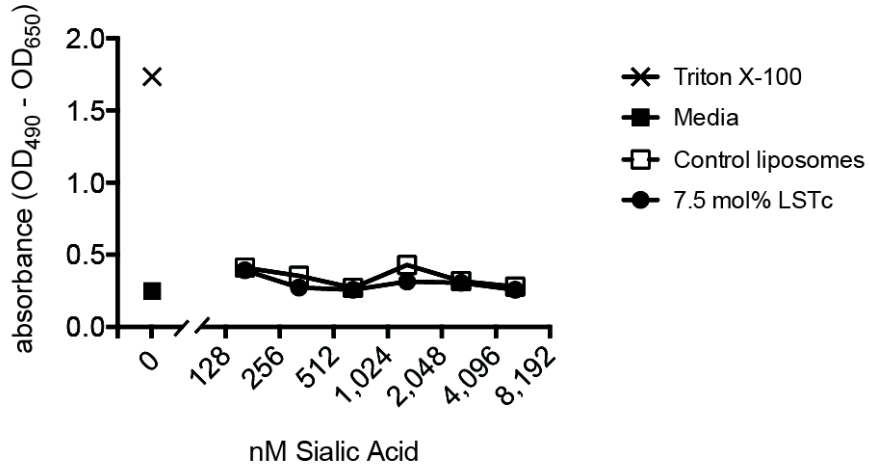
Decoy liposomes were also not toxic *in vivo*. Overt toxicity in mice was measured by weight loss and behavior changes, as compared to mice that received mocek, saline treatment. Mice treated with LSTc-containing decoy liposomes and saline showed no signs of toxicity or weight loss after treatment (Figure 3.6B). In addition, lungs were harvested from mice four days post-treatment and IL-1 β levels were examined.

Decoy liposomes containing LSTc remain active for long periods

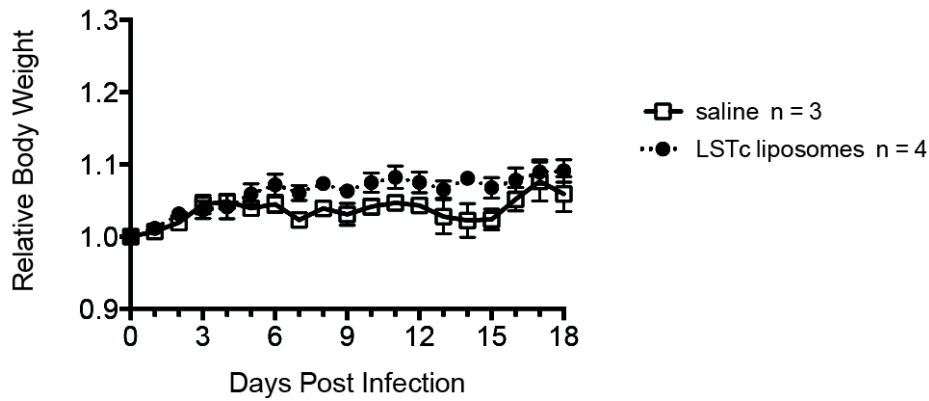
In order to be a useful therapeutic, LSTc decoy liposomes must be both chemically and biologically stable over long periods of time. Liposomes can be lyophilized and stored

Figure 3.6 Decoy liposomes are not toxic *in vitro* or *in vivo*.

A.



B.



C.

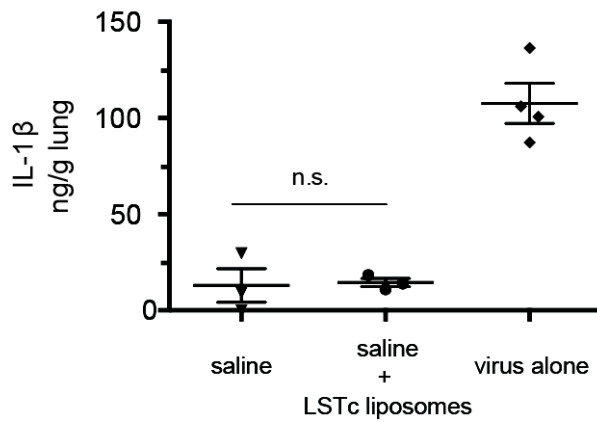


Figure 3.6 Decoy liposomes are not toxic *in vitro* or *in vivo*.

A, Control or LSTc-containing decoy liposomes were serially diluted 2-fold and incubated with MDCK cells for one hour before testing for LDH release. Triton X-100 treated cells (**x mark**) resulted in 100% cell death and media (PBS-1%BSA) treated cells (**filled square**) was used as the background control. Decoy liposomes with 7.5 mol% LSTc (**filled circles**) did not cause cytotoxicity at any dilution, including the highest concentration tested, 5250 nM SA. Control liposomes (**open squares**), at equivalent concentrations of lipid, also did not cause cytotoxicity. **B and C**, C57BL/6 mice were given intranasal saline (**open squares**), or 170 μ M SA of 7.5 mol% LSTc decoy liposomes diluted in saline (**filled circles**) and monitored for gross pathology and weight loss (**B**). Mice that received decoy liposomes did not show any signs of sickness, had normal weight retention, and were not any different from mice that received saline alone. **C**, lung IL-1 β levels were tested four days post-infection from mice that received saline, or 170 μ M SA of 7.5 mol% LSTc decoy liposomes diluted in saline or PR/8 alone. Mice that received LSTc decoy liposomes did not have any elevation of IL-1 β after liposome treatment, as compared to saline treated mice.

for long periods without losing their chemical and physical properties. However, once resuspended into a liquid buffer, it is possible that they could degrade over time. It is critical that the decoy liposomes maintain the inhibitory properties described above. To measure stability, I tested an individual preparation of 7.5 mol% LSTc decoy liposomes against PR/8 IAV infectivity, stored the liposomes at 4°C in PBS for over a year before challenging PR/8 IAV infectivity (Figure 3.7). After up to 15 months of storage, at 100 nM SA, the LSTc decoy liposomes inhibited $86.8 \pm 1.5\%$ PR/8 infectivity (Figure 3.7 black squares). This inhibition was similar to the 84.3% PR/8 inhibition observed when the liposomes were first tested a year earlier (Figure 3.7 grey triangles) and similar to liposome preps used in experiments above (see Figure 3.5A, black circles). These data indicate that LSTc-containing decoy liposomes are biologically stable and remain active against IAV after long periods of liquid storage at 4°C.

Decoy liposomes containing LSTc block viral growth of Influenza A virus in MDCK cells

To investigate the decoys' ability to inhibit IAV during multiple rounds of infection, I infected MDCK cells with IAV in the presence of increasing concentrations of decoy or control liposomes, and allowed continued viral replication and spread in the presence of either decoy or control liposomes. Control liposomes or decoy liposomes with 7.5 mol% LSTc at concentrations of 1 nM to 1,000 nM LSTc (10-fold increments) were added to MDCK cells 30 minutes before addition of PR/8. After one hour, all inoculating virus was removed, and LSTc decoy or control liposomes were replenished to the same concentrations

Figure 3.7 LSTc-containing decoy liposomes are stable.

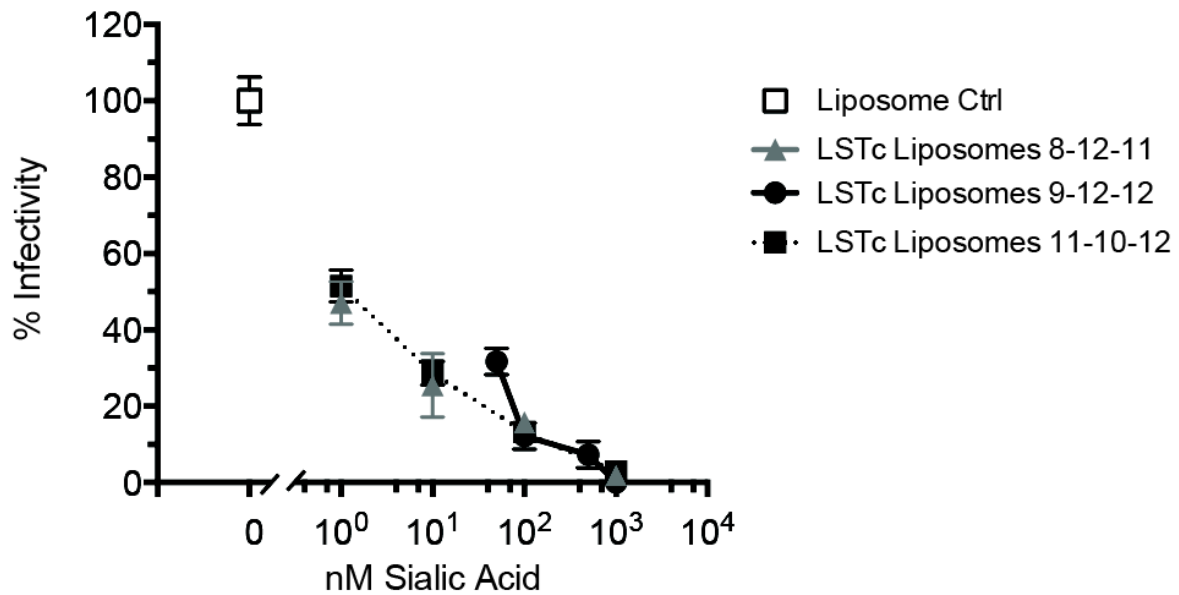


Figure 3.7 LSTc-containing decoy liposomes are stable.

PR/8 (50 PFU/well) was incubated with control liposomes or LSTc-containing decoy liposomes before the addition to MDCK cells. Plaques per well of virus treated with control liposomes (0 mol% LSTc) are defined as 100% infectivity (**open square**), and virus treated with decoy liposome with 7.5 mol% LSTc are expressed as the percent reduction from its respective control. Decoy liposomes first tested in August 2011 (**grey triangles**) inhibited PR/8 IAV to statistically similar levels as decoy liposomes tested in September 2011 (**circles**) and November 2012 (**filled squares, dotted line**). The data represent the average \pm S.E. of biological repeats, done in duplicate.

as during the infection, in serum-free media to allow virus replication in host cells. Twenty-four hours after infection, supernatants were sampled and tested for PR/8 plaque-forming units. The amount of virus recovered from wells treated with highly concentrated LSTc decoy liposomes was significantly reduced compared to wells with control liposomes, or with PR/8 and assay medium alone (Figure 3.8). Infected MDCK cells treated with 100 or 1,000 nM LSTc decoy liposomes had viral titers below the limit of detection, over 100-fold less than control liposome-treated cells (decoy liposomes 2.7 ± 0 vs. control liposomes 4.8 ± 0.07 ; $p \leq 0.001$, based on \log_{10} -transformed PFU/mL data) (Figure 3.8). 10 nM LSTc decoy liposomes also significantly inhibited PR/8 replication (2.8 ± 0.2 vs. control liposomes 4.8 ± 0.07 ; $p \leq 0.01$) (Figure 3.8). Decoy liposomes diluted to 1 nM LSTc or less did not prevent PR/8 replication (4.6 ± 0.04 vs. control liposomes 4.8 ± 0.07 ; $p = 0.069$). These results suggest that adhesion of viral particles to LSTc decoy liposomes depletes the amount of free virus capable of infecting in successive rounds of replication, and that this interaction is long-lasting because the bound virus is not cleared in this *in vitro* system.

Decoy liposomes containing LSTc extend survival of Influenza A virus-infected mice

To investigate the decoys' ability to inhibit IAV in a physiological setting, I evaluated the effects of LSTc-containing decoy liposomes on mice infected with a lethal dose of IAV. LSTc decoy liposomes or control liposomes were co-incubated with 1,000 PFU of PR/8 at 37°C for 30 minutes. This dose of PR/8 typically causes 90% lethality (LD₉₀) in C57BL/6

Figure 3.8 Inhibition of influenza A virus replication by LSTc decoy liposomes.

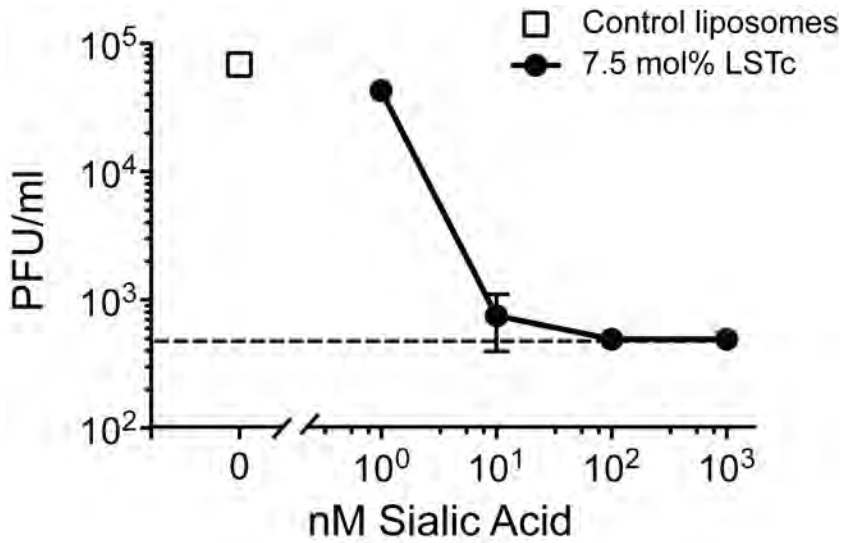


Figure 3.8 Inhibition of influenza A virus replication by LSTc decoy liposomes.

Control or LSTc-containing decoy liposomes were added onto confluent monolayers of MDCK cells 30 min before infection with PR/8 (multiplicity of infection 0.01). After infection, cells were incubated in the presence of liposomes for 48 h. Viral growth was measured by a plaque forming unit assay and plotted as PFU/ml versus total LSTc concentration present in the solution. Control liposomes did not inhibit IAV growth (**open squares**); however, increasing concentrations of 7.5 mol% LSTc decoy liposomes inhibited PR/8 infectivity (**filled circles**). The dotted line denotes the limit of detection of the assay. Data are representative of a single independent experiment repeated once, each with similar results.

mice following intratracheal delivery. The prediction was that any IAV not initially associating with LSTc decoy liposomes could subsequently infect susceptible cells within the lungs. Thus, mice administered virus with LSTc decoy liposomes might be expected to succumb to IAV infection less quickly than mice administered virus in combination with control liposomes or mice receiving virus alone.

Mice that received control liposomes and 1,000 PFU of PR/8 died at the same rate as mice that received 1,000 PFU of PR/8 alone (Figure 3.9A, median survival of 8 days for both groups, Log Rank test, $\chi^2 = 0.01$, $p = 0.9$). However, mice that received LSTc decoy liposomes and 1,000 PFU of PR/8 had significantly extended survival, with a median survival of 12 days compared to 8 days for mice that received control liposomes and 1,000 PFU of PR/8 (Log Rank test, $\chi^2 = 13.6$, $p \leq 0.01$), resulting in a 33.3% mean increase in lifespan post-infection (Figure 3.9A). The median survival and survival curve slope was reproducible over multiple experiments (the data in Figure 3.9A and B represents the sum of three independent experiments with a combined $n \leq 19$ mice for each group). Weight loss after IAV infection is a standard proxy for severity of disease. Mice that receive larger doses of IAV typically have more severe weight loss after infection as well as increased mortality (data not shown and Powell, Dwyer et al. 2006).

To test the effect of the mole percentage of LSTc contained on each liposome *in vivo*, I challenged mice with a lethal dose of PR/8 IAV, as described above, but with decoy liposomes containing 15 mol% LSTc. 15 mol% LSTc decoy liposomes did not have significantly higher potency against IAV *in vitro* (Figure 3.5 and data not shown), but this may not apply to an *in vivo* infection environment. As seen previously, mice that received control liposomes and 1,000 PFU of PR/8 died with similar kinetics as mice that received

Figure 3.9 LSTc decoy liposomes extend survival after lethal influenza A virus challenge.

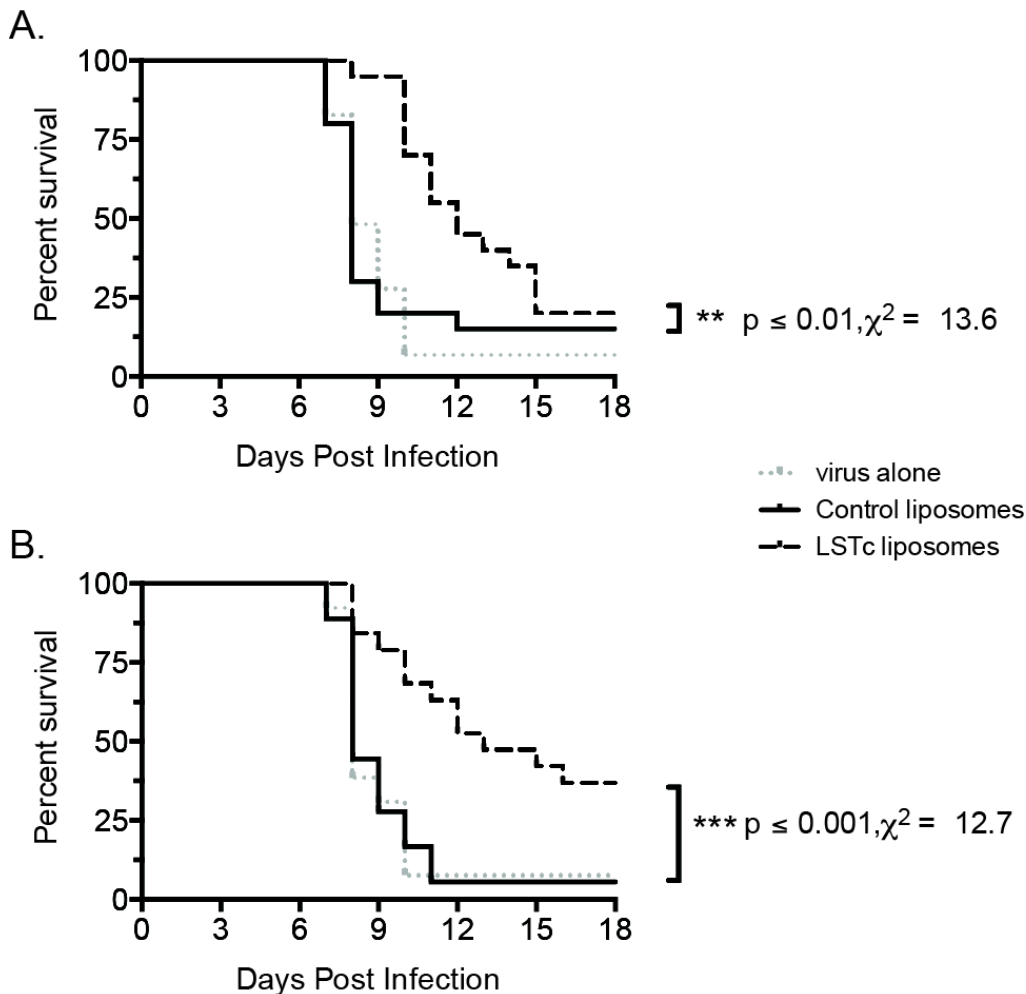


Figure 3.9 LSTc decoy liposomes extend survival after lethal influenza A virus challenge.

1,000 PFU of PR/8 was incubated with control liposomes or LSTc-containing decoy liposomes with **(A)** 7.5 mol% LSTc or **(B)** 15 mol% LSTc at 37°C for 30 min, then used for intratracheal infection of C57BL/6 mice. Mice were monitored daily for survival. **A.** Mice that received LSTc decoy liposomes and PR/8 (**dashed black line**) had a 33% increase of mean survival time post-infection as compared with mice that received control liposomes and PR/8 (**solid black line**) or PR/8 alone (**gray dotted line**). The LSTc decoy liposome and PR/8-treated mice survival advantage was statistically significant ($\chi^2 = 13.6, p \leq 0.01; n \leq 19$ for each strain). **B.** Mice that received decoy liposomes with 15 mol% LSTc had a significant 38.5% time to death increase and was statistically significant ($\chi^2 = 12.7, p \leq 0.001; n \geq 18$) as compared to mice that received control liposomes. Data shown are combined from three independent experiments, each having similar results.

1,000 PFU of PR/8 alone (Figure 3.9C, median survival of 8 days for both groups, Log Rank test, $\chi^2 = 2.3$, $p = 0.13$). Mice that received 15 mol% LSTc decoy liposomes and 1,000 PFU of PR/8 had significantly longer survival times, with median survival of 13 days, a 38.5% mean increase over control liposomes and PR/8 (Log Rank test, $\chi^2 = 12.7$, $p \leq 0.001$), a day longer than 7.5 mol% LSTc decoy liposomes (not a significant increase, Log Rank test, $\chi^2 = 0.7$, $p = 0.4$). The overall molarity of SA in the decoy liposome dose was 170 μM SA, the same as amount as 7.5 mol% LSTc liposomes above. The survival trend and median survival time were reproducible over several experiments; the data presented here are the sum of 3 experiments, with combined numbers listed. These data are consistent with the co-incubation data showing 7.5 mol LSTc decoy liposomes increase survival and further support the hypothesis that decoy liposomes make long-lasting interactions that neutralize virus in the physiological setting of an infected lung.

IAV titers were not significantly different three days post-infection between mice that received co-incubated control liposomes and virus and mice that received co-incubated LSTc decoy liposomes and virus or mice that received virus alone (Figure 3.10A). In addition, lung IL-1 β levels were also not significantly different three days post-infection between all three treatment groups (Figure 3.10B). These data sample only a small window of the overall infection, and therefore form an incomplete picture of the viral and cytokine profile throughout infection. Additional time points would be required for a full understanding of the viral load and cytokine in control and decoy liposome treated mice, and additional cytokine screening would be required for a complete picture of the pulmonary cytokine milieu.

Figure 3.10 Mice that received LSTc decoy liposomes do not have altered viral titers or IL-1 β levels four days post influenza A virus infection.

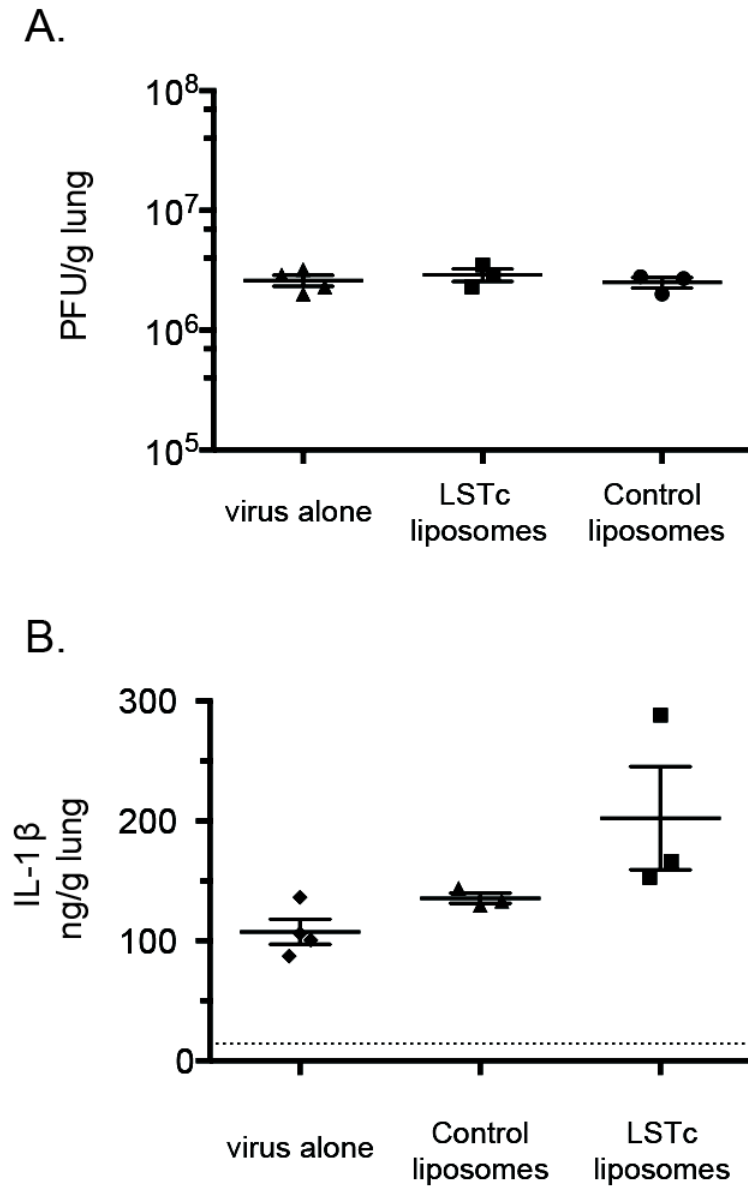


Figure 3.10 Mice that received LSTc decoy liposomes do not have altered viral titers or IL-1 β levels four days post influenza A virus infection.

350 PFU of PR/8 was incubated with control or LSTc-containing decoy liposomes at 37 °C for 30 min, and used for intratracheal infection of C57BL/6 mice. Mice from each treatment (n=3) were sacrificed 4 days post-infection; lungs were removed and tested for viral titers (**A**) and IL-1 β cytokine levels (**B**). Mice that received LSTc decoy liposomes and PR/8 did not have significantly different viral titers or IL-1 β as compared to mice that received control liposomes and PR/8 or virus alone.

Decoy liposomes are not effective as therapeutics or prophylactics for Influenza

A virus infection

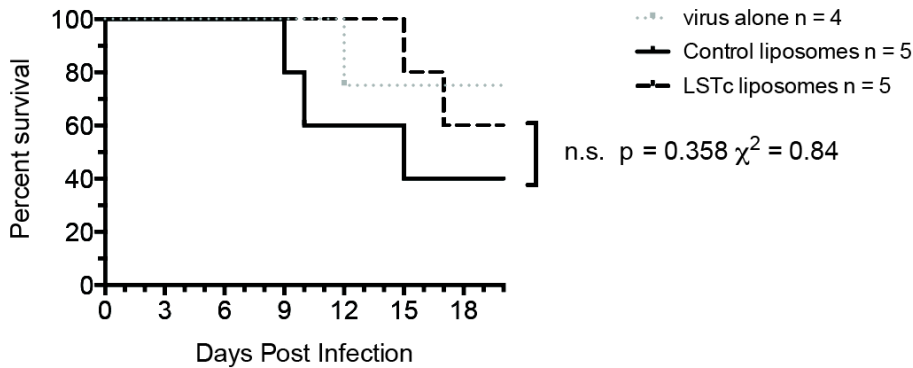
To extend the co-incubated survival data above, I treated mice with decoy liposomes in a more clinically relevant setting, either before or after PR/8 IAV infection.

Therapeutically treated mice were infected with 350 PFU of PR/8 IAV, rested for thirty minutes, and then treated with either 170 μ M SA LSTc-containing decoy liposomes or an equivalent amount of control liposomes. Mice were monitored daily for weight loss and survival. The median survival for control liposomes-treated mice was 15 days, and undefined for decoy liposomes treated mice. Decoy liposome-treated mice had 60% survival at the end of the experiment, thus median survival was undefined. The time-to-death for the decoy liposome-treated mice was not statistically significant from control liposome-treated mice (Figure 3.11A, Log Rank test, $\chi^2 = 0.84$, $p = 0.36$), but because of the small number of mice used with this protocol, it is possible increased group sizes would give more statistical power.

To test the liposomes' efficacy as a prophylactic, I administered decoy liposomes containing 7.5 mol% LSTc to mice one hour before challenging them with 1,000 PFU of PR/8. When co-incubated, this dose of SA is protective against this dose of PR/8, but it was no longer protective prophylactically (Figure 3.11B). Mice given either control liposomes or decoy liposomes before infection had mean survival times of nine or ten days (Log Rank test, $\chi^2 = 2.3$, $p = 0.13$). These data demonstrate that the decoy liposomes can make and maintain long-lasting interactions with its target virus when co-incubated in a relatively small volume, but when introduced into an organ with large surface area as the lung, an effective dose for prophylactic or therapeutic treatment must be higher than tested here.

Figure 3.11 Therapeutic or prophylactic treatment of infected mice with LSTc decoy liposomes is not protective.

A.



B.

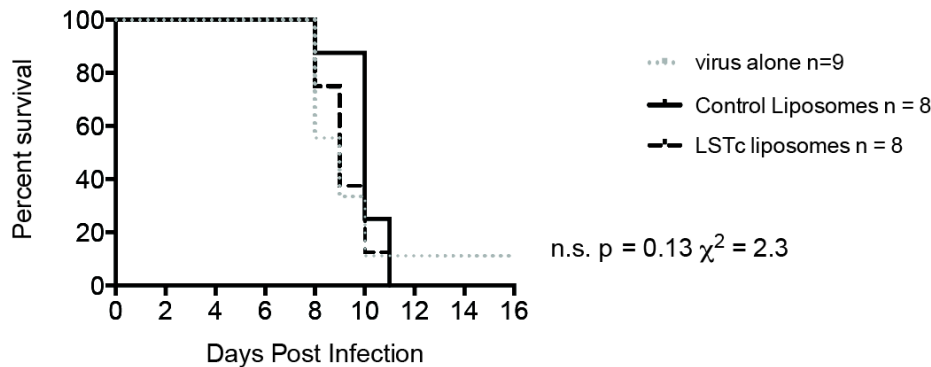


Figure 3.11 Therapeutic or prophylactic treatment of infected mice with LSTc decoy liposomes is not protective.

C57BL/6 mice were treated with control of LSTc-containing decoy liposomes after (A) or before (B) intratracheal PR/8 infection and were monitored daily for survival. **A**, Therapeutic treatment: mice were infected with 350 PFU of PR/8 by intratracheal the route, rested for 30 minutes and then treated with 170 μ M SA LSTc-containing decoy liposomes (**dashed black lines**), an equivalent amount of control liposomes (**solid black line**) or a mock saline treatment (virus alone, **grey dotted line**). Mice that received LSTc decoy liposomes infection had a slight, but not statistically significant increase of mean survival time as compared with mice that received control liposomes and PR/8 or PR/8 alone. **B**, Prophylactic treatment: mice were treated with 170 μ M SA LSTc-containing decoy liposomes, an equivalent amount of control liposomes or a mock saline treatment, rested for 1 h and then infected with 1,000 PFU of PR/8 by intratracheal the route. Mice that received decoy liposomes before infection had no change in survival times as compared to mice that received control liposomes or mock infection (B). Data shown are from one experiment.

Use of sialic acid containing decoy liposomes to prevent influenza A virus infection

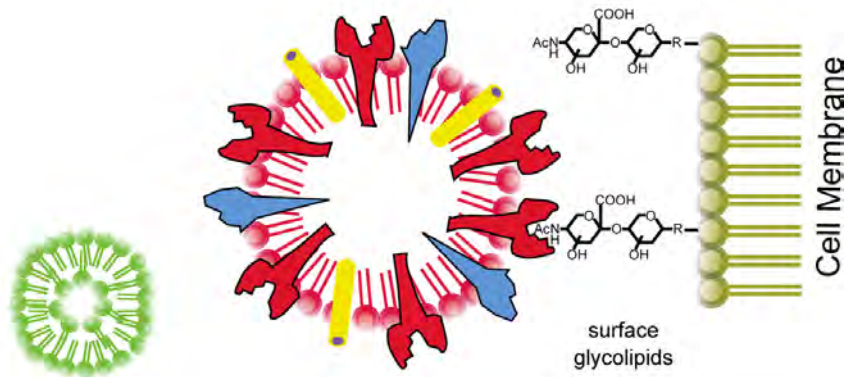
Discussion

Decoy receptors have the potential to attenuate infections by diverting the pathogen away from susceptible tissues (Asher, Cerny et al. 2005). Pathogen receptor mimics are especially suited for use as decoys, because the target virus is unlikely to develop resistance through mutation. Viruses require binding specificity and avidity to replicate efficiently and transmit between hosts. My approach uses liposomes to create a modifiable platform of synthetic decoy receptors that can form multivalent bonds with multiple strains of IAV that results in viral neutralization (Figure 3.12). In order for a treatment to neutralize it must either block a required enzymatic function, such as IAV's neuraminidase or M2 ion channel, or stimulate the immune system to block viral replication, such as the yearly vaccine. The LSTc decoy liposomes described here fall into the former category, and act by binding the flu's HA receptor on the receptor-binding site blocking its normal function of binding to cell surface-associated SA. Furthermore, the decoy liposomes are multivalent and can theoretically create immuno-complexes of many bound virions and liposomes. Viruses bound in large complexes would be non-infectious and more likely to be phagocytosed by leukocytes.

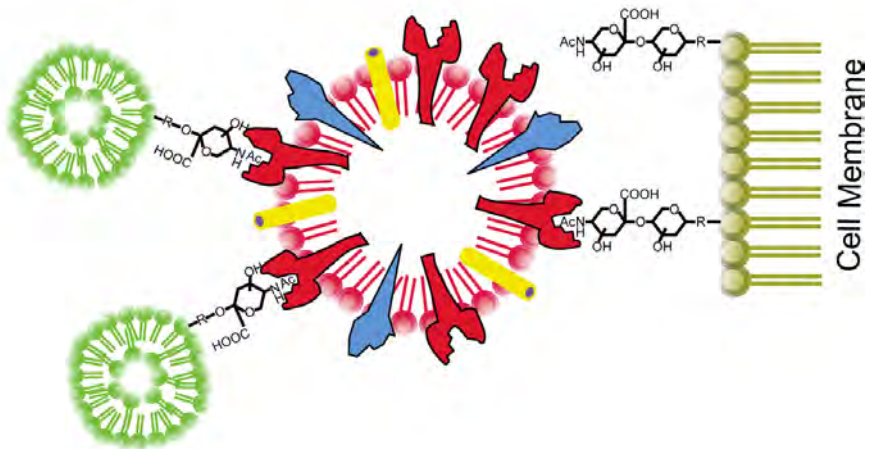
Previous research has shown that SA-bearing receptor molecules can bind and inhibit IAV strains (Pritchett, Brossmer et al. 1987). Indeed, many different sialosides containing a single SA residue can inhibit IAV hemagglutination (Pritchett, Brossmer et al. 1987; Sauter, Bednarski et al. 1989; Toogood, Galliker et al. 1991; Weinhold and Knowles 1992; Sparks, Williams et al. 1993). Because IAV HA forms polyvalent interactions with the host cell, these mono-sialosides have relatively weak inhibitory properties, the strongest having an IC_{50} of 3.7

Figure 3.12 Summary: LSTc-containing decoy liposomes inhibit influenza A virus binding and infection.

A



B



C

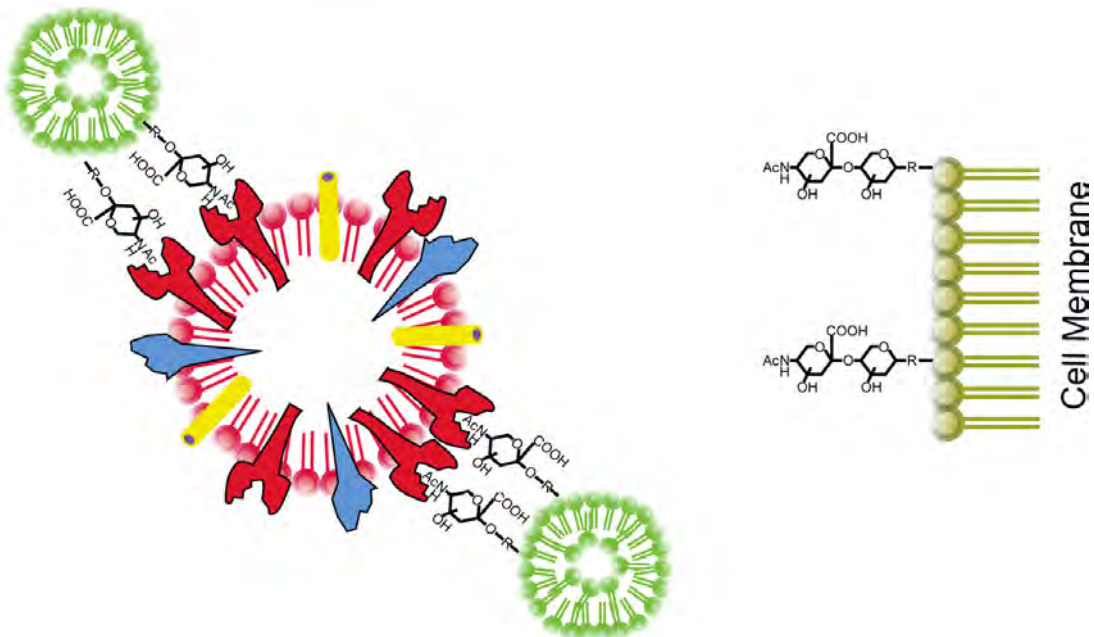


Figure 3.12 Summary: LSTc-containing decoy liposomes inhibit influenza A virus binding and infection.

A, IAV infects host cells by first attaching to α 2-6 terminally linked SA. Control liposomes that do not contain LSTc do not inhibit IAV adhesion or infection. **B**, decoy liposomes with limited amounts of LSTc on their surfaces do not form highly multivalent interactions with IAV and only partially inhibit binding to host cells. **C**, decoy liposomes with 5 mol% or more LSTc on the surface are capable of competitively binding multiple strains of IAV, thereby preventing binding and infection of host cells.

μM (Weinhold and Knowles 1992). To take advantage of the multivalent nature of HA binding, several groups created polymer-based sialosides, which are more potent inhibitors of RBC hemagglutination (Glick, Toogood et al. 1991; Spaltenstein and Whitesides 1991; Lees, Spaltenstein et al. 1994; Mammen, Dahmann et al. 1995; Kiessling and Pohl 1996). While the IC_{50} concentrations for HAI were significantly improved, the evidence that polymerized sialosides are capable of inhibiting infectivity is not particularly compelling (Spevak, Nagy et al. 1993; Itoh, Hetterich et al. 1995; Reuter, Myc et al. 1999). Gamian *et al.* (1991) were unable to block H3N2 IAV infection of embryonated chicken eggs with polyvalent SA glycoconjugates or their monovalent parental building blocks. Mochalova *et al.* (1994) and Tuzikov *et al.* (2000) were able to prevent some IAV strains from infecting MDCK cells, but the doses required to block infection were significantly higher than those required to block RBC hemagglutination. In contrast, our decoy liposomes inhibited infectivity at similar concentrations as they inhibited hemagglutination. One important distinction between decoy liposomes and polymer-based sialosides is their potential toxicity when used *in vivo*. The decoy liposomes are constructed with derivatives of lipids found in the human body, such as phosphatidylcholine, and the entire liposome structure is non-toxic, whereas some polymer-based sialosides can cause cell death at high doses.

Decoy liposomes are highly adaptable and can be modified with many components while retaining their anti-viral inhibitory properties. Therefore, our collaborators and I used DOPC along with LSTc-DOPE glycolipid, to create multivalent, polymer-like decoy liposomes. DOPC is an ideal liposome lipid backbone because of its neutral charge and low melting temperature that makes the lipid membrane fluid at body temperature. The liposome platform is highly flexible (described in detail in the next chapter), and it accommodates various modification

including changes to the ratio of different lipid components used or addition of a lipid-conjugated fluorophore for tracking. The lipid acyl chain length and double bond give the lipids a low melting temperature so that at body temperature the lipid bilayer will be fluid, allowing for efficient movement of the LSTc glycan through the liposome surface as a means of increasing the multivalency of HA-LSTc interactions. The lipids used to create our decoy liposomes should be versatile inhibitors and as I have described here, where other decoy liposome formulations have fallen short.

These LSTc-containing decoy liposomes competitively bound to both H1N1 and H3N2 subtypes of IAV (Table 3.1 and Table 3.2), while control liposomes lacking LSTc did not. Increasing the percentage of LSTc displayed on the surface of our decoy liposomes increased the HAI titer against IAV. I also tested monovalent LSTc, the building block used to create our decoy liposomes. Monovalent LSTc did not inhibit hemagglutination, even when tested at concentrations well in excess of the estimated molarity of LSTc incorporated into decoy liposomes. Monovalent SA analogs have dissociation constants for HA of approximately 2 mM SA (Pritchett, Brossmer et al. 1987; Sauter, Bednarski et al. 1989; Glick, Toogood et al. 1991). I tested monovalent LSTc at 5 mM and saw no inhibition of IAV. These data suggest that our decoy liposomes act as multivalent, polymer-like decoys; based on the IC_{90} concentrations need to inhibit hemagglutination. Polymer sialosides IC_{90} values are in the micro to nanomolar range, and the 7.5 mol% LSTc decoy liposomes inhibited IAV in the same overall range, from 1 μ M SA for Philippines IAV, down to less than 50 nM SA for PR/8 IAV (Table 3.2). Based on these data alone, the decoy liposome platform appears to be a promising non-toxic alternative to the cytotoxic sialoside polymers. Furthermore, the interaction was virus-specific, as high

concentrations of LSTc decoy liposomes did not competitively bind to SeV (Table 3.2), while clearly capable of inhibiting IAV.

The HAI results suggest that the hypothesized method of action is correct, that the decoy liposomes bind directly to HA and prevent RBC agglutination. This is supported by the literature showing that the SA-containing glycans LSTc and LSTa bind to multiple subtypes of HA (Ha, Stevens et al. 2001; Russell, Stevens et al. 2006; Lin, Xiong et al. 2012). I confirmed that this HA-LSTc interaction is direct using fluorescently labeled decoy liposomes and IAV covalently modified with Alexa Fluor 647. Only LSTc-containing decoy liposomes, but not control liposomes, bound to fluorescently labeled IAV (Figure 3.2). The size of the fluorescent punctate staining suggests that many decoy liposomes have bound to a number of IAV virions, forming a larger complex. Additionally, electron micrographs of PR/8 bound to LSTc decoy liposomes also support the possibility of complex formation (Dr. James Comolli, personal communications).

Alexa Fluor labeled virus can also be used to track viral binding to target cells. Here I present data with the human lung epithelial cell line, A549, an IAV permissive cell with predominantly α 2-6 linked SA. When WSN HA-647 was mixed with control liposomes, strong binding to A549 cells was observed, whereas less binding was observed when virus was mixed with LSTc-containing decoy liposomes (Figure 3.4). These data demonstrate that the LSTc-containing decoy liposomes bind directly to the IAV virion, and that this binding prevents adhesion to sialylated cells.

Building on the binding data above, I used the permissive A549 cells to examine whether decoy liposomes can also bind to IAV budding from a human cell. All of the IAV strains tested so far were passaged through either chicken eggs or canine MDCK cells, and therefore binding

virus coming from A549 cells demonstrates that there is no human-specific post translational modification that prevents decoy liposome action. Indeed, LSTc-containing decoy liposomes bound to A549 cells infected with PR/8 for 18 hours, but they did not bind to uninfected cells. Control liposomes did not bind to either infected or uninfected cells (Figure 3.3 and data not shown). These data establish that our decoy liposomes can bind to not only intact virions, but also to budding and cell-associated HA. This experiment cannot determine the fate or infectivity of the surface-associated virus bound to decoy liposomes, but it is possible that decoy liposomes bound to an infected cell surface may trap newly released virus and form larger immunogenic complexes at a site of infection.

The ability of LSTc decoy liposomes to bind to IAV, as observed data above, also protected cells from infection with multiple strains of H1N1 and H3N2 IAV (Figure 3.5). The degree of binding and inhibition of infectivity was also dependent on the percentage of functionalized LSTc lipids incorporated into decoy liposomes. Decoy liposomes with only 1 mol% of their surfaces functionalized with LSTc did not block hemagglutination and blocked only a small fraction of infectious virus. Increasing the mole percent of LSTc increased HAI and reduced infectivity. Decoy liposomes with 7.5 mol% LSTc inhibited IAV most efficiently; they significantly decreased infectivity at the lowest tested concentrations of LSTc, inhibiting PR/8 at an effective concentration of 10 nM SA. All other series of LSTc decoy liposomes did not significantly inhibit IAV at this concentration. In contrast, the monovalent form of LSTc did not inhibit either PR/8 or Philipines when tested at equimolar (data not shown) or at far higher concentrations of LSTc incorporated into decoy liposomes (Figure 3.5). The inability of monovalent LSTc to inhibit IAV agrees with published data that show other monovalent SA analogs, while able to block hemagglutination, they are incapable of inhibiting IAV infectivity

(Gamian, Chomik et al. 1991; Mochalova, Tuzikov et al. 1994; Tuzikov, Gambaryan et al. 2000). LSTc incorporated into our decoy liposomes can make polymer-like, multivalent interactions with influenza virus due to the increased efficacy of the liposomes compared to monovalent LSTc.

The LSTc-containing decoy liposomes are specific for IAV. I tested decoy liposomes containing 7.5 mol% LSTc against multiple strains of IAV, and show that they are capable of binding and inhibiting not just the H1N1 PR/8, but also the Beijing, H3N2 Philippines, and X-31 strains (Table 3.2 and Figure 3.5B). They do not, however, inhibit either SeV hemagglutination (Table 3.2) or RSV infectivity (Figure 3.5B). Control liposomes with DOPG lipid in place of LSTc glycolipids did not inhibit any of the viruses tested. Furthermore, lack of infectivity is not a result of toxicity; neither control nor LSTc-containing decoy liposomes caused any cytotoxicity *in vitro* (Figure 3.6A) or gross toxicity *in vivo* (Figure 3.6B), demonstrating that the reduction in infectivity is probably a result of viral neutralization. Inhibition of IAV is thus specific for the binding of HA to α 2-6 linked SA, and is not a non-specific adhesion mediated by some other interaction.

While each of the IAV strains tested was inhibited by LSTc decoy liposomes, the degree of inhibition for each IAV strain varied considerably. Each of the four strains tested is a conventional research strain propagated in chicken eggs. PR/8, which exhibited the greatest degree of inhibition (see Table 3.2), is a commonly used H1N1 strain that has been extensively passaged in MDCK cell culture, and is adapted to growth in mice. The extensive MDCK cell culture suggests that may have a small live-to-dead virion ratio, where less virus particles are defective than other strains. Preliminary particle counts suggest this hypothesis (Dr. James Comolli, personal communications). X31 and Philippines are each mouse-adapted reassortant

strains. Beijing 262/95 is a relatively recent human clinical isolate that resembles modern H1N1 variants that emerged after 1994 (McDonald, Smith et al. 2007) and has undergone relatively little selection in the laboratory. One might expect that the Beijing human isolate would be most greatly inhibited by LSTc decoy liposomes given its adaptation to the human airway, which has a high prevalence of α 2-6 linked SA (Ibricevic, Pekosz et al. 2006). However, the Beijing strain, like the other viruses used in this study, was expanded in chicken eggs, which may have allowed for the selection of virions that favor binding to α 2-3 linked SA. Human RBC and MDCK cells, which were used in binding and infectivity assays, respectively, display a combination of α 2-6 and α 2-3 linked SAs. The affinity between virus and host, either in the presence or absence of decoy liposomes, is influenced by the virion's preferential binding to host α 2-3 linked SA. Of note, the antigenic subtype did not appear to predispose viruses to greater or lesser susceptibility to LSTc decoy liposomes.

While the decoy liposomes can inhibit IAV infectivity, the amount of virus tested above is much smaller than the amount of virus that would be present in an actual infection. To test the decoy liposome's ability to inhibit viral spread of larger amounts of virus, I used a serum-free system to allow continued replication in the presence or absence of LSTc-containing liposomes. Decoy liposomes, but not control liposomes, inhibited viral replication (Figure 3.8). The ability of LSTc decoy liposomes to inhibit viral replication in this system shows that they can block not only the initial infection event, but will remain active for days at body temperature and block progeny virus from re-infecting new target cells. The amount of IAV in this experiment is also much higher than in the initial infection studies (Figure 3.5), and here the LSTc decoy liposomes reduced the infectious titers by more than two logs, demonstrating significant efficacy against large amounts of virus.

MDCK cells are widely used in IAV studies because they are permissive to IAV infection and propagation, and allow for analysis of viral binding, infection, and viral growth kinetics. MDCK cells express both α 2-6 and α 2-3 linked SA, which presents a higher bar for inhibition with the LSTc decoy liposomes, which only prevent IAV from binding α 2-6 linked SA. Here, I have further demonstrated that the inhibition by LSTc decoy liposomes seen in MDCK cells is also true in a human respiratory epithelial cell line (A549 cells) as well as *in vivo* in mice.

In addition to binding IAV and protecting cells from infection, our decoy liposomes also extended survival of mice challenged with a lethal dose of IAV (Figure 3.9). Mice had significantly longer survival times when infected with a LD₉₀ of IAV pre-incubated with LSTc decoy liposomes than mice infected with the LD₉₀ pre-incubated with control liposomes. Mice that received decoy liposomes with 15 mol% LSTc and IAV also had significantly longer survival times than co-incubated virus and control liposomes (Figure 3.9B).

When used for more clinically relevant prophylactic or therapeutic treatment of IAV-infected mice, the decoy liposomes were not protective. Therapeutically treated mice first infected with PR/8 thirty minutes before being given LSTc decoy liposomes had the same time-to-death as infected mice that received control liposomes (Figure 3.11A). Likewise, dosing mice with LSTc decoy liposomes before a lethal PR/8 infection did not reduce mortality (Figure 3.11B). Taken together, these data suggest that the dose of decoy liposomes that extended survival when co-incubated with IAV, 170 μ M SA, was insufficient when given before or after infection. It is possible that a higher dose of decoy liposomes would be protective, but this has not been possible due to technical limitations, resulting in a lack of sufficient quantities of decoy liposomes from our collaborators. The average airway surface area of an adult mouse is approximately 600 cm², an area considerably larger than the volume of co-incubated virus and

decoy liposomes (0.3 cm^2). When given alone, the decoy liposomes would be diluted throughout the lung, greatly reducing their local concentration. The co-incubation data suggests that the initial dosage would need to be increased by at least 3 logs to be effective. However, these data demonstrate that when co-incubated, LSTc decoy liposomes are capable of maintaining long-lasting interactions with IAV while in the hostile environment of the respiratory tract. Both an overall negative charge and a surface glycan enable liposomes to persist in the lungs (Deol and Khuller 1997), and our decoy liposomes contain both. While co-incubating decoy liposomes with virus does not reflect a typical therapeutic delivery system, these mouse experiments demonstrate a proof-of-concept that LSTc decoy liposomes remain active and inhibitory *in vivo*. The extended survival of these mice suggests that the IAV binding and neutralization observed *in vitro* also occurs *in vivo*.

In this chapter I have shown that decoy liposomes containing LSTc have higher avidity for IAV than monovalent LSTc alone. Decoy liposomes bind directly to IAV virions and bound IAV cannot attach to SA-bearing epithelial cells. Furthermore, virus bound to decoy liposomes are not infectious. This block is virus-specific, and decoy liposomes specifically block IAV, but not other respiratory viruses that do not bind to α 2-6 linked SA. LSTc-containing decoy liposomes can also block subsequent rounds of viral infection *in vitro*. When co-incubated with virus, decoy liposomes maintain long-lasting association with virus *in vivo*, significantly extending survival times of mice given decoys and a lethal dose of IAV. These results show that the decoy receptor liposome platform is a valid method for combating IAV, and that the platform can be modified to combat other pathogens with defined host receptors.

Chapter IV

Optimizing the anti-influenza A virus liposome platform

Introduction

In the previous chapter, I described the use of novel, LSTc-bearing decoy liposomes as a potential IAV therapeutic. In this chapter I will discuss how various modifications to the decoy liposomes provided a better understanding of the properties required for inhibition. I also will describe changes I made to the decoy glycolipid and their inhibitory effect on IAV. Our liposome modifications demonstrate that a highly fluid, low curvature liposome is required to achieve efficient inhibition. This inhibition is most likely dependent on the movement of SA glycolipids along the liposome surface, so that they can form multivalent interactions with IAV virions that increase the overall binding strength, decrease the dissociation rate and prevent the virus from binding and infecting a target cell.

Optimizing the anti-influenza A virus liposome platform

Results

Large, low curvature decoy liposomes are more efficient at inhibiting IAV

The initial liposomes tested were formed by extrusion through a 20 nm pore (see Materials and Methods), resulting in liposomes with an average radius of 31.6 ± 1 nm. Previous studies have shown that larger liposomes have less surface curvature and less line tension, which is the energy between two lipid domains. Liposomes with less line tension have less structured lipid micro-domains and more lipid mobility (Baumgart, Hess et al. 2003). Decoy liposomes with more lipid fluidity, and therefore more LSTc mobility, theoretically should be more effective. To increase the decoy liposome fluidity our collaborators increased the liposome size by using a larger lipid extrusion pore. Using a 200 nm pore extruder, our collaborators increased the average liposome radius to 56.8 ± 3.5 nm. To limit generation of multilamellar bodies, lipid bilayers within a larger liposome, extruder pores larger than 200 nm were not tested. Multilamellar decoy liposomes would have internal LSTc-DOPE and would result in available LSTc presented at the surface.

To determine the effect of liposome size on IAV infectivity, I co-incubated PR/8 with control or 7.5 mol% LSTc-containing decoy liposomes extruded through either a 20 nm or 200 nm extrusion pore before infecting MDCK cell monolayers. Increasing liposome size increased the inhibition of LSTc decoy liposomes (Figure 4.1). At the lowest concentration tested, 1 nM SA, 20 nm extruded LSTc liposomes did not inhibit PR/8 ($120 \pm 3.4\%$ infectivity of controls), but 200 nm extruded LSTc liposomes significantly inhibited PR/8 $53.1 \pm 3.1\%$ ($p \leq 0.01$). The difference between these decoy liposomes was greatest at low concentrations of SA; the

Figure 4.1 Larger decoy liposomes with less surface curvature are more efficient at inhibiting influenza A virus.

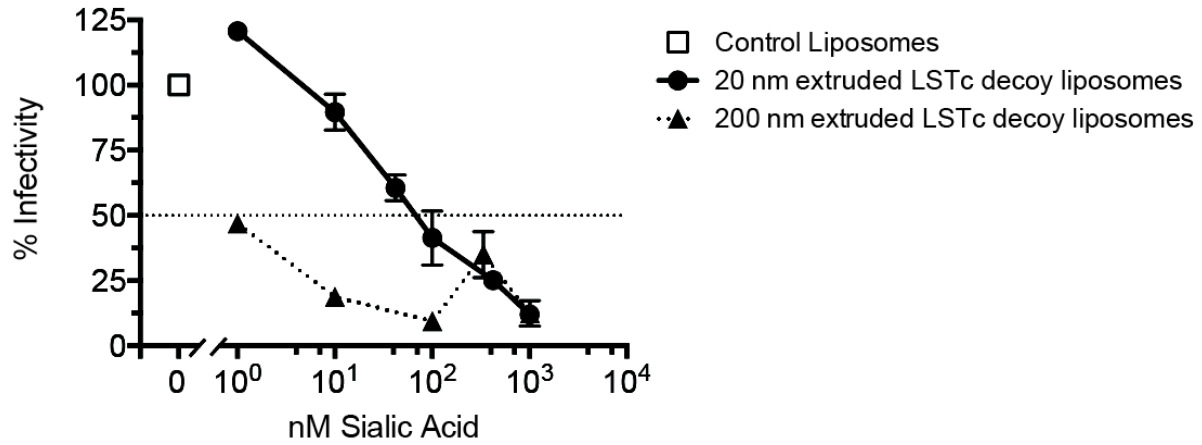


Figure 4.1 Larger decoy liposomes with less surface curvature are more efficient at inhibiting influenza A virus.

PR/8 (30 PFU/well) was incubated with control liposomes, 20 nm pore extruded or 200 nm pore extruded LSTc-containing decoy liposomes before the addition to MDCK cells. Plaques per well of virus treated with control liposomes (0 mol% LSTc) are defined as 100% infectivity (**open squares**). Decoy liposomes with 7.5 mol% LSTc extruded through a 200 nm pore filter (**dotted triangles**) significantly inhibited PR/8 more than decoy liposomes extruded a 20 nm pore filter (**circles**). The data represent the average \pm S.E. of two experiments.

inhibitory advantage of 200 nm pore extruded liposomes diminished as the concentration of SA increased. At high concentrations of SA, both 20 and 200 nm extruded LSTc liposomes inhibited PR/8 to the same extent, approximately 70% inhibition at 300 nM SA and greater than 87% inhibition at 1,000 nM SA. These data suggest that larger decoy liposomes with less curvature can make more interactions with IAV per liposome and therefore block infectivity more efficiently.

Osmotic crushing slightly improves the efficacy of LSTc decoy liposomes

In addition to changing the liposome curvature by increasing overall size, our collaborators altered their curvature by osmotic crushing. Osmotic crushing results in truncated, "squashed" sphere liposomes (Figure 4.2A) that have a high curvature equator region and flattened, lower curvature polar regions (Foo, Chan et al. 2003). As seen with the larger liposomes, lower curvature may increase their LSTc glycolipid mobility and therefore the decoy's efficacy. LSTc decoy liposomes were created with the same protocol described previously, but extruded into 15 mM PBS, instead of 150 mM PBS. Immediately before each infectivity experiment, I diluted liposomes to the desired SA concentration in 150 mM PBS, causing osmotic outflow from the liposome interior and crushing into truncated sphere liposomes. I tested the effect of crushing on IAV infectivity as described above, with co-incubation of control and LSTc decoy liposomes with PR/8 IAV. Osmotically crushed LSTc decoy liposomes had a slight, but significant increased efficacy against PR/8 infectivity (Figure 4.2B). At the highest concentration tested, 100 nM SA, crushed liposomes inhibited $61.1 \pm 1.7\%$ of PR/8 as compared to $37 \pm 9.5\%$ ($p \leq 0.05$). The increase was modest, about 1.5 fold, suggesting that either the degree of crushing achieved was small or that areas of high curvature (the equator region) created micro-domains

Figure 4.2 Osmotic crushing does not significantly affect influenza A virus inhibition.

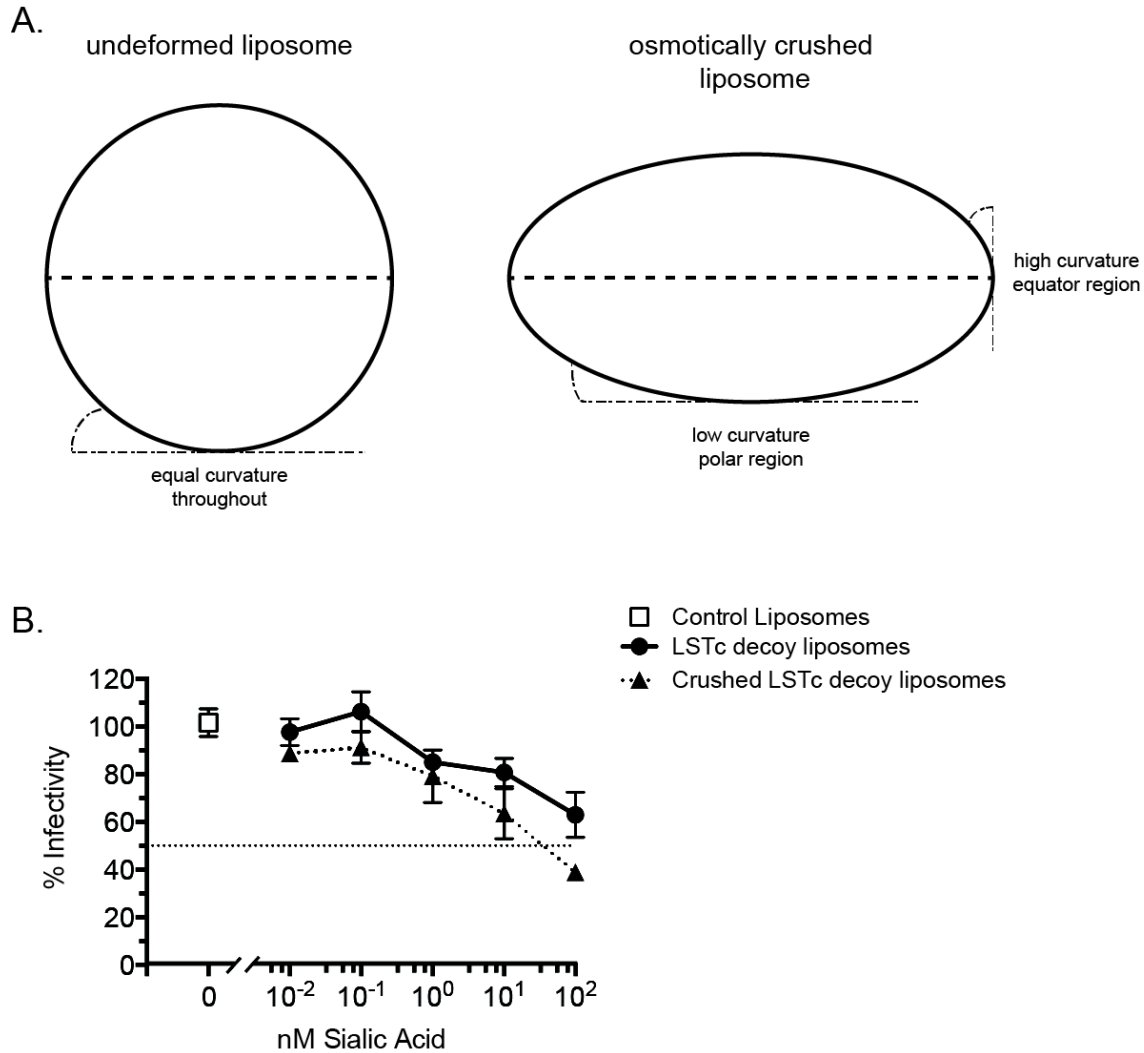


Figure 4.2 Osmotic crushing does not significantly affect influenza A virus inhibition.

(A) Schematic representation of undeformed, spherical liposomes (left) that have equal curvature throughout the sphere and osmotically crushed (right) liposomes that have an equator region (**dotted line**) with high curvature and two low curvature polar regions. (B) PR/8 (30 PFU/well) was incubated with control liposomes, LSTc-containing decoy liposomes and osmotically crushed LSTc-containing decoy liposomes before the addition to MDCK cells. Plaques per well of virus treated with control liposomes (0 mol% LSTc) are defined as 100% infectivity (**open square**). Osmotically crushed decoy liposomes (**dotted triangles**) inhibited PR/8 infectivity slightly better than spherical decoy liposomes (**circles**). The data represent the average \pm S.E. of two experiments. Figure 4.2 Increasing fluidity of the decoy liposome's surface increases efficacy.

that limited LSTc mobility across the liposome. I did not perform direct, electron microscopy measurement of liposome crushing.

Increasing the fluidity of the liposome lipid bilayer increases efficacy of LSTc decoy liposomes

Inclusion of cholesterol into a lipid bilayer has a two-fold effect on lipid fluidity. In rigid, gelled bilayers, cholesterol interferes with the packing of hydrophobic tails and increases the lipid diffusion coefficient. In highly fluid bilayers, cholesterol increases the mechanical rigidity and decreases the diffusion coefficient by reducing the free space between the lipid tails (Rubenstein, Smith et al. 1979). In order to test the impact of cholesterol on our decoy liposomes, our collaborators incorporated 30 mol% cholesterol during liposome construction and tested the impact on IAV infectivity, as described above. At 1 or 10 nM SA, decoy liposomes with 7.5 mol% LSTc and 30 mol% cholesterol inhibited PR/8 infectivity significantly better than decoy liposomes with no cholesterol (Figure 4.3); 62% vs no inhibition ($120 \pm 3.4\%$ of control, $p \leq 0.001$) at 1 nM SA and $60.3 \pm 1.7\%$ vs $10.3 \pm 6.9\%$ ($p \leq 0.05$) inhibition at 10 nM SA. At these low SA concentrations of decoy liposomes, the addition of cholesterol increased inhibition by 68%. At 100 nM SA, decoy liposomes with cholesterol inhibited PR/8 slightly better than decoy liposomes without cholesterol, but it was not significant ($58.6 \pm 10.3\%$ vs $77.6 \pm 1.7\%$ infectivity $p = 0.21$). And at the highest concentration tested, 1,000 nM SA, decoy liposomes with and without cholesterol inhibited PR/8 infectivity to similar levels, both greater than 87%. Control liposomes with 30 mol% cholesterol did not affect PR/8 infectivity. These data demonstrate that cholesterol affects the decoy liposome inhibitory properties, most likely by

Figure 4.3 Increasing fluidity of the decoy liposome's surface increases efficacy.

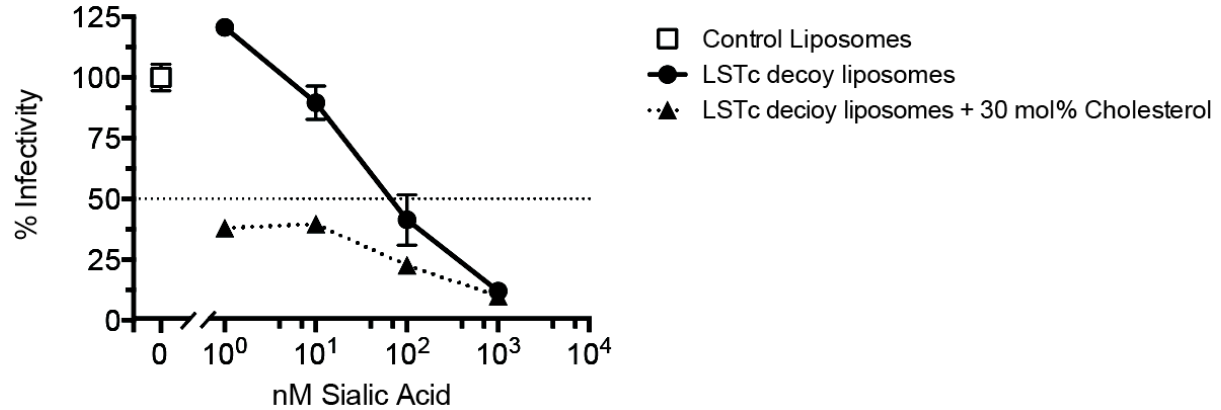


Figure 4.3 Increasing fluidity of the decoy liposome's surface increases efficacy.

PR/8 (30 PFU/well) was incubated with control liposomes, LSTc-containing decoy liposomes with and without 30 mol% cholesterol before addition to MDCK cells. Plaques per well of virus treated with control liposomes (0 mol% LSTc) are defined as 100% infectivity (**open square**). 7.5 mol% LSTc decoy liposomes with 30 mol% cholesterol (**dotted triangles**) significantly inhibited PR/8 infectivity more efficiently than decoy liposomes with 7.5 mol% LSTc without cholesterol (**circles**). The data represent the average \pm S.E. of two experiments.

improving the fluidity of the lipid bilayer, increasing the diffusion of the LSTc–DOPE glycolipid thereby increasing its bio-availability.

PEGylation of decoy liposomes abrogates their inhibitory properties

Incorporation of polyethylene glycol (PEG)-conjugated lipids into liposomes has been shown to extend blood circulation times and to decrease phagocytosis, increasing the *in vivo* half-life of the liposomes (Blume and Cevc 1993). Therefore, our collaborators constructed liposomes with 10 mol% PEG-1000–DOPE and 10 mol% less of the neutral lipid, DOPC. The addition of PEG did not have an effect on control liposome size or polydispersity index (PDI). LSTc-containing decoy liposomes with PEG were slightly smaller than control liposomes, but did not differ in their PDI measurements (data not shown). Although PEGylated, 7.5 mol% LSTc decoy liposomes did inhibit PR/8 infectivity, they inhibited significantly less than decoy liposomes without PEG at all concentrations tested, $23.5 \pm 1.4\%$ vs. $52.9 \pm 2.8\%$ (PEGylated decoy liposomes vs decoy liposomes, $p \leq 0.05$) of PR/8 infectivity at 1 nM SA and 60.8% vs. $98 \pm 1.4\%$ PR/8 ($p \leq 0.05$) at 1,000 nM SA (Figure 4.4). The addition of PEG-1000 into our decoy liposomes resulted in approximately a two-fold decrease of efficacy *in vitro*. This is most likely from steric interference between the PEG molecule and the LSTc glycan, effectively masking the LSTc glycan from HA. These data suggest that while PEGyled liposomes have longer *in vivo* half-life and therefore may be useful in a drug delivery context, but they are not suited for decoy receptor presentation on a liposome surface.

Figure 4.4 Addition of PEG reduces decoy liposome's inhibitory properties.

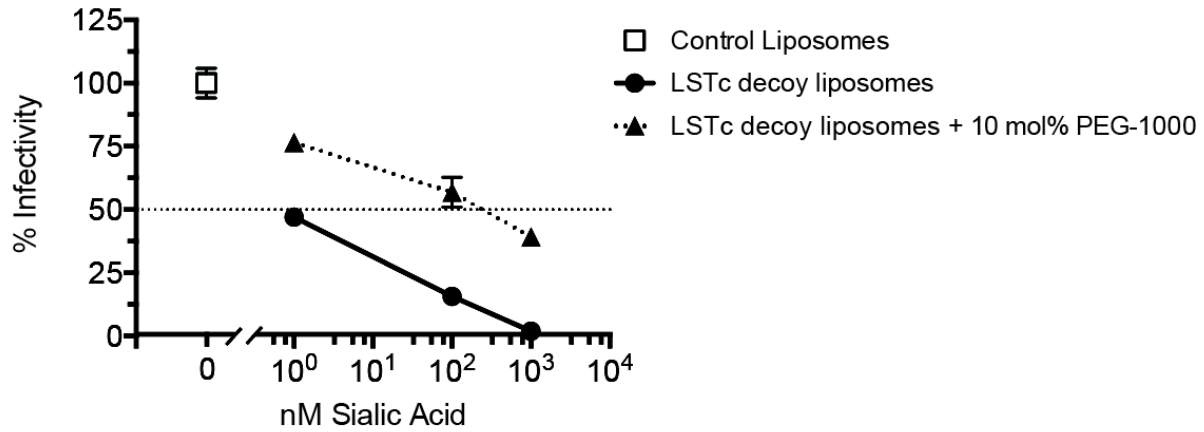


Figure 4.4 Addition of PEG reduces decoy liposome's inhibitory properties.

PR/8 (30 PFU/well) was incubated with control liposomes, LSTc decoy liposomes and LSTc decoy liposomes with PEG-1000 before the challenge on MDCK cells. Plaques per well of virus treated with control liposomes (0 mol% LSTc) are defined as 100% infectivity (**open square**). PEGylated decoy liposomes (**dotted triangles**) inhibited significantly less PR/8 infectivity than LSTc decoy liposomes with 7.5 mol% LSTc and no PEG (**circles**). The data represent one representative experiment that was repeated twice and presented as biological repeats \pm S.E.

Additional decoy liposome surface negative charge does not increase IAV inhibition

Surface charge, or zeta potential, is a major determinant of the interaction between two charged bodies in a microscopic environment, such as an invading virus and a susceptible epithelial cell. Viruses, which have relatively neutral zeta potentials, are attracted to negatively charged (with a significant portion of the charge coming from SA) cell surfaces (Hagenaars, Mastrobattista et al. 2009). To electrically attract IAV to the decoy liposomes, our collaborators increased the negative charge of the liposomes, either by incorporating additional negative lipid (DOPG) or negatively charged LSTc-DOPE and co-incubated them with PR/8 IAV before infecting MDCK cells (Figure 4.5). Control liposomes with either 7.5 or 15 mol% negative charge from DOPG lipid did not inhibit PR/8 infectivity. Increasing the negative charge to 15 mol% per decoy liposomes by either increasing the percentage of LSTc to 15 mol% (Figure 4.5) or by additional DOPG lipid (data not shown) did not significantly affect PR/8 infectivity as compared to decoy liposomes with 7.5 mol% negative charge. Inhibition of PR/8 infectivity was consistently better with 7.5 mol% negatively charge decoy liposomes, despite doubling the amount of LSTc glycolipids per liposome, at all concentrations tested, from 10 nM SA to 1,000 nM SA. These data demonstrate that increasing the negative charge of LSTc decoy liposomes does not increase PR/8 inhibition. The increase in negative charge may have been too small, or the additional negative charge may have created an unfavorable repulsion between the MDCK cells and the decoy liposomes.

Figure 4.5 Increasing negative charge of decoy liposomes does not affect influenza A virus inhibition.

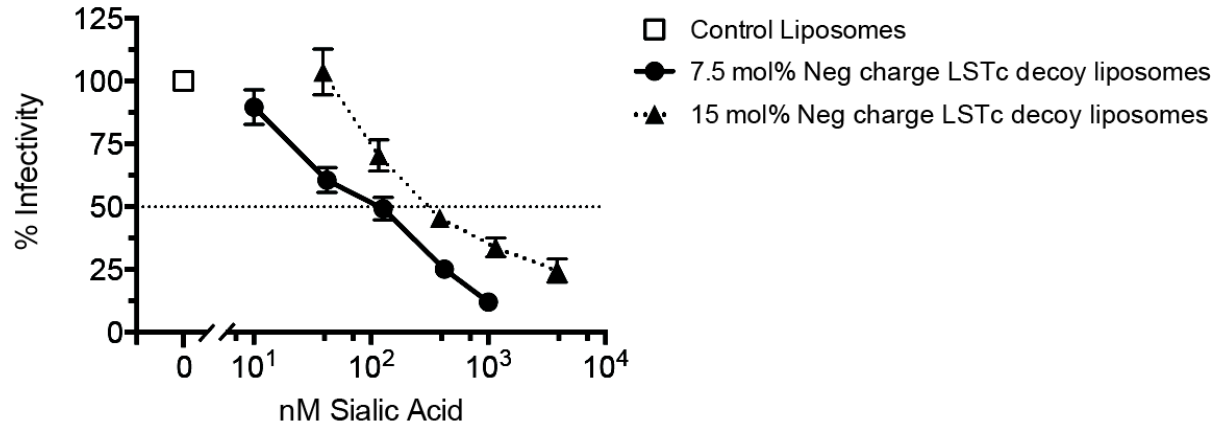


Figure 4.5 Increasing negative charge of decoy liposomes does not affect influenza A virus inhibition.

PR/8 (30 PFU/well) was incubated with control liposomes or LSTc-containing decoy with one of two negative charges before the addition to MDCK cells. Plaques per well of virus treated with control liposomes (0 mol% LSTc) are defined as 100% infectivity (**open square**). Decoy liposomes with 7.5 mol% negative charge and LSTc (**circles**) inhibited better than decoy liposomes with 15 mol% negative charge and LSTc (**dotted triangles**). The data represent the average \pm S.E. of three experiments.

Combining decoy liposomes and the NA inhibitor oseltamivir increases decoy liposome efficacy

One concern with decoy receptor therapy for IAV is that NA removes terminal SA, normally from infected cell surfaces, but potentially also in the form of decoy LSTc. Bacterial NA cleaves human LSTc in a crude preparation of breast milk (Martin-Sosa, Martin et al. 2003), and viral NA removes SA from purified monovalent LSTc *in vitro* when assayed by proton NMR (Kristina Prachanronarong and Celia Schiffer, personal communication). Therefore, to examine the effect of IAV NA on LSTc decoy liposomes binding and inhibition, I combined decoy liposomes with and without the neuraminidase inhibitor (NAi) oseltamivir and tested the effect on infectivity. Inclusion of oseltamivir with LSTc decoy liposomes increased inhibition of PR/8 infectivity (Figure 4.6). As expected, oseltamivir mixed with control decoys (Figure 4.6, clear bars) did not significantly affect infectivity. Oseltamivir alone would only inhibit budding IAV, and all drug treatments are washed out before replication begins. LSTc decoy liposomes alone also inhibit PR/8 (Figure 4.6, left grouping), as seen previously. Adding oseltamivir to the co-incubation and one-hour infection resulted in further inhibition of PR/8 infectivity. When combined with 386 nM SA of LSTc decoy liposomes, 1 μ M oseltamivir (Figure 4.6B, cross-hatched bars) significantly reduced PR/8 infectivity by an additional 30% ($48 \pm 4.9\%$ decoy liposomes alone vs 25.5% PR/8 infectivity for LSTc decoy liposomes and 10 μ M oseltamivir, $p \leq 0.05$).

Higher concentrations of LSTc decoy liposomes had additional synergistic effects with oseltamivir. Co-incubating 1,160 nM SA of LSTc decoy liposomes (Figure 4.6, grey bars) with oseltamivir and PR/8 resulted in an additional 60% decrease of infectivity when incubated with both decoy liposomes and 10 μ M oseltamivir (Figure 4.6C), as compared to decoy liposomes

Figure 4.6 Combining LSTc decoy liposomes with the NA inhibitor oseltamivir improves decoy inhibition of influenza A virus.

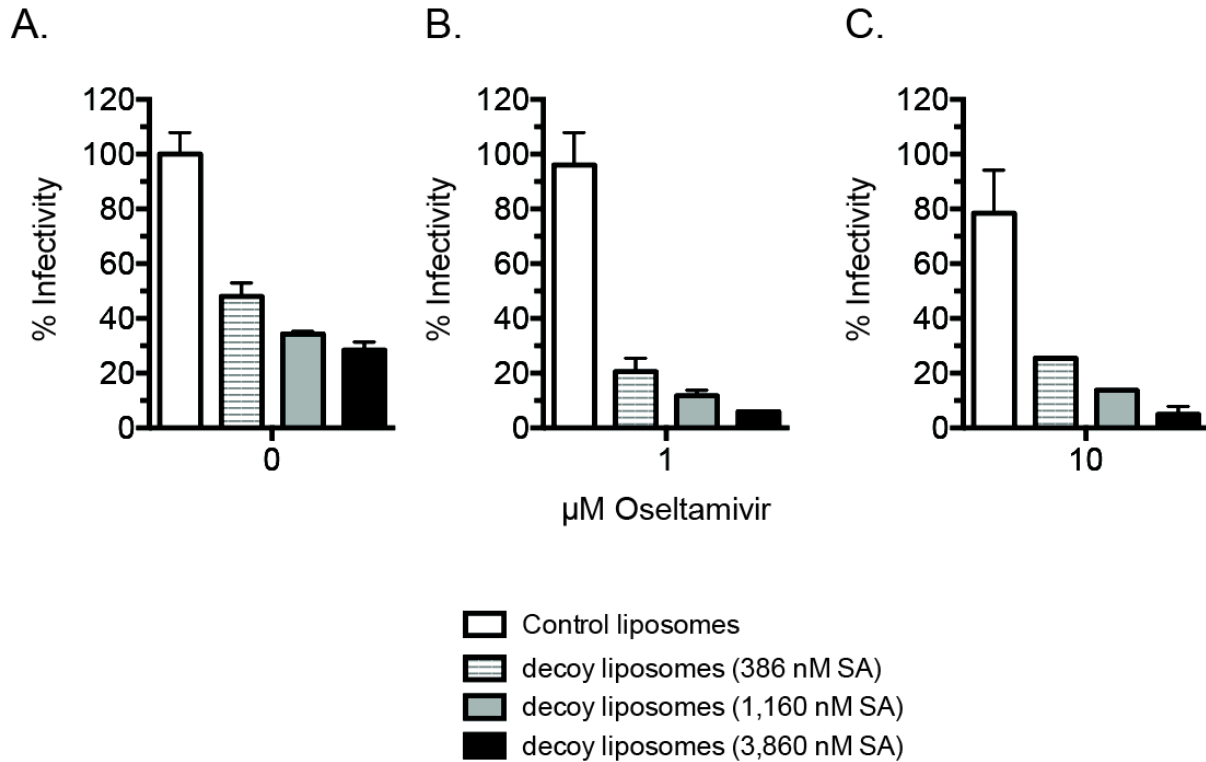


Figure 4.6 Combining LSTc decoy liposomes with the NA inhibitor oseltamivir improves decoy inhibition of influenza A virus.

PR/8 (30 PFU/well) was incubated with control liposomes or LSTc-containing decoy liposomes with or without the NAI oseltamivir before the addition to MDCK cells. Infection lasted for 1 hour at 37°C before virus and drug treatments were washed away and plaques allowed to develop. Plaques per well of virus treated with control liposomes (0 mol% LSTc and 0 μM oseltamivir) are defined as 100% infectivity (A, **clear bar**), and PR/8 samples treated with LSTc decoy liposomes and oseltamivir are expressed as the percent reduction from their respective control. **A-C.** Inhibition of PR/8 infectivity with control liposomes (**clear bars**) or increasing amounts of LSTc-containing decoy liposomes; 386 nM SA (**horizontal hatching**), 1,160 nM SA (**grey**) or 3,860 nM SA (**black**) and 0 μM (A), 1 μM (B) or 10 μM oseltamivir. The data are biological repeats of one independent representative experiment, repeated three times, all with similar results.

alone, 13.7% vs. $34.3 \pm 1\%$ ($p \leq 0.01$) PR/8 infectivity, respectively. At the highest LSTc concentration tested, 3,860 nM SA of decoy liposomes (Figure 4.6, black bars), inclusion of oseltamivir resulted in 82% of additional inhibition, with the combination of 3,860 nM SA decoy liposomes and 10 μM oseltamivir (Figure 4.6C) inhibiting all but $4.9 \pm 2.9\%$ infectivity as compared to $28.4 \pm 2.9\%$ infectivity ($p \leq 0.05$) with decoy liposomes and no oseltamivir. Addition of less oseltamivir, 1 μM , followed the above trend of increasing inhibition of LSTc decoy liposomes, but to a lesser degree, as expected (Figure 4.6B). These data demonstrate that decoy liposomes act synergistically with oseltamivir to inhibit IAV.

Decoy liposomes with the $\alpha 2$ -3 linked SA-containing glycolipid inhibit IAV

IAV binds to terminal SA, linked in either an $\alpha 2$ -6 or an $\alpha 2$ -3 linkage to the penultimate sugar residue, depending on which host species they are adapted to infect. The human upper respiratory tract has glycans with $\alpha 2$ -6 linked SA, and therefore I have focused primarily on decoy liposomes decorated with that linkage. However, highly virulent H5N1 avian strains that infect humans (Chandrasekaran, Srinivasan et al. 2008) and recent avian or swine crossover strains bind to $\alpha 2$ -3 linked SA (Pappas, Viswanathan et al. 2010). Therefore, our collaborators created decoy liposomes functionalized with $\alpha 2$ -3 linked SA, via the glycolipid LS-Tetrasaccharide A (LSTa). LSTa glycan underwent the same purification, chemical linking and quality controls as described for LSTc in Chapter 3. LSTa-containing liposomes had similar polydispersity indexes as LSTc-containing liposomes.

To test IAV binding of LSTa-containing decoy liposomes, I utilized the standard HAI assay and found that LSTa decoy liposomes inhibited all IAV strains tested, except Beijing H1N1 (Table 4.1). All the strains that were inhibited by LSTa-containing decoy liposomes have

Table 4.1 Assessment of LSTa decoy liposomes by hemagglutination inhibition assay of multiple strains of influenza A virus.

Virus	HAI Titer	IC₉₀ (μM SA)
Philippines H3N2	180	0.16 (± 0.8)
X-31 H3N2	16	1.8 (± 2.9)
HK 68 H3N2	90	0.32 (± 0.3)
Victoria H3N2	16	1.8 (± 5.1)
Beijing H1N1	No inhibition	> 14.6

Table 4.1 Assessment of LSTa decoy liposomes by hemagglutination inhibition assay of multiple strains of influenza A virus.

LSTa decoy liposomes competitively bind to several strains of influenza virus. Decoy liposomes containing 30 mol% LSTa are effective at inhibiting hemagglutination of Philippines, X-31, and HK68 IAV strains. IC₉₀ values are shown as molarity of sialic acid ± the 95% confidence interval. Hemagglutination of Beijing IAV is not inhibited by 30 mol% LSTa decoy liposomes at the highest concentration tested.

been described to bind to α 2-3 linked SA. The Beijing 95 is a more recent isolate, and is believed to have had less egg passage, and therefore less α 2-3 adaptation. Control liposomes lacking LSTa did not cause any HAI when tested at the same lipid concentrations as LSTa liposomes. Like LSTc liposomes, liposomes with 30 mol% LSTa inhibited Philippines with HAI titers of 180 and an IC₉₀ of 0.16 μ M SA, X-31 with HAI titers of 16 and an IC₉₀ of 1.8 μ M SA, HK 8/68 with HAI titers of 90 and an IC₉₀ of 0.32 μ M SA, and Victoria 3/75 (H3N2) with HAI titers of 16 and an IC₉₀ of 1.8 μ M SA. I also tested Beijing 262/95 (H1N1) against the 30 mol% LSTa liposomes, but it did not inhibit hemagglutination at the highest concentration tested, 14.6 mM SA, which is roughly three logs more LSTa decoys than what was inhibitory for the other IAV strains. Interestingly, Beijing IAV is inhibited only by LSTc-containing decoy liposomes (see Table 3.2), which suggests that it binds exclusively to α 2-6 linked SA, whereas all of the other strains tested appear to be promiscuous binders that bind both α 2-6 and α 2-3 linked SA. While LSTa decoy liposomes inhibited IAV, the degree of HAI was less than that of LSTc-containing liposomes; this may be due to any of a number of factors, including the binding strength of HA to α 2-3 linked SA, susceptibility of LSTa to viral NA, and proper incorporation and presentation of LSTa into decoy liposomes.

Decoy liposomes with the α 2-3 linked SA glycan inhibit influenza virus infectivity

To investigate the impact of LSTa-containing decoy liposomes on infectivity, I co-incubated several strains of IAV with control or decoy liposomes with 30 mol% LSTa before infecting MDCK cell monolayers. LSTa decoy liposomes significantly inhibited all IAV strains tested (Figure 4.7). At the highest concentration tested, 14,585 nM SA, LSTa decoy liposomes inhibited PR/8 up to $40.6 \pm 7.2\%$, Philippines up to 31%, X31 up to $56.7 \pm 3.9\%$,

Figure 4.7 LSTa decoy liposomes inhibit influenza A virus infection of MDCK cells.

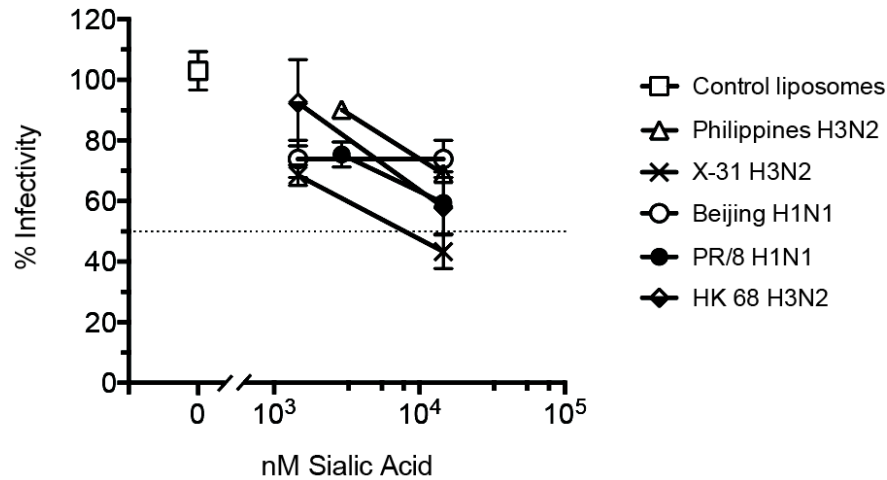


Figure 4.7 LSTa decoy liposomes inhibit influenza A virus infection of MDCK cells.

Decoy liposomes containing 30 mol% LSTa inhibit multiple strains of IAV. Decoy liposomes inhibited Philippines (**open triangles**, 50 PFU/well), X-31 (**crosses**, 50 PFU/well), Beijing (**open circles**, 15 PFU/well), PR/8 (**filled circles**, 30 PFU/well), and HK68 (**half closed diamonds**, 60 PFU/well) strains of IAV. The data are representative averages \pm S.E. of one experiment for Philippines, X-31, Beijing and HK68 and two experiments for PR/8.

HK68 up to $42 \pm 0.8\%$ and Beijing $26.1\% \pm 4.3\%$ of infectivity as compared to control liposomes. Unlike LSTc decoy liposomes, all of the strains tested, except Beijing, were inhibited to similar levels by both doses. The overall degree of inhibition obtained here was less than comparative doses of LSTc-containing decoy liposomes, perhaps due to strain preference for α 2-6 linked SA over α 2-3 SA. Supporting this is the relative lack of inhibition of Beijing IAV, a strain that is reported to have less cell culture adaptation than the other common research strains (McDonald, Smith et al. 2007). In previous studies, an H3N2 strain had a 5-fold preference for LSTc over LSTa with the HAI assay (Pritchett, Brossmer et al. 1987). Together with the HA data above, these data demonstrate that LSTa decoy liposomes can also inhibit IAV binding and infectivity.

LSTc- and LSTa-containing decoy liposomes synergistically inhibit IAV infectivity

Many of the key emerging avian and swine IAV strains that successfully infect humans can bind to both α 2-3 and α 2-6 linked SA, and it is therefore reasonable to expect that a population of decoys that contained both SA linkages might inhibit IAV to a greater degree than either one alone. To test this hypothesis, I performed a ‘checkerboard’ experiment by co-incubating PR/8 with either LSTc liposomes or LSTa liposomes individually, or with a combination of both types at varying concentrations and assayed for infectivity on MDCK cell monolayers. LSTc liposomes alone inhibited PR/8 by $84.7 \pm 1.7\%$ at 11,600 nM SA (Figure 4.8, left grouping), which is in line with the degree of inhibition seen in Chapter 3 (see Figure 3.5). When used individually, LSTa liposomes also inhibited PR/8 to a similar extent as seen above, to $39 \pm 3.4\%$ at 15,600 nM SA (Figure 4.8, white bars). Again these results confirm that LSTc decoy liposomes are more effective at inhibiting IAV than LSTa decoy liposomes. When

Figure 4.8 Combining LSTc- and LSTa-containing decoy liposomes increases inhibition of influenza A virus.

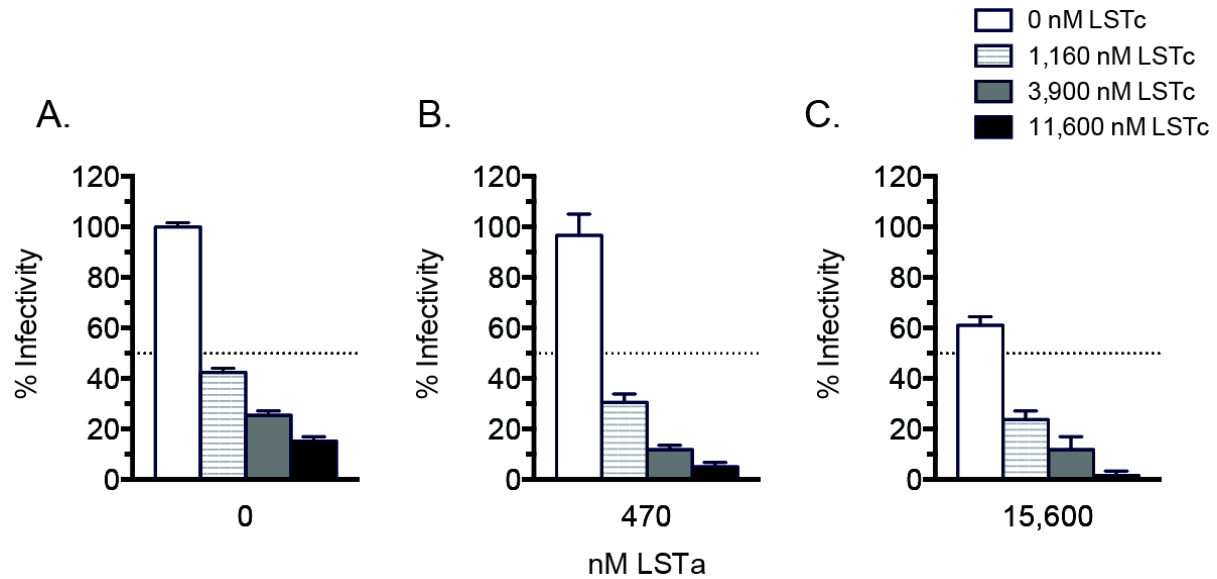


Figure 4.8 Combining LSTc- and LSTa-containing decoy liposomes increases inhibition of influenza A virus.

PR/8 (30 PFU/well) was incubated with control liposomes, LSTc-containing decoy liposomes, LSTa-containing decoy liposomes or a mixture of LSTc- and LSTa-containing decoy liposomes before the addition to MDCK cells. Plaques per well of virus treated with control liposomes (0 mol% LSTc and 0 mol% LSTa) are defined as 100% infectivity (A, **clear bar**), and PR/8 samples treated with different liposome formulations are expressed as the percent reduction from its respective control. (A-C) Samples received the indicated amount of decoy liposomes with 15 mol% LSTa and increasing amounts of LSTc-containing decoy liposomes, either control liposomes (**clear**), 1,160 nM SA (**horizontal hatching**), 3,900 nM SA (**grey**) or 11,600 nM SA (**black**), as indicated in the key. The data represent biological repeat average \pm S.E. of one representative of two experiments.

combined, LSTc and LSTa decoy liposomes had a synergistic effect. At a constant concentration, 1,160 nM SA, of LSTc liposomes, 470 nM SA or 15,600 nM SA of LSTa-containing liposomes inhibited PR/8 infectivity $69.5 \pm 3.4\%$ and $76.3 \pm 3.4\%$, respectively, from a baseline inhibition of $57.6 \pm 1.7\%$ when challenged with LSTc decoy liposomes alone (Figure 4.8). When used together, this represents an additional 32% increase of inhibition above either LSTc or LSTa liposomes alone. Higher doses of LSTa decoy liposomes also results in synergy. LSTc-containing decoy liposomes at 3,900 nM SA inhibited PR/8 infectivity to $74.5 \pm 1.7\%$ in the absence of LSTa liposomes, but inhibition increased to $88.1 \pm 1.7\%$ and $88.1 \pm 5\%$ when combined with either 470 nM SA or 15,600 nM SA LSTa-containing liposomes, an additional 18% inhibition increase. Finally, 11,600 nM SA of LSTc-containing liposomes alone inhibited $84.7 \pm 1.7\%$ PR/8 infectivity. Addition of LSTa at 470 and 15,600 nM SA increased the inhibition to 94.9 ± 1.7 and $98.3 \pm 1.7\%$ of all PR/8 inhibited, resulting in an additional 16% increase of inhibition as compared to either decoy liposomes alone. Inhibition was most dramatic when low concentrations of both LSTc- and LSTa-containing decoy liposomes were combined, due in part to the almost complete inhibition of IAV at the tested viral dose (30 PFU/well). The synergistic effect can be seen when 470 nM SA of LSTa liposomes (3.4% inhibition alone) and 1,160 nM SA LSTc liposomes (57.6% inhibition alone) are combined, resulting in 69.5% inhibition. These data suggest a mixture of decoy liposomes would effectively combat a strain of IAV that retains the ability to bind to both $\alpha 2-3$ and $\alpha 2-6$ linked SA.

Optimizing the anti-influenza A virus liposome platform

Discussion

The data presented here describe several diverse modifications made to the decoy liposome platform, including changing the decoy receptor to target IAV strains adapted to other host species. Using liposomes to achieve polymer-like, multivalent decoys makes it easily adaptable, which is not true for polymer-based decoy receptors. The results presented in this chapter demonstrate that changing liposome size, fluidity, and charge can improve efficacy of IAV inhibition. In addition, the decoy receptor can be changed to LSTa, and along with LSTc-containing decoy liposomes, can synergistically target IAV. LSTa decoy liposomes may also target avian adapted IAV strains. These data highlight the adaptability of the decoy liposome system, and with the creation of decoy liposomes containing LSTa, indicate that additional glycolipid decoy mimics can be utilize to target additional pathogens.

Generation of liposome formulations for enhanced IAV inhibition

The basic decoy liposome formulation showed promising inhibition against IAV with the SA-containing molecule, LSTc. In an attempt to improve inhibition, our collaborators and I modified several aspects of the platform to determine the optimal formulation for IAV inhibition. Doubling the size of the decoy liposome increased inhibition by almost five fold at low concentrations of SA (Figure 4.1). These data indicate that low decoy curvature is very important for optimal interactions between LSTc and HA. Baumgart *et al.* (2003) have shown that liposomes with minimal curvature have less line tension, and therefore less of a diffusion barrier between lipid components as compared to liposomes with higher curvature (Baumgart, Hess et

al. 2003). Further increase in liposome size is not technically feasible in this study due to the formation of multilammellar vesicles created with larger extruder pores, which would reduce the amount of LSTc available at the vesicle exterior for binding to virus and thus negate the positive effects of further curvature reduction.

Osmotic crushing is another method of changing liposome curvature. Osmotically crushed liposomes are shaped like truncated spheres that have two polar regions with low curvature and an equator region with high curvature. As shown previously, large decoy liposomes with low curvature were more inhibitory. We hypothesized that crushed decoy liposomes would interact more efficiently with IAV via their two low curvature domains. Crushing our decoy liposomes resulted in a small but significant increase in IAV inhibition (Figure 4.3), but crushed liposomes were less effective than the larger, spherical liposomes tested above. It is possible that the high curvature equator region prevented LSTc glycolipids from migrating from one polar domain to the other.

Liposome fluidity can be adjusted by changing the membrane components. Adding cholesterol into a lipid bilayer affects lipid packing and makes the bilayer more fluid (Rubenstein, Smith et al. 1979). Cholesterol also increases liposome fluidity, and it has been shown to increase lateral diffusion and reduce line tension (Coderch, Fonollosa et al. 2000). The addition of 30 mol% cholesterol improved the PR/8 inhibition of LSTc decoy liposomes by three fold (Figure 4.2), suggesting that cholesterol enhanced the ability of LSTc decoy glycans to diffuse through the liposome membranes, increasing the bio-availability of the LSTc decoy.

Addition of PEG to liposome was previously shown to increase *in vivo* half-life (Blume and Cevc 1993). Increased *in vivo* half-life would improve the efficacy of our decoy liposomes, allowing more time for a patient's adaptive immune response to clear the virus, thus decreasing

mortality. Decoy liposomes with long half-lives may act more like a molecular sink, and could be administered to patients less often. Unfortunately, inclusion of PEG-1000 onto our decoy liposomes abrogated their ability to inhibit PR/8 IAV (Figure 4.4). PEG increases the circulation times of drug delivery decoys, but in the context of decoy liposomes, PEG appears to mask the LSTc glycolipid. The molecular weight of PEG-1000 and LSTc are comparable, suggesting that there may be steric interference between PEG and LSTc glycolipid. In addition, PEGylated liposomes were previously shown to have reduced lipid fluidity (Blume and Cevc 1993), which would make the LSTc glycolipid less able to migrate through the membrane and bind to IAV. For these reasons, PEGylated decoy liposomes are not a viable option for extending *in vivo* half-life.

The outcome of an interaction between two lipid membranes is partially dependent on their electrostatic properties. In the context of an enveloped viral infection, such as IAV, the net membrane charge, or zeta potential, of the virion and of the target host cell are critical for infection. Using decoy liposomes as a therapy further complicates the equation, introducing a third lipid membrane that must have a favorable zeta potential for interaction with the appropriate partners – strong for the virus and weak for cell membranes. IAV has a relatively neutral zeta potential of about -20 mV (Hagenaars, Mastrobattista et al. 2009). Mammalian cells have a strong negative charge. Liposomes with 7.5 mol% of negatively charged lipids, similar to the decoys liposomes used here, also have a relatively neutral zeta potential, of about -25 mV (Woodle and Lasic 1992). Therefore increasing the negative charge of the decoy liposomes may make them more attractive to the less negatively charged IAV and less attractive to the very negative host cells, which may impede decoy liposome function. In addition, negatively charged liposomes were shown to have longer *in vivo* lifespans in the lung environment as compared to

neutral liposomes (Deol and Khuller 1997). Therefore, our collaborators doubled the mole percent of negatively charged molecules, either by adding negative lipid in place of neutral lipid or by adding negatively charged LSTc. Doubling the negative charge on decoy liposomes did not increase PR/8 inhibition; rather, inhibition was slightly reduced (Figure 4.5). This contradicted our initial hypothesis and may result from electrostatic repulsion of decoy liposomes from the cell monolayer, where the competitive binding of decoy LSTc to virus would be most effective at blocking IAV attachment to SA on susceptible cells.

One potential problem of using a decoy receptor drug is that some pathogens, IAV included, enzymatically remove their host receptor during the course of infection. IAV NA on budding virions removes terminal SA from glycolipids and glycoproteins on the infected cell and on IAV itself. Desialylation allows IAV release from an infected cell by preventing nascent HA from binding the infected cell or other virions (See Figure 1.2). The NA inhibitors Oseltamivir and Zanamivir prevent release of budding virus and effectively neutralize the virus (Collins, Haire et al. 2008). The SA on both LSTc and LSTa are theoretically vulnerable to NA and could be cleaved when the decoy liposome binds to IAV. The literature suggests that unpurified human LSTc is cleavable by bacterial NA (Martin-Sosa, Martin et al. 2003). Moreover, purified monovalent LSTc is cleavable by viral NA (Kristina Prachanronarong and Dr. Celia Schiffer, personal communication) and therefore NA may cleave decoy liposomes LSTc negatively affecting inhibition.

To examine the effect of NA cleavage on LSTc decoy liposomes, I mixed decoy liposomes with or without the NA inhibitor, oseltamivir, and compared PR/8 inhibition. At all concentrations of decoy liposomes tested, addition of oseltamivir increased inhibition of infectivity (Figure 4.6). The effect was most dramatic at high concentrations of decoy liposomes

and fairly high concentration of oseltamivir, which resulted in an additional 80% of infectivity inhibition. These data demonstrate that the LSTc-containing decoy liposomes act synergistically with oseltamivir to further inhibit IAV infectivity. In addition, NA may remove some SA from the decoy liposomes, and this may explain some of the inhibition differences between the IAV strains tested against LSTc-containing decoy liposomes (see Figure 3.4B and Table 3.2), because NA activity levels differ by strain.

The linkage of SA to the penultimate sugar residue can be made NA resistant, and previous decoy studies have found this modification makes decoy receptors more efficient (Itoh, Hetterich et al. 1995; Sun, Kanie et al. 2000). These data demonstrate that my decoy liposomes would benefit from an LSTc molecule with an NA-resistant linkage, which can be created in the laboratory. Another potential solution would be to load the decoy liposome interior with a NAI. Loading would result in a local, high Oseltamivir concentration at the decoy liposome, as oseltamivir would escape slowly through the lipid bi-layer. This approach would not only make the decoy liposomes more efficient, it would help deliver a proven anti-IAV drug to the site of infection. This could be used as a method of targeting NA inhibitors to infected respiratory cells, preventing release of budding virus, with lower NAI doses and possibly reduced toxicity.

Decoy liposomes with α 2-3 linked SA inhibit IAV binding and infectivity

IAV that is adapted to infect humans predominantly binds to α 2-6 SA, while avian and swine adapted strains bind to α 2-3 SA. There is evidence of strains emerging from the avian and swine population and infecting humans, bind to both α 2-6 and α 2-3 SA before the adaptation to α 2-6 linked SA binding is fixed (Glaser, Stevens et al. 2005). Furthermore, humans have α 2-3 linked SA in the lower respiratory tract, and when avian-adapted IAV reaches this area, life-threatening pneumonia can develop. Therefore, our collaborators created decoy liposomes with

LSTa, a glycan with α 2-3 linked terminal SA. LSTa decoy liposomes were able to bind and inactivate several IAV strains tested, but to a lesser degree than LSTc-containing decoy liposomes. The reduced affinity was seen with both the HAI and infectivity assay and most likely represents a preference of each strain for α 2-6 linked SA. Notably, a more recent clinical isolate, Beijing IAV, was inhibited less by LSTa decoy liposomes than the strains adapted to mouse infection, such as PR/8 or X-31 (Figure 4.7 and Table 3.1). Combining LSTc- and LSTa-containing decoy liposomes increased the degree of inhibition against PR/8 IAV (Figure 4.8), demonstrating synergy between two decoy receptors against a promiscuous binder IAV. These data suggest that some virions in a virus population may favor one linkage over another, and a mix of decoy liposomes can effectively target such viruses. Combined decoy treatment may also be useful when combating a strain with unknown binding preferences. It would be interesting to test LSTa decoy liposomes against an avian-specific IAV strain, as it may demonstrate the true potential of LSTa decoy liposomes against other antigenic IAV subtypes.

The data presented here have determined that optimal inhibition occurs when decoy liposomes have low curvature and highly fluid lipid membranes. In addition, decoy liposomes with LSTa, a glycolipid with α 2-3 linked SA, inhibited all but one IAV strains tested and acted synergistically with LSTc-containing decoy liposomes to further inhibit IAV. These data demonstrate the adaptability of the decoy liposome platform and how they could be modified for use in different applications and potentially different diseases. The decoy liposomes tested here have been especially made for use in the lung, but they could easily optimized for other uses, such as *in vitro* binding arrays.

Chapter V

Heparin sulfate decoy liposomes inhibit respiratory syncytial virus and herpes simplex virus

Preface

This Chapter contains information relating to the creation of decoy liposomes containing the decoy glycolipid HS-octa, and their use as a therapeutic against RSV, HSV and PIV3. Dr. Zachary Shriver's laboratory created and purified HS-octa glycans and constructed LSTa-glycolipids. Dr. Deborah Fygenon and her laboratory were responsible for constructing the HS-octa decoy liposomes. I tested the liposomes in all experiments described below, including infectivity assays, growth inhibition studies, and statistical analysis. Natasha Qaisar and Serna Pham performed the PIV3 HAI assays.

Introduction

In the previous two chapters I described the creation and optimization of sialic acid-bearing decoy liposomes as a potential IAV therapeutic. In this chapter I will discuss developing the decoy liposome platform to target a new set of viruses by utilizing a new decoy receptor glycolipid. My findings demonstrate that decoy liposomes with heparin sulfate octasaccharides (HS-octa) inhibit HS-binding viruses better than the HS-octa building block in solution or the full-length heparin, and in addition, HS-octa decoy liposomes are not anticoagulants.

Heparan sulfate (HS) is a broad group of related, linear chain glycosaminoglycans (GAGs) made up of 10 to 200 disaccharide repeats, containing *N*-acetyl-D-glucosamine and an uronic acid. While all HS-GAGs have the same basic disaccharide repeat, each member is chemically distinct from further modifications to each repeat. HS-GAGs can be sulfonated with either an N- or O-linkage, and they have three sites per disaccharide repeat for O-sulfonate attachment. Epimerization of the uronic acid can add further variety to each HS-GAG family member. With so many possible modifications, HS-GAG family members differ widely in structure. Heparin is one HS-GAG family member, it is highly sulfonated, giving it the highest negative charge density of all known biological molecules. It is made mostly by mast cells and is used clinically as a potent anticoagulant. Clinical heparin is a pleiotropic population of heparin chains that vary in length and molecular weight, which range from 5,000 to 40,000. It is a well-studied HS-GAG and many binding partners have been described (Iozzo 1998). Important here, the heparin domains required for its anticoagulant properties have been defined: heparin binds to antithrombin III and the factor IIa /Xa complex (Petitou, Herault et al. 1999). Antithrombin III binding requires a specific pentasaccharide repeat of heparin / HS and a second,

distal binding saccharide partner on the same chain. Shorter oligosaccharides of heparin, also generalized as heparan sulfates by the literature, do not possess the longer binding sites of these clotting factors and therefore are not anticoagulants (Dr. Zachary Shriver, personal communication and Petitou, Hérault et al. 1999).

Many pathogens bind to HS-GAGs, which taken together, are expressed ubiquitously on cell surfaces throughout the body. HS-binding viruses use HS either for initial attachment or as a sole host ligand (Zhu, Li et al. 2011). Due to its many sulfonate and carboxylate groups, HS-GAGs have highly negative charge densities and HS-binding viruses have evolved attachment proteins with clusters of positively charged amino acids, forming heparan-binding domains (HBD). Because HS is a linear repeating molecule, it is thought to make multiple interactions with many HBDs on a single virion and to make multivalent interactions with virus. Here our collaborators and I have created and tested HS-octa decoy liposomes that inhibit HS-binding viruses. These data, along with LSTc and LSTc functionalized decoy liposomes may be used in the future as an adaptable platform to target many different important pathogens.

Heparin sulfate decoy liposomes inhibit respiratory syncytial virus and herpes simplex virus

Results

Heparin sulfate oligosaccharide liposomes

While all of the liposome formulations described above had a wide range of modifications; they all had sialic acid as the decoy receptor for IAV inhibition. Replacing the decoy receptor glycan allows the decoy liposome platform to target other important pathogens. One such glycan receptor is heparin / heparan sulfate GAGs. HS is a representative of a family of long, linear polysaccharides found abundantly throughout the body, both in the extracellular matrix and attached to cell membranes. Many viruses have been discovered to bind to HS, as either an initial receptor before binding a protein receptor or as specific receptor (Zhu, Li et al. 2011). Specifically, HS has been demonstrated to play an important role in respiratory syncytial virus (RSV) (Krusat and Streckert 1997) and herpes simplex virus (HSV) (WuDunn and Spear 1989).

Therefore our collaborators created decoy liposomes decorated with HS oligosaccharides, in order to inhibit HS-binding viruses. The starting HS molecule used was clinical heparin, which consists of a population of heparin chains of varying lengths, with an average molecular weight of 15,000. Heparin was cut into smaller fractions with heparinase and purified by anion exchange chromatography. The negative charge on each disaccharide repeat allows for fairly pure populations of specific numbers of sugar residues (Zachary Shriver, personal communication). An octasaccharide (referred here as HS-octa) was chosen for use in the decoy liposomes due to its lack of anticoagulation properties and because it has enough binding motifs while not being too large to cause liposome destabilization or incorporation issues. HS-octa

decoy liposomes were created in the same manner as for the LSTc–DOPE liposomes described in Chapter 3. Compounds 1 – 4, as described in Figure 3.1 were created with the same method, and purified HS-octa was covalently attached to the DOPE lipid-linker (compound 4).

HS-octa decoy liposomes were extruded with the same protocol as for LSTc decoy liposomes, they were also extruded through a 200 nm extruder pore, and had average radii of 57.6 ± 2.1 nm and PDI of 0.136 ± 0.01 , which are similar to the sizes and polydispersity of LSTc decoy liposomes. Our collaborators generated a series of HS-octa decoy liposomes with increasing mole percentages of HS-octa incorporated in each liposome to test the optimal density of HS-octa required for inhibition. The maximum mole percentage of HS-octa incorporation was 30 mol%, decoy liposomes with less HS-octa had DOPG incorporated as needed to retain a 30 mol% of negatively charged lipid. Of note, DOPG has less of a negative charge per molecule than HS-octa–DOPE. Liposomes with 0 mol% HS-octa and 30 mol% DOPG were used as control liposomes.

Heparin and HS-octa inhibition is specific for HS-binding viruses

In order to test the heparin decoy glycan for species-specific inhibition, I co-incubated RSV A2, HSV kos and PR/8 IAV with full-length heparin sulfate, HS-octa in solution or media control before infecting Vero or MDCK cell monolayers. Full-length heparin inhibited RSV and HSV (Figure 5.1 A, B), as established by the literature (WuDunn and Spear 1989; Feldman, Audet et al. 2000), but the same concentrations of heparin did not inhibit IAV (Figure 5.1C), which has also been previously shown (Martinez and Melero 2000). In my hands, neither full-length or the octasaccharide inhibited IAV, demonstrating that the process of creating the HS-

Figure 5.1 Heparin sulfate and HS-octa specifically inhibit RSV and HSV infection of Vero cells.

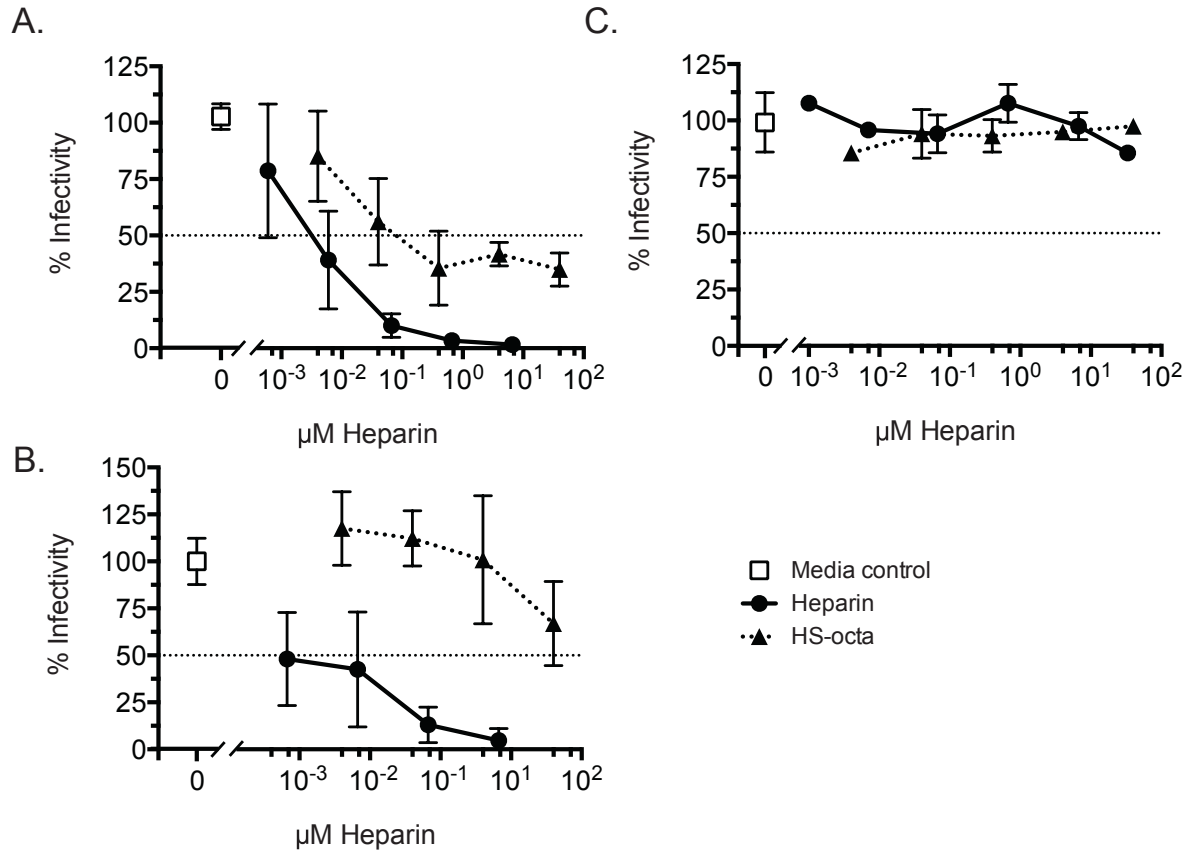


Figure 5.1 Heparin sulfate and HS-octa specifically inhibit RSV and HSV infection of Vero cells.

A, RSV (50 PFU/well), **B** HSV (50 PFU/well) and **C**, IAV (PR/8, 50 PFU/well) were incubated with full-length heparin, HS-octa saccharide or media control before addition to Vero (**A** and **B**) or MDCK cells (**C**). Full-length heparin (**circles**) inhibited RSV and HSV to a greater extent than HS-octa saccharide (**triangles**). Neither inhibited IAV. Data are represented as percent reduction, with media control (**open squares**) defined as 100% infectivity. The data represent the average \pm S.E. of two experiments for HSV and RSV and one experiment for PR/8 IAV.

octa does not introduce any non-specific inhibition properties or contamination. Full-length heparin was very efficient at blocking RSV infectivity, inhibiting $60.1 \pm 10.8\%$ of RSV at as little as $0.006 \mu\text{M}$ HS. Higher doses resulted in up to 96% inhibition (Figure 5.1A). As expected, HS-octa was less efficient at inhibiting RSV than the full-length heparin. HS-octa blocked 44% of RSV infectivity when used at $0.04 \mu\text{M}$ HS-octa and blocked approximately 60% of RSV infectivity inhibition at the highest concentration tested, $40 \mu\text{M}$ HS-octa.

A similar trend resulted when HSV was challenged with full-length heparin and HS-octa. Full-length heparin blocked 52% HSV infectivity at the lowest concentration tested, $0.006 \mu\text{M}$ HS and up to 95% HSV infectivity at $6.6 \mu\text{M}$ HS (Figure 5.1B). HS-octa in solution did not inhibit HSV strongly, blocking only 33% of HSV infectivity at the highest concentration tested, $40 \mu\text{M}$ HS-octa. The difference between the full length and octasaccharide is expected because the shorter HS-octa has fewer negatively charged side groups available for binding to the virus and reduced steric hindrance. The full-length heparin however, cannot be used therapeutically either in solution or complexed into a decoy liposome due to its potent anticoagulant properties. These data confirm that the HS-octa building block remains inhibitory to HS-binding viruses, and does not have a binding gain-of-function to the unrelated virus, IAV. These data also validate the use of HS-octa as a receptor in decoy liposomes, for species-specific inhibition of HS-binding viruses.

Decoy liposomes with HS-octa inhibit Respiratory syncytial virus

Next I assessed decoy liposomes functionalized with HS-octa glycolipids linked to DOPE at different mole percentages on RSV infectivity. Our collaborators created a series of liposomes containing increasing mole percentages of HS-octa glycolipid, and control liposomes

containing the negatively charged lipid, DOPG, in place of decoy. The series ranges from control liposomes (0 mol% HS-octa and 30 mol% DOPG) to 30 mol% HS-octa (and no DOPG). To calculate the molarity of HS-octa in solution, I multiplied the mole percent input of HS-octa-DOPE by the total lipid concentration, as described above for the LSTc liposomes. Increasing concentrations of decoy liposomes with HS-octa inhibited RSV infectivity (Figure 5.2A) in these cells, while control liposomes did not. At low concentrations (0.001 μ M HS-octa), all decoy liposome formulations tested inhibited RSV weakly. Increasing the mole percentage of HS-octa per decoy liposomes increased RSV inhibition, in a dose dependent manner. Decoy liposomes with 3 mol% HS-octa (Figure 5.2A, open diamonds) weakly inhibited RSV, blocking only $30 \pm 18.2\%$ RSV infectivity at 1 μ M HS-octa, the highest concentration tested. 7.5 mol% HS-octa liposomes were more effective, inhibiting $26.6 \pm 4.8\%$ ($p \leq 0.005$) and $48.3 \pm 2.6\%$ ($p \leq 0.0001$) RSV infectivity at 0.1 and 1 μ M HS-octa, respectively. Unlike LSTc decoy liposomes, where efficacy plateaued at 7.5 mol% LSTc incorporation (see Figure 3.5), decoy liposomes with 10 mol% HS-octa inhibited better than 7.5 mol% HS-octa decoy liposomes, blocking $39 \pm 5.9\%$ of RSV infectivity at 0.1 μ M HS-octa. Decoy liposomes with 30 mol% HS-octa inhibited RSV to the greatest extent, blocking $76.5 \pm 3.9\%$ of RSV infectivity ($p \leq 0.0001$) at very low concentrations (0.01 μ M HS-octa). Increasing concentrations of 30 mol% HS-octa decoy liposomes had an even more pronounced inhibition effect, blocking $90.2 \pm 2.2\%$ ($p \leq 0.0001$) and $98.1 \pm 1.9\%$ RSV infectivity ($p \leq 0.0001$) at 0.1 μ M and 1 μ M HS-octa, respectively as compared to control liposomes.

The HS-octa decoy liposomes blocked RSV infectivity to a greater extent than the heparin controls. As seen previously, full-length heparin in solution inhibited RSV with an IC_{50} of approximately 10 μ M HS-octa (Figure 5.2A and B grey diamonds) and the non-liposome

Figure 5.2 HS-octa decoy liposomes inhibit RSV infectivity.

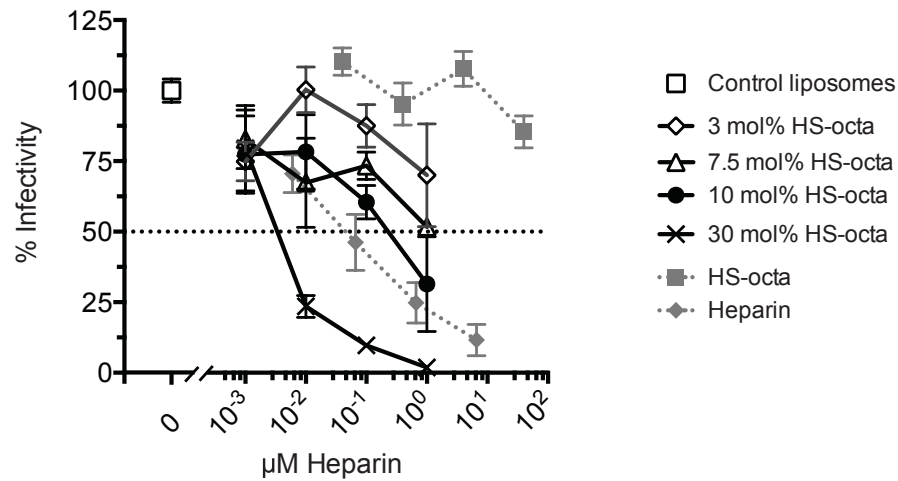


Figure 5.2 HS-octa decoy liposomes inhibit RSV infectivity.

RSV (30 PFU/well) was incubated with control liposomes, LSTc-containing decoy liposomes, full-length heparin or HS-octa before the addition to Vero cells. Plaques per well of virus treated with control liposomes (0 mol% HS-octa) are defined as 100% infectivity (**open square**), and virus treated with different liposome formulations are expressed as the percent reduction from its respective control. Decoy liposomes with 30 mol% HS-octa (**X-es**) inhibited PR/8 to the greatest extent. Decoy liposomes with 10 mol% HS-octa (**circles**) also significantly inhibited infection; however, decoy liposomes with 3 mol% HS-octa (**open diamonds**) or 7.5 mol% HS-octa (**open triangles**) poorly inhibited infection. HS-octa building block (**grey squares**) inhibited weakly, and the anticoagulant, full-length heparin (**grey diamonds**) inhibited both viruses, slightly less than 30 mol% HS-octa decoy liposomes. The data represent the average \pm S.E. of two experiments for RSV.

associated HS-octa building block inhibited weakly, blocking only $14.6 \pm 5.7\%$ of RSV infectivity at the highest concentration tested, $40 \mu\text{M}$ HS-octa. The HS-octa decoy liposomes inhibited RSV approximately four logs lower concentrations of the octamer heparin saccharide used to create them. These data demonstrate that incorporation of HS-octa into liposomes increases RSV inhibition, presumably by allowing glycolipid migration through the bilayer and increasing the bio-availability of HS-octa binding motifs despite the shorter chain length of HS-octa, as compared to full-length heparin.

Decoy liposomes containing HS-octa block Respiratory syncytial virus growth

To investigate whether the decoy liposomes inhibit more than one round of viral replication, I infected Vero cells with RSV either before liposome treatment or co-incubated in the presence of increasing concentrations (in 10-fold increments) of decoy or control liposomes. All inoculating virus was removed and viral replication and spread occurred in viral growth media in the presence of the same treatment of control or decoy liposomes as during infection. When liposomes were added 15 minutes after infection (Figure 5.3A), the highest doses decoy liposomes with 10 mol% or 30 mol% inhibited viral growth. Decoy liposomes with 10 mol% HS-octa significantly inhibited RSV titers at the highest concentration tested, $1 \mu\text{M}$ HS-octa, resulting in only $3,000 \pm 500$ PFU/ml as compared to control liposome treated cells that had $15,250 \pm 1750$ PFU/ml of RSV ($p \geq 0.05$). Decoy liposomes with 30 mol% HS-octa also inhibited RSV at $1 \mu\text{M}$ HS-octa and at $10 \mu\text{M}$ HS-octa inhibition of RSV increased to $1,250 \pm 250$ PFU/ml RSV ($p \geq 0.01$). At $0.1 \mu\text{M}$ and lower concentrations of HS-octa, neither decoy liposome formulations inhibited RSV replication.

Figure 5.3 RSV replication in Vero cells is blocked by HS-octa decoy liposomes.

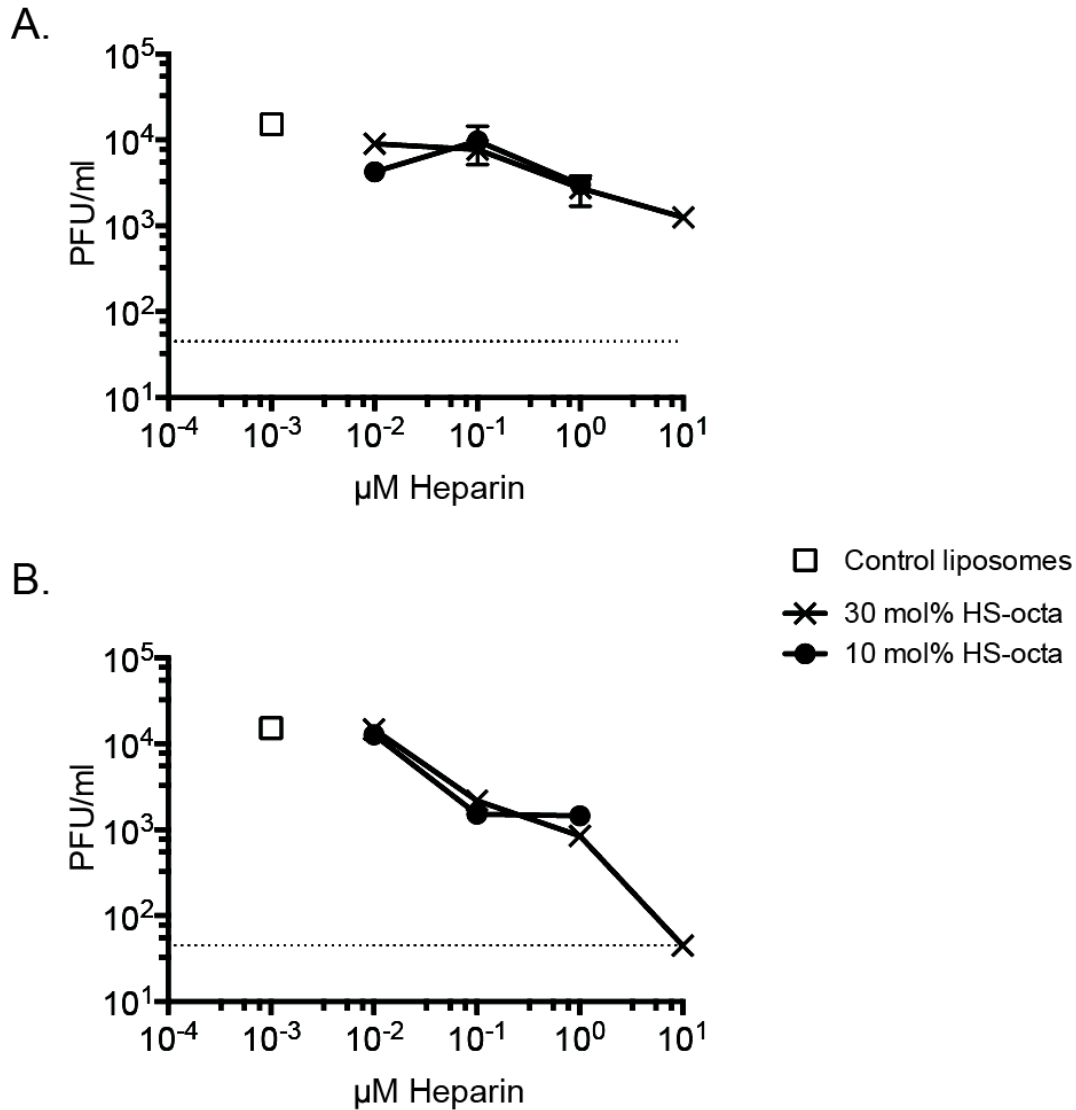


Figure 5.3 RSV replication in Vero cells is blocked by HS-octa decoy liposomes.

Control or HS-octa decoy liposomes were **A**, mixed with RSV 30 minutes before or **B**, added 15 minutes after RSV onto confluent monolayers of Vero cells. RSV was used at a multiplicity of infection of 1. After infection, cells were incubated in the presence of control or decoy liposomes for 24 h. Viral growth was measured by a plaque forming unit assay and plotted as PFU/mL versus total HS-octa concentration present in the solution. Control liposomes did not inhibit RSV growth (**open squares**); however, increasing concentrations of 30 mol% HS-octa (**X-es**) and 10 mol% HS-octa (**circles**) decoy liposomes inhibited RSV infectivity. The dotted line denotes the limit of detection of the assay. Data are biological repeats \pm S.E. from one experiment.

Additional inhibition was seen when RSV and liposomes were co-incubated for 30 minutes before infection of Vero cells, decoy liposomes with 10 mol% and 30 mol% significantly reduced viral titers compared to titers from cells treated with co-incubated RSV and control liposomes (Figure 5.3B). At 0.1 μ M HS-octa, both sets of decoy liposomes inhibited approximately one log of viral titers; $1,525 \pm 175$ PFU/ml for 10 mol% HS-octa liposomes and $2,175 \pm 125$ PFU/ml for 30 mol% HS-octa liposomes. Increasing the concentration 10 fold did not significantly affect RSV inhibition by 10 mol% decoy liposomes, suggesting a plateau for these decoys. However inhibition was increased with the 30 mol% decoy liposomes, RSV titers were down to 850 ± 50 PFU/ml at 1 μ M HS-octa ($p \geq 0.01$ compared to 0.1 μ M HS-octa) and at the highest concentration tested, 10 μ M HS-octa, RSV titers were below the limit of detection, 45 PFU/ml. The lack of virus at the highest dose most likely represents a 100% block of the initial infection and not a block of replication.

Decoy liposomes with HS-octa liposomes inhibit Herpes Simplex Virus

Many diverse viruses have been described that bind to heparan. Therefore, I investigated whether the inhibitory effect of HS-octa decoy liposomes on RSV also applies to HSV-1, a DNA alpha herpes virus. HSV has been shown to bind heparan and heparan-related molecules (WuDunn and Spear 1989), in addition to host protein receptors. I co-incubated the liposomes containing 10 mol%, 30 mol% HS-octa or control liposomes with HSV kos before infecting Vero cell monolayers. Like RSV, control liposomes and low concentrations of 10 mol% and 30 mol% HS-octa decoy liposomes did not block HSV infectivity (Figure 5.4). Increasing concentrations of 10 mol% liposomes significantly inhibited HSV, blocking $57 \pm 6.3\%$ ($p \leq 0.001$) at 1 μ M HS-octa. Furthermore, 10 μ M HS-octa of 10 mol% decoy liposomes blocked

Figure 5.4 HS-octa decoy liposomes inhibit HSV infectivity.

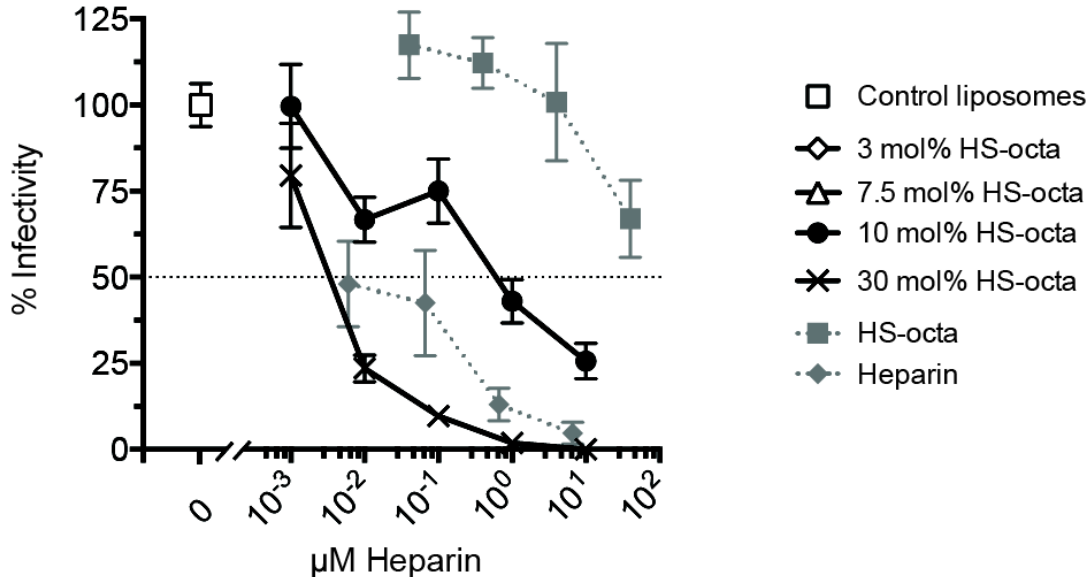


Figure 5.4 HS-octa decoy liposomes inhibit HSV infectivity.

HSV (25 PFU/mL) were incubated with control liposomes, LSTc-containing decoy liposomes, full-length heparin or HS-octa before the addition to Vero cells. Plaques per well of virus treated with control liposomes (0 mol% HS-octa) are defined as 100% infectivity (**open square**), and virus treated with different liposome formulations are expressed as the percent reduction from its respective control. Decoy liposomes with 30 mol% HS-octa (**X-es**) inhibited PR/8 to the greatest extent. Decoy liposomes with 10 mol% HS-octa (**circles**) also significantly inhibited infection; however, decoy liposomes with 3 mol% HS-octa (**open diamonds**) or 7.5 mol% HS-octa (**open triangles**) poorly inhibited infection. HS-octa building block (**grey squares**) inhibited weakly, and the anticoagulant, full-length heparin (**grey diamonds**) inhibited both viruses, slightly less than 30 mol% HS-octa decoy liposomes. The data represent the average \pm S.E. of two experiments for RSV and HSV.

74.4 ± 3.6% HSV infectivity ($p \leq 0.001$). Like RSV, HSV was inhibited to the greatest extent by decoy liposomes containing 30 mol% HS-octa. At only 0.01 μM HS-octa, decoy liposomes with 30 mol% HS-octa inhibited 76.5 ± 3.9% of RSV infectivity ($p \leq 0.0001$); achieving the same amount of HSV inhibition as 10 μM HS-octa of decoy liposomes with 10 mol% HS-octa. Almost 100% inhibition of HSV infectivity was achieved at 1 μM HS-octa, with 98.1 ± 1.9% ($p \leq 0.0001$) inhibition, and an increase to 10 μM totally inhibits HSV infectivity (Figure 5.4).

As was true for RSV and the HS building blocks, HSV was only weakly inhibited by HS-octa in solution (Figure 5.4, grey diamonds). When incorporated into decoy liposomes, the efficacy of HS-octa improved by roughly 5 logs for 10 mol% HS-octa liposomes and by about 7 logs for 30 mol% HS-octa liposomes. Full-length heparin in solution inhibited HSV infectivity better than free HS-octa, as with RSV, but it was not as inhibitory as the 30 mol% HS-octa liposomes. These data demonstrate that the decoy liposome platform can be functionalized to target other classes of virus and that the inhibitory properties depend on the abundance of decoy on the liposomal surface.

Decoy liposomes containing HS-octa block herpes simplex virus replication

To determine if the HS-octa decoy liposomes could inhibit HSV infectivity and replication, I co-incubated one of two doses of HSV with control or decoy liposomes, in 10-fold increments of HS-octa before infection of vero cell monolayers. Virus and liposome treatment was removed after one hour and HSV replication was allowed to continue for 48 hours in the same concentration of control or decoy liposomes as during infection. The presence or absence of HSV-induced cell cytotoxicity was used as the measurement of HSV replication or decoy liposome protection, respectively. High concentrations HS-octa decoy liposomes blocked HSV-

induced cell death, as seen by loss of crystal violet-stained cell monolayers, but not by control liposomes (Figure 5.5). Vero cells infected with 10 MOI of HSV kos and treated with 1 or 10 μ M HS-octa decoy liposomes containing 30 mol% HS-octa were protected (Figure 5.5A). An MOI of 10 ablated the vero cell monolayer when HSV was diluted alone in media (media control) or in the presence of control liposomes with equivalent lipid levels as the highest concentrated decoy liposome treatment. At 1 MOI, decoy liposomes containing 30 mol% HS-octa protected Vero cells from HSV-induced cytotoxicity at a dose of 0.1 μ M HS-octa and above (Figure 5.5B), while control liposomes did not. These data demonstrate that HS-octa decoy liposomes are capable of inhibiting larger amounts of HSV virus, and that they remain protective for multiple rounds infection.

Decoy liposomes with HS-octa inhibit human parainfluenza virus 3 hemagglutination

Human parainfluenza virus 3 (PIV3) is a member of the *paramyxoviridae* family and is the etiological agent that causes human parainfluenza disease that causes upwards of five million lower respiratory tract infections in children every year in the US alone (Henrickson, Kuhn et al. 1994). PIV3 binds to both α 2-3 linked SA and HS for cell entry (Amonsens, Smith et al. 2007). In addition, PIV3 agglutinates RBCs. HS-octa decoy liposomes will provide an alternative binding option and will inhibit hemagglutination when present in sufficient quantity. I tested the HS-octa decoy liposomes against PIV3 in the standard HAI assay. Decoy liposomes with 30 mol% HS-octa inhibited PIV3 agglutination, while control liposomes at equal lipid concentrations did not (Table 5.1). HS-octa decoy liposomes with 30 mol% HS-octa had HAI titers of 32 and an IC_{90} of 3.97 μ M HS-octa. The building block, HS-octa in solution did not

Figure 5.5 HS-octa decoy liposomes inhibit replication and HSV-induced cytotoxicity of Vero cells.

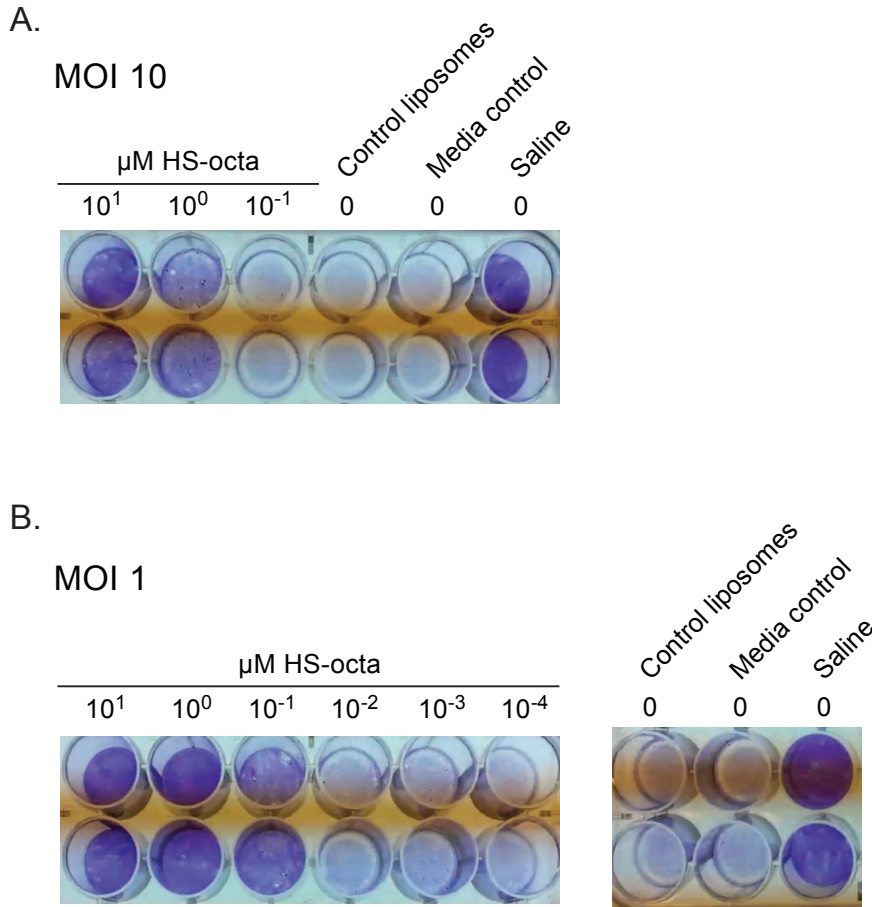


Figure 5.5 HS-octa decoy liposomes inhibit replication and HSV-induced cytotoxicity of Vero cells.

Control or HS-octa decoy liposomes were mixed with **A**, 10 MOI or **B**, 1 MOI of HSV kos 30 minutes before addition onto confluent monolayers of Vero cells. After infection, cells were incubated in the presence of control or decoy liposomes for 48 h. Viral growth was measured by HSV-induced cytotoxicity, as seen by a loss of crystal-violet stained monolayers and displayed with total HS-octa concentration present in the solution. Control liposomes did not inhibit HSV growth (0 $\mu\text{M HS-octa}$); however, 30 mol% HS-octa decoy liposomes inhibited HSV infectivity, at 1 μM and 0.1 $\mu\text{M HS-octa}$ when challenged with 10 MOI or 1 MOI of HSV, respectively. Data shown are from one experiment.

Table 5.1 Assessment of HS-octa decoy liposomes by hemagglutination inhibition assay of human parainfluenza virus 3.

Decoy	HAI Titer	IC₉₀ (μM HS)
Control liposomes	No inhibition	N/A
HS-octa decoy liposomes	32	3.97 (± 1.62)
HS-octa in solution	No inhibition	> 120,000
Full-length heparin in solution	64	83 (± 95.2)

Table 5.1 Assessment of HS-octa decoy liposomes by hemagglutination inhibition assay of human parainfluenza virus 3.

HS-octa decoy liposomes competitively bind to human PIV3. Decoy liposomes containing 30 mol% HS-octa are effective at inhibiting hemagglutination of PIV3, while neither the building block HS-octa in solution nor control liposomes inhibit. HS-octa decoy liposome inhibition is significantly greater than the full-length heparin ($p \leq 0.05$). IC₉₀ values are shown as molarity of heparin / HS-octa ± the 95% confidence interval.

inhibit hemagglutination at the highest concentration tested, 120,000 μM HS. Full-length heparin did inhibit, but significantly less than HS-octa decoy liposomes ($p \leq 0.05$), having HAI titers of 64 and an IC₉₀ of 83 μM HS. These data demonstrate that HS-octa decoy liposomes competitively bind PIV3 and suggest that they will bind to many other viruses that have been described to bind to heparan sulfate.

Heparin sulfate decoy liposomes inhibit respiratory syncytial virus and herpes simplex virus

Discussion

The data presented in this chapter describe the construction of heparin octasaccharide decoy liposomes that inhibit the HS-binding viruses, RSV, HSV and PIV3. Using the proven decoy liposome platform, our collaborators have created decoy liposomes with a glycolipid receptor capable of binding to a large number of viruses and that inhibit more strongly when incorporated into liposomes than when in solution alone. These new HS-octa decoy liposomes are a proof-of-principle that the liposome platform is effective against many other viruses that have well described host glycan receptors and in conjunction with glycan arrays, the platform could be used to target emerging virus strains

A second human glycan molecule widely used by many viruses is heparin / heparan GAGs. Heparan sulfate is a ubiquitous molecule secreted by many cells throughout the body and many viruses have evolved to bind HS, at least as an initial attachment. One specific HS-GAG is heparin, a highly sulfonated HS that HS-binding viruses readily attach. Heparin is commercially available and is used clinically as a potent anticoagulant (Zhang, McCallum et al. 2008). Our collaborators created a defined eight-sugar residue heparin oligosaccharide, or HS-octa, that does not have anticoagulant activity and as described above, binds to viruses as a building block for incorporation into decoy liposomes. I confirmed findings in the literature that full-length heparin blocks RSV and HSV infectivity, but does not affect IAV (Figure 5.1). HS-octa retains some of full-length heparin's inhibitory properties; reducing infectivity by approximately one log for RSV, four logs for HSV, and it remains non-inhibitory for IAV. The

reduced potency is to be expected: soluble HS inhibits viruses by binding to specific, positively charged domains on viral surface attachment and fusion proteins, and the number of binding motifs is reduced on HS-octa as compared to full-length heparin (Feldman, Hendry et al. 1999; Adamson, Thammawat et al. 2012). My hypothesis is that HS-octa will be more bio-available when incorporated into liposomes than it is in solution, and therefore more likely to form inhibitory multivalent interactions with HS-binding viruses.

Decoy liposomes functionalized with HS-octa blocked RSV and HSV infectivity, and the degree of inhibition depended on the mole percent of HS-octa. Decoy liposomes with 3 mol% of HS-octa did not significantly inhibit RSV, but decoy liposomes with 7.5 mol% HS-octa significantly inhibited RSV infectivity at higher concentrations tested, reaching an IC_{50} at 1 μ M HS-octa. Increasing to 10 mol% HS-octa lowered the IC_{50} to approximately 0.2 μ M HS-octa. Decoy liposomes with 30 mol% HS-octa, the highest mole percent tested, had the most profound effect, blocking 76% of RSV infectivity at 0.01 μ M HS-octa, and achieving an approximate IC_{50} at 0.004 μ M HS-octa. None of the other HS-octa decoy liposomes tested inhibited RSV at all when used at such low concentrations of HS-octa.

All of the inhibitory decoy liposomes containing HS-octa inhibited RSV to a greater extent than the building block, HS-octa in solution. Furthermore, decoy liposomes containing 10 mol% HS-octa were as effective as full length heparin at inhibiting RSV, and decoy liposomes with 30 mol% HS-octa inhibited RSV one to two logs better than the full-length heparin. These data suggest that the 10 mol% HS-octa liposomes can make the same quantity and quality of interactions with RSV as can the full-length molecule, despite the difference in chain length. In addition, increasing the percentage of glycan percentage to 30 mol% HS-octa allows even more interactions with RSV, making it an even more potent inhibitor.

HS-octa decoy liposomes are also strong inhibitors of HSV. Like RSV, the degree of inhibition depends on the percentage of HS-octa incorporated into each liposome. I focused on 10 and 30 mol% HS-octa liposomes because they were the most effective RSV inhibitors. Decoy liposomes with 10 mol% and only 0.01 μM HS-octa significantly inhibited HSV infectivity, and inhibition increased to 75% 10 μM HS-octa. With an IC_{50} of 1 μM HS-octa, these decoy liposomes inhibited better than HS-octa in solution, which never attained 50% inhibition, even at 40 μM HS-octa. Decoy liposomes with 30 mol% HS-octa inhibited to the greatest extent, achieving an IC_{50} near 0.003 μM HS-octa. Decoy liposomes with 30 mol% and 0.01 μM HS-octa inhibited three times the amount of HSV as decoy liposomes with 10 mol% HS-octa and twice the amount of HSV as full-length heparin at similar concentrations. As seen above with RSV, liposomes with higher mole percentages of HS-octa are more effective inhibitors of HSV, despite the fact that there are fewer liposomes per volume when used at equimolar concentrations. These data demonstrate that decoy liposomes can be made to inhibit additional pathogens, as long as their target glycan is known.

The data presented above demonstrate that HS-octa decoy liposomes inhibit the initial infection step. To examine replication over subsequent rounds of infection, I tested decoy liposomes with HS-octa against RSV and HSV in an environment that allows for continued viral replication. In order to investigate whether the decoy liposomes inhibit viral replication, I infected Vero cells with RSV before adding liposomes (Figure 5.3A). Post-infection treatment of decoy liposomes with either 10 mol% or 30 mol% resulted in a significant reduction of viral titers as compared to control liposomes, albeit to a lesser extent than co-incubation treatment. Decoy liposomes inhibited to a greater degree when they were co-incubated with RSV before infection (Figure 5.3B). Decoy liposomes containing either 10 mol% or 30 mol% HS-octa

significantly reduced RSV titers, and the highest dose of 30 mol% HS-octa liposomes reduced RSV titers to the lower limit of detection (Figure 5.3B). The difference of decoy liposome inhibition seen between post-infection and co-incubation most likely represents neutralization of the infecting inoculum and not inhibition of subsequent RSV replication. It is possible that therapeutic treatment will have limits due to RSV's syncytia method of spreading; an RSV infected cell can fuse with cellular membranes from surrounding uninfected cells, without requiring virus to enter the supernatant, making inhibiting viral spread more difficult.

HS-octa decoy liposomes also impede HSV replication and spread. When co-incubated with a high dose of HSV (10 MOI), decoy liposomes with 30 mol% and at least 10 μ M HS-octa protected Vero cell monolayers from HSV-induced lysis. A ten-fold lower dose of virus, 1 MOI, decoy liposomes with 30 mol% and as little as 1 μ M HS-octa blocked HSV replication. Equivalent amounts of control liposomes did not block cell death at either HSV dose. These data have the caveat of co-incubation before infection and therefore may represent, at least in part, neutralization of the initial inoculum. For a true measure of inhibition to be obtained, this experiment needs to be performed with HSV infection before liposome treatment.

The data described here demonstrate that HS-octa incorporated into decoy liposomes allows for optimal binding of HS-octa and HS-binding viruses, most likely by glycolipid migration through the liposome membrane. Independent movement through the fluid bi-layer increases availability of virus binding motifs per liposome, unlike full-length HS-GAGs, which must move as a unit. When one section of the full-length HS is bound, the rest of the chain has significant movement constraints, resulting in sub-optimal confirmations for additional HBS binding. The reduction of HS chain length and incorporation into liposomes results in an increase in bio-availability of the binding motifs, despite the reduction of the total number of

theoretical binding moieties on the full-length HS. This increase of binding partners is what I hypothesize to be the driving force behind the additional inhibition seen with my decoy liposomes; their method of action is from binding and providing steric interference of virus attachment and fusion proteins so that they cannot infect cells.

The data presented here demonstrate that the glycolipid can be exchanged so that the resulting decoy liposomes will bind and inhibit a new virus, or in the case of HS-octa decoy liposomes, a set of viruses. This offers a promising start to describing the inhibitory properties of HS-octa decoy liposomes to two important HS-binding viruses. However there are many more, such as HIV, Ross River virus, and Venezuelan equine encephalitis virus to name only a few. I fully expect HS-octa decoy liposomes to be inhibitory against these viruses as well. Furthermore, exchanging the decoy glycolipid will allow decoy liposomes to target even more viruses in the future.

Chapter VI

Conclusions and Future Directions

I have endeavored to extend the knowledge of the chemistry and applicability of decoy drugs with decoy liposomes. My results in chapters 3 through 5 show that decoy liposomes can be used effectively to target important pathogens such as IAV, RSV and HSV. In addition I demonstrate here that the liposome platform can be modified to create decoys that neutralize additional pathogens with additional decoy glycolipids. It was previously shown that monomeric LSTc and LSTa tightly bind to IAV HA, and that an SA-containing polymer binds to HA more tightly than the monomeric building block. These previous studies led us to incorporate LSTc into decoy liposomes, thus increasing the valency of SA, so that it inhibits IAV infectivity better than monomeric SA and SA-containing polymers. Furthermore, work presented here shows that the liposome formulation can be modified in many ways to enhance or hinder inhibition. In particular, increasing liposome size and including cholesterol increased the liposomes' efficacy as a decoy platform. In addition, our collaborators changed the decoy glycan to create decoy liposomes that target different pathogens. Overall, the findings presented here demonstrate that the receptor-binding pocket is a valid and important therapeutic target, not only for IAV but also heparin binding viruses and suggest that decoy liposomes could be made with additional glycolipids to target more viruses and possibly any pathogen with a well-defined host receptor, including bacteria and protozoa.

In chapter 3, I examined the ability of LSTc-containing decoy liposomes to bind and inhibit IAV. The field of antiviral therapeutics has been largely devoted to small molecule inhibitors that make high affinity, specific binding events to their target, for example the

neuraminidase inhibitors. However, a second class of inhibitors, decoy receptor molecules, has slowly been gaining attention. Decoy receptors rely on many, weak-affinity binding events to create an overall strong interaction. Indeed, many biological processes utilize this multivalent interaction mechanism, especially when involving protein–carbohydrate interactions (Kießling and Pohl 1996). Many studies have shown that during IAV infection, a multivalent interaction between HA and SA is required for efficient viral binding (Kießling and Pohl 1996). In most of these studies multivalency was achieved by attaching SA to a polymer backbone. Several groups have used SA-containing liposomes to achieve the multivalency (Kingerywood, Williams et al. 1992; Spevak, Nagy et al. 1993; Sun, Kanie et al. 2000; Guo, Sun et al. 2002). The liposome chemistry and SA linkages were different in each study and the results varied. In all cases, the decoy liposomes were an improvement over the monomeric building block (if tested) and other monomeric SA in the literature.

While the decoy liposome studies showed that liposomes could be used to achieve polymer-like multivalency, they also demonstrated much room for improvement. The previous studies all used an SA residue linked either directly to the lipid backbone, or to a steric linker. Here, SA linked to a long sialylated glycan increased binding to multiple subtypes of HA (Chandrasekaran, Srinivasan et al. 2008; Xu, Newhouse et al. 2009). Indeed LSTc-containing decoy liposomes were able to bind and inhibit both H3N2 as well as H1N1 IAV, whereas Sun *et al.* (2000) could not inhibit H1N1 PR/8 IAV with their single SA residue glycolipid. Furthermore, all but two studies performed only HAI assays with their SA-containing decoy liposomes. HAI is a fast and efficient method to test competitive binding, but hemagglutination inhibition does not always correlate to infectivity inhibition (Gamian, Chomik et al. 1991). Spevak *et al.* (1993) tested their liposomes against H3N2 IAV, but had conflicting results

between decoy liposomes that inhibited infectivity and those that blocked hemagglutination. This discrepancy may be due to the chemical make up and techniques used for construction. Their lipid backbone contained only one acyl chain, which would allow for tighter packing of the lipid tails, and they were irradiated to create ellipsoid liposomes, which have an area of high curvature around the plane of ellipse and a corresponding area of low curvature. The higher degree of lipid packing and uneven curvature may have contributed to their inconsistent data. Taking all of these data together, I hypothesized that a decoy liposome formulation with low curvature and highly fluid lipids and containing lipid linked LSTc would bind many strains of IAV and block infection.

The LS-Tetrasaccharide family has been shown to bind tightly to multiple subtypes of HA (Eisen, Sabesan et al. 1997; Skehel and Wiley 2000; Ha, Stevens et al. 2001; Russell, Stevens et al. 2006), and its binding conformation has been detailed for both human- and avian-adapted viruses (Xu, Newhouse et al. 2009). Indeed Pritchett *et al.*, (1987) used LSTc as a monomeric decoy inhibitor of IAV and saw relatively strong HAI inhibition, as compared to other monomeric SA decoys. I examined whether inclusion of LSTc (or for α 2-3 SA binding viruses, LSTa) into liposomes would increase the inhibition properties by creating a polymer-like decoy capable of multivalent interactions with IAV. The LSTc-containing decoy liposomes had HAI IC₉₀ in range for the H3N2 viruses tested, and better IC₉₀ for PR/8 IAV than other decoy liposomes. The inhibitory concentrations were better than all monomeric and most SA-containing polymer decoys. The binding data alone demonstrate that the LSTc decoy liposomes were able to create strong, multivalent interactions with IAV. Furthermore, the decoy liposomes inhibited infectivity, attaining IC₅₀ concentrations in a very tight range to the concentrations detected in the HAI assay, unlike previous work, that required more decoys to inhibit infectivity

than HAI (Spevak, Nagy et al. 1993). The infectivity inhibition seen here showed that an increasing mole percentage of LSTc per liposome correlated to increased inhibition, where previous work saw a disconnect between HAI and infectivity (Spevak, Nagy et al. 1993). Our data also saw a plateau of efficacy when increasing the mole percent of LSTc to at least 7.5 mol% into decoy liposomes. Decoy liposomes with 10 mol% LSTc or more per liposomes had no significant improvement over the inhibition seen with 7.5 mol% LSTc decoy liposomes as others have also seen (Spevak, Nagy et al. 1993).

Our LSTc decoy liposomes also formed stable, long-term interactions with virus. As shown *in vitro*, when decoy liposomes were mixed with virus and left in the presence of replicating virus, they were able to prevent IAV spread. As seen *in vitro*, when premixed with virus before inoculation decoy liposomes significantly extended survival *in vivo*. Protection was restricted to premixing virus and liposomes. When administered before or after infection, the doses we were able to deliver were not sufficient to protect from an IC₉₀ dose of virus. This difference in protection is most likely due to the immense surface area of the lung and the liposomes would be diluted significantly when given in a small volume to mice. This could be remedied by using a higher dose of liposomes, but unfortunately our collaborators have not been able to produce sufficient decoys to perform these studies.

These data demonstrate the need to optimize the liposome formulation for better inhibition. In chapter 4, I present a number of adaptations to the liposome formulation designed to improve viral infectivity inhibition. Incorporation of cholesterol and increasing liposome size produced the most dramatic improvement in liposome efficacy. Addition of the NAI oseltamivir increased virus replication inhibition by decoy liposomes, demonstrating synergy. Of note, the SA linkage in monomeric LSTc is cleavable by IAV neuraminidase. NA cleavage of decoy

receptors has hampered the IAV decoy field since its inception. SA decoys with linkages resistant to NA inhibit IAV better than sensitive parent molecules (Guo, Sun et al. 2002). Improving my LSTc-decoy liposomes to make them NA resistant would be a very interesting avenue to pursue in future studies.

Mixing decoy liposomes with different IAV receptors improved efficacy over that of a single decoy liposome population alone. Many IAV strains emerging from avian or swine circulation can infect humans, and bind to both α 2-6 and α 2-3 linked SA. Therefore, I challenged IAV with a mix of decoy liposomes presenting both SA linkages. Infectivity inhibition was synergistic when both types of SA were used, suggesting that the decoy liposome platform may be useful for targeting newly emergent strains, to which a vaccine has not yet been created. Novel, antigenically different IAV isolates still bind to either the canonical α 2-6 or α 2-3 linked SA (Glaser, Stevens et al. 2005; Pappas, Viswanathan et al. 2010; Lin, Xiong et al. 2012). A newly emerged, potentially pandemic IAV strain may spread rapidly when there is little pre-existing immunity (Dawood, Iuliano et al. 2012). The decoy liposomes described here, if stockpiled in advance, could theoretically be used against future novel antigenic strains.

The liposome platform may also be able to function as a second-generation glycan array. Glass coverslip fixed arrays do not allow for proper display of glycans, and incorporation of a wide range of SA-containing molecules could be used to quickly assay the binding preference of a new clinical IAV isolate. Recent work has shown that a colorimetric assay can be used with LSTc and LSTa dendrimers (Hobbie, Viswanathan et al. 2013). Using decoy liposomes as a monitoring platform would be an exciting new application, if effective.

The liposome backbone can be further adapted to target other pathogens by linking any defined receptor to the lipid backbone. Here I present data that demonstrate neutralization of

additional pathogens with heparan sulfate octasaccharide functionalized decoy liposomes. Decoy liposomes containing HS-octa are able to inhibit the HS-binding viruses RSV, HSV and PIV3, in much the same manner as seen with IAV and LSTc decoy liposomes. A mole percent incorporation series of HS-octa into liposomes showed a positive correlation between amount of HS-octa decoy molecule included per liposome with the amount of infectivity inhibition for RSV and HSV. Unlike LSTc decoy liposomes, there was no inhibition plateau at middling levels of HS-octa - the highest mole percent attempted, 30 mol% HS-octa, inhibited both viruses to the largest extent. This difference is possibly due to the size of each HS-octa chain. HS-octa has a molecular weight of 2,500 and extends eight sugar residues away from the liposome surface, whereas LSTc has a molecular weight of 1,000 and extends only five residues from the liposome surface. Additionally, HS-octa has a higher negative charge density than LSTc, and this may increase the order of HS-octa glycolipids on the surface before encountering virus. The negative charge of HS-octa would be neutralized when bound to virus, due to the charged amino acids in the viral HBD, allowing for re-ordering and more fluidity of the remaining un-bound HS-octa on the liposome surface.

When decoy liposomes were added to cell monolayers, infected with RSV, inhibition of spread was only modest. This is possibly due to RSV's method of spreading via syncytia fusion with cell-to-cell spread without virion release (Gower, Pastey et al. 2005). HS-octa decoy liposomes were able to block a large inoculum of HSV virus from replicating and killing Vero cells, to date this experiment has only been done with premixing virus and liposomes. HS-octa apparent binding constants can be approximated by inhibition of a hemagglutinating virus. HAI of PIV3 demonstrated that decoy liposomes with 30 mol% HS-octa had an IC_{90} of 20 μ M HS-octa, representing a roughly 20 fold increase over full-length heparin. The HS-octa building

block in solution did not inhibit agglutination at the highest concentration tested, which was also true for monomeric LSTc, so both types of decoy liposomes saw significant efficacy over their free building blocks. These data demonstrate that decoy liposomes can be adapted to additional viruses. The number of viruses and bacteria that have known glycan receptors is quite large, and HS-octa liposomes can theoretically target at least 25 viruses, including HIV (Zhu, Li et al. 2011). In the near future it would be interesting to characterize decoy liposome inhibition of additional HS-binding viruses and greatly expand the number of decoy molecules incorporated into liposomes, creating an adaptable platform capable of targeting many pathogens.

The data presented here demonstrate that decoy liposomes can inhibit viruses in a species-specific manner and can be created to target different viruses. However, these decoy liposomes are not an anti-viral silver bullet. The liposome platform has a number of substantial hurdles that must be overcome before they can become more than a promising concept. The majority of the inhibition data demonstrated here was obtained under optimized conditions, where virus and decoy liposomes were premixed before addition to target cells. The decoy liposomes are inhibitory when premixed, but the inhibition is greatly reduced or completely eliminated (data not shown) when decoy liposomes are added after or at the exact same time as IAV. Likewise *in vivo*, adding LSTc decoy liposomes either before, or after IAV infection did not protect mice as compared to mice that received control liposomes (Figure 3.11). The lack of inhibition in these experiments may be a kinetic or dosing issue. The decoy liposome were created in order to mimic the glycan topology of cellular SA, but cell-associated SA may form a better interaction with IAV when presented to virus at the same time, and therefore may outcompete the decoy liposomes.

It is also possible that when adding decoy liposomes after or at the same time as infection, a higher dose may be required to see similar levels of inhibition as seen with premixing. One drawback that has hampered this body of work is that decoy liposomes are not small molecule inhibitors and they require a number of purification and chemical synthesis steps, and have been at times of limited supply. And unfortunately, some avenues of investigation were not pursued due to a lack of decoy liposomes. Another drawback of decoy liposomes is their ability to be used in an efficient manner in some infection routes. Respiratory infections are ideal targets for decoy liposomes because they can be easily administered into the lungs. Other possible liposome delivery models include intravenous (Immordino, Dosio et al. 2006) and intracranial (Krauze, Noble et al. 2007) routes, but decoy liposomes have yet to be tried in these models. Decoy liposomes may not be well suited for treating other infectious agents, for example, decoy liposomes may not be effective for dermal infections, such as HSV dermatitis. In addition, to be long-lasting in the circulation, liposomes should be PEGylated, and I have shown here that PEGylation reduces the currently formulated LSTc-DOPE decoy liposomes.

Overall, the data presented in this dissertation demonstrate the validity and utility of decoy liposomes to target and neutralize a highly conserved region on viruses, the receptor binding site. Here I present data on inhibiting IAV, RSV and HSV infectivity. With additional study, I believe decoy liposomes could be used against additional viruses, bacteria and other pathogens. Maturation of liposome science, along with research into the best binding ligands for pathogens could bring the efficacy of decoy liposomes on par with small molecule inhibitors and may be a valid therapeutic for sick patients.

Appendix A

RIP3-dependent programmed necrosis is required for a proper danger signal during influenza A virus infection

The following data is from other IAV research I conducted while in the Finberg and Kurt-Jones laboratory. While it is important research on the biology of IAV infection, it is not an integral component to the data presented in this dissertation and will not be submitted for publication in its current state. However, it represents an initial foray into the field of programmed necrosis and IAV disease that may impact future research done in the lab.

I would like to thank the following researchers who helped me in this project. Dr. Francis Chan, PhD (University of Massachusetts Medical School, Worcester, MA) for kindly provided the RIP3 knockout mice, Anna Cerny for genotyping and animal husbandry, and Dr. Susan Swain (University of Massachusetts Medical School, Worcester, MA) for mouse-adapted PR/8 IAV.

Introduction

Influenza normally presents as a self-limiting upper respiratory tract infection. Scientists have elucidated many of the innate and adaptive immune pathways critical for response to IAV. The virus undergoes lytic replication in pulmonary epithelial cells, stimulates a robust proinflammatory cytokine response, and results in a large leucocyte influx into the lungs. Leukocytes and cytokines activate and mature DCs, which help activate IAV-specific B-cells which finally clear the infection (Seibert, Rahmat et al. 2013). Programmed necrosis is a proinflammatory death process, unlike apoptosis, which is anti-inflammatory, and has been described to be important during viral infections, including vaccinia virus (Cho, Challa et al. 2009), murine cytomegalovirus (Upton, Kaiser et al. 2010), mouse hepatitis virus and lymphocytic choriomeningitis virus (Mocarski, Upton et al. 2012). Programmed necrosis is an actively mediated cell death pathway, dependent on receptor-interacting protein (RIP) 1 and RIP3. IAV, like many important viruses, modulates the host apoptosis mechanism for its own advantage, and RIP3-dependent necrosis may be an especially important mechanism of cell death when apoptosis is blocked in infected cells (Mocarski, Upton et al. 2012). RIP3-dependent necrosis can be activated by death receptors of the TNF Receptor (TNFR) superfamily, as well as by TNFR-independent pathways during viral infection (Mocarski, Upton et al. 2012). RIP3 knockout mice are unable to undergo programmed necrosis, while having normal immune activation. The data presented here will delve into the requirement of RIP3-dependent necrosis for an immediate innate anti-IAV immune response.

Materials and Methods

Mouse infection and lung collection – Sex matched C57BL/6 wild type mice were purchased from the Jackson Laboratory (Bar Harbor, ME). RIP3^{-/-} mice were bred in-house. Mice were 8 to 10 weeks of age at the time of infection. Mice were infected with 490 HA units of PR/8 IAV either by the intranasal route (for histology studies) or by the intratracheal route (for all other studies). Mice were given an overdose of anesthesia and lungs were removed.

Histopathology – Lungs from infected and mock mice were removed as described above, except they were first inflated with 10% buffered formalin, removed and fixed for 24 h in 10% buffered formalin in tissue Tek histology cassettes. Sectioning and H&E staining was performed by the University of Massachusetts Medical school DERC core facility.

Collection and analysis of BAL cells – Mice were infected as described above, except as noted. Three days post-infection, mice were given an overdose of anesthesia, and BAL cells were harvested by lavaging the lung four consecutive times with one mL of PBS. BAL cells from each individual mouse were kept separate as biological repeats, n = 3 per infected genotype and n = 1 per naïve genotype. BAL cells were stored on ice before use. BAL cells were pelleted by centrifugation at 1400 rpm for 5 minutes and counted. Cells were stained for the following groups of surface markers, either (1) FITC conjugated Ly-6G, PE conjugated CD11b, APC conjugated 7/4 and PacBlue conjugated F4/80 or (2) FITC conjugated Nk 1.1, PE conjugated CD11b, APC conjugated CD11c and PacBlue conjugated B220. Cells were analyzed as described in Chapter 2.

Viral titers and cytokine lungs – Mice were infected and lungs were harvested as described above. Excised lungs were frozen in 300 μ L sterile PBS at -80°C prior to use. Lung samples were thawed on ice, homogenized and clarified. Viral titers were attained by serial dilution of the samples, and assayed as described in chapter 2. Cytokine levels were assayed from the clarified lung homogenates by commercial ELISA kits according to the manufacture's instructions.

Myeloperoxidase levels – Lungs were harvested from infected mice as described above, except for the following. Lungs were harvested days 1 and 3 post-infection. Lungs were homogenized, clarified at 10,000 rpm for 15 minutes at 4°C . Lung pellets were resuspended in hexadecyl-trimethyl ammonium bromide, sonicated and snap frozen to crack the tissue homogenate. MPO rates were determined with O-dianisidine dihydrochloride and absorbance was read at 450 over a period of thirty minutes to obtain a rate of MPO activity.

RIP3-dependent programmed necrosis is required for a proper danger signal during influenza A virus infection

Results

RIP3^{-/-} mice have increased pulmonary pathology after IAV infection

To investigate the quality of their immune response to IAV, I infected RIP3^{-/-} or littermate controls with PR/8 IAV by intratracheal delivery and removed lungs three days post-infection for histopathology analysis. RIP3^{-/-} mice had similar overall gross lung morphology, with the same lung area affected by infection (Figure 1). However, RIP3^{-/-} mice had exacerbated local pathology foci, and enhanced inflammatory cuffing, or cellular debris in the large airways (Figure 2A and B). RIP3 knockout mice also had large areas of perivascular nuclear dust, a sign of inflammation and cell death, often from infiltrating neutrophils (Figure 2C) that were not present in the wild type lungs. Finally, RIP3^{-/-} lungs had signs of vasculitis and vessel wall breakdown, while the wild type did not (Figure 2D and E). Taken together, these data demonstrate that RIP3^{-/-} mice have worse pathology after infection and suggest that the lack of RIP3-dependent necrosis puts them at a significant disadvantage when challenged with IAV.

RIP3^{-/-} mice have higher viral titers from IAV infection

To investigate the disparity of the lung pathology seen between RIP3^{-/-} mice and littermate controls, I tested the extent of viral replication in the lungs of infected mice. I harvested lungs from RIP3^{-/-} and wild type infected mice one and three days post infection and titrated lung homogenates on MDCK cells (Figure 3). RIP3^{-/-} and wild type mice had similar pulmonary titers one day post-infection (Figure 3.A) but, 3 days post-infection, RIP3^{-/-} mice

Figure 1. Wide field H&E staining of infected mouse airways.

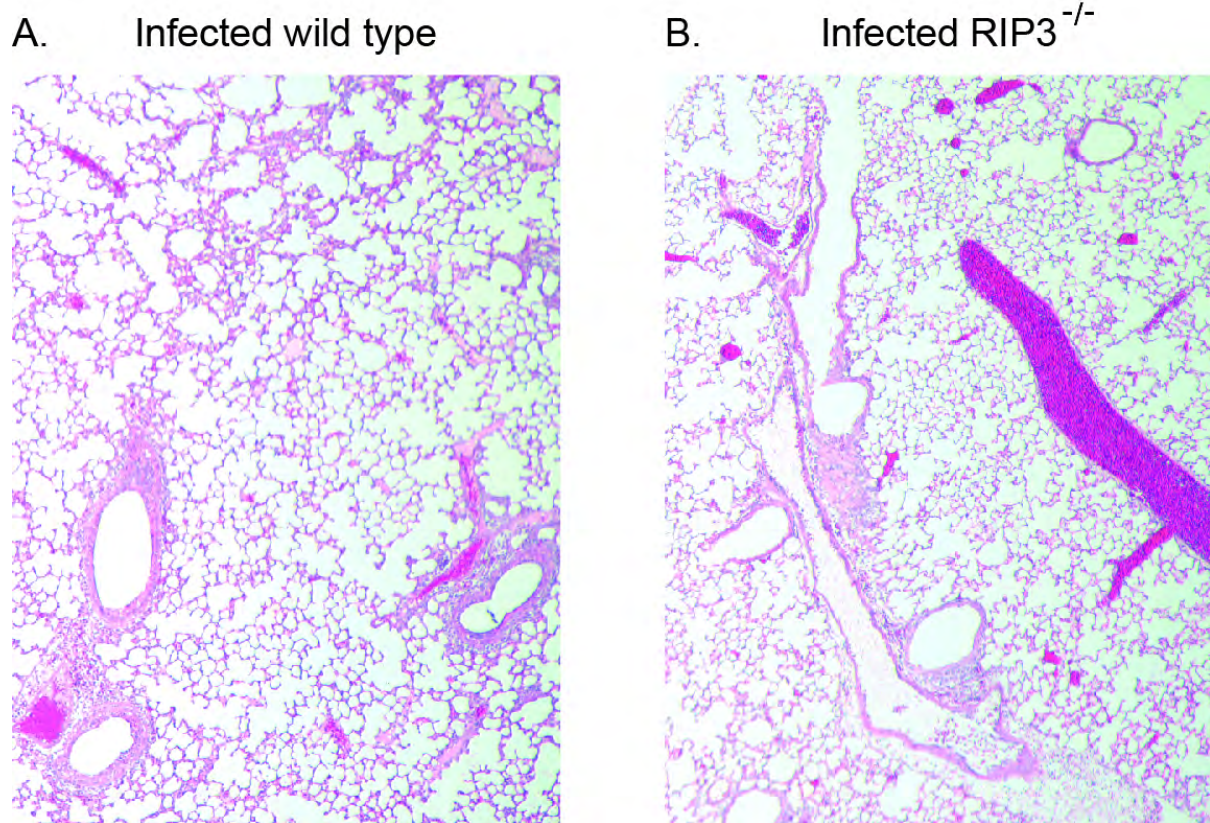


Figure 1. Wide field H&E staining of infected mouse airways.

Groups of wild type mice (**A**) and RIP3^{-/-} mice (**B**) were infected with PR/8 IAV, lungs were inflated, removed and fixed in buffered formalin. Tissue sections were prepared as described in Materials and Methods and stained with eematoxylin and eosin (H&E). Images were acquired with the same camera settings, at 20X magnification and adjusted for size and contrast using Adobe Photoshop, using the same settings for both.

Figure 2. Detailed H&E staining of infected mouse lungs.

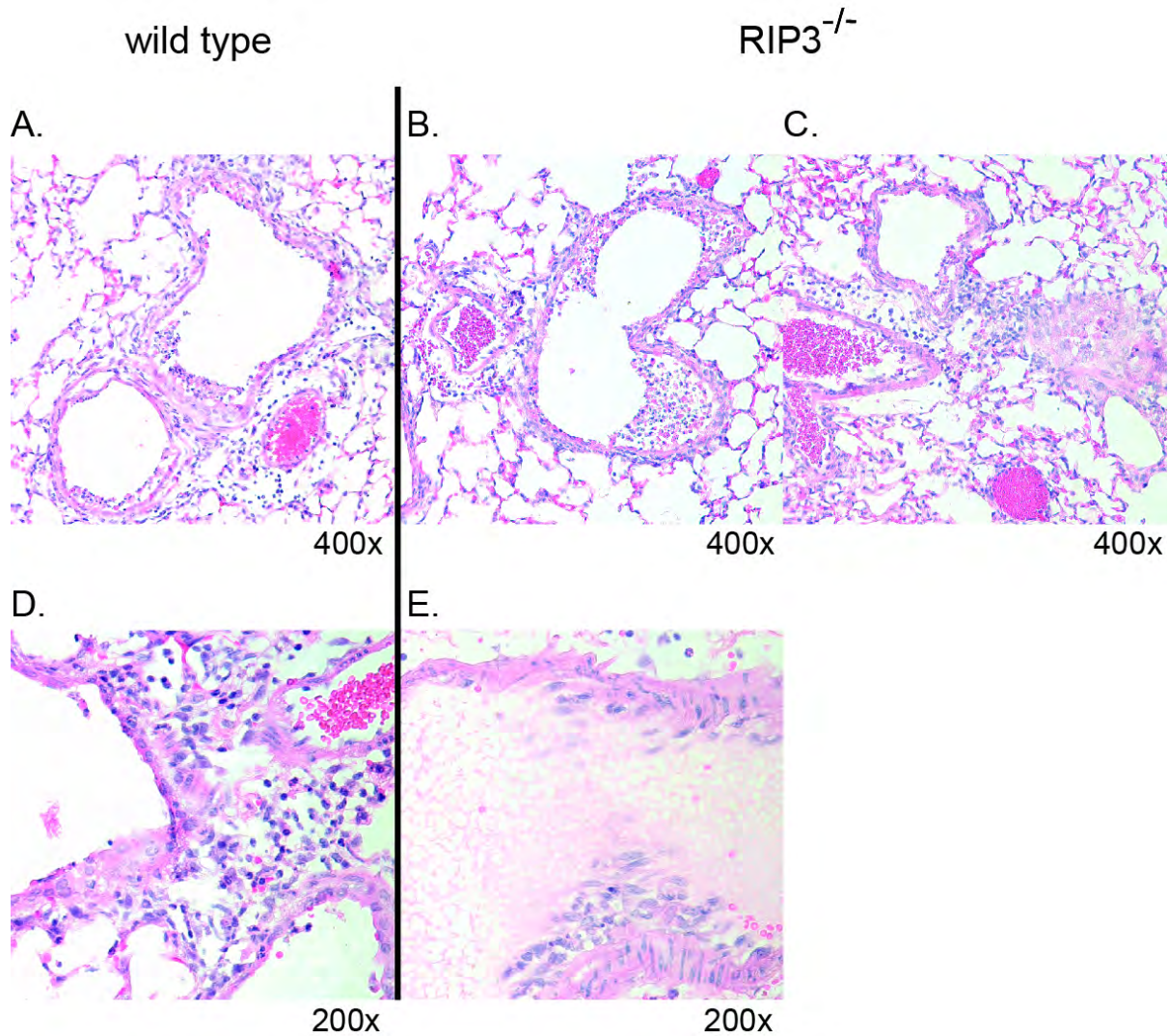


Figure 2. Detailed H&E staining of infected mouse lungs.

Groups of wild type mice (**A and D**) and RIP3^{-/-} mice (**B, C and E**) were infected with PR/8 IAV, lungs were inflated, removed and fixed in buffered formalin. RIP3^{-/-} mice had enhanced inflammatory cuffing (**B**), large areas of perivascular nuclear dust (**C**), and vasculitis (**E**). Tissue sections were prepared as described in Materials and Methods and stained with H&E. Images were acquired at either 400X (**A-C**) or 200X (**D, E**). Images were acquired with the same camera settings, at the magnification listed and adjusted for size and contrast using Adobe Photoshop, using the same settings for all images.

Figure 3. RIP3^{-/-} mice have higher viral titers after IAV infection

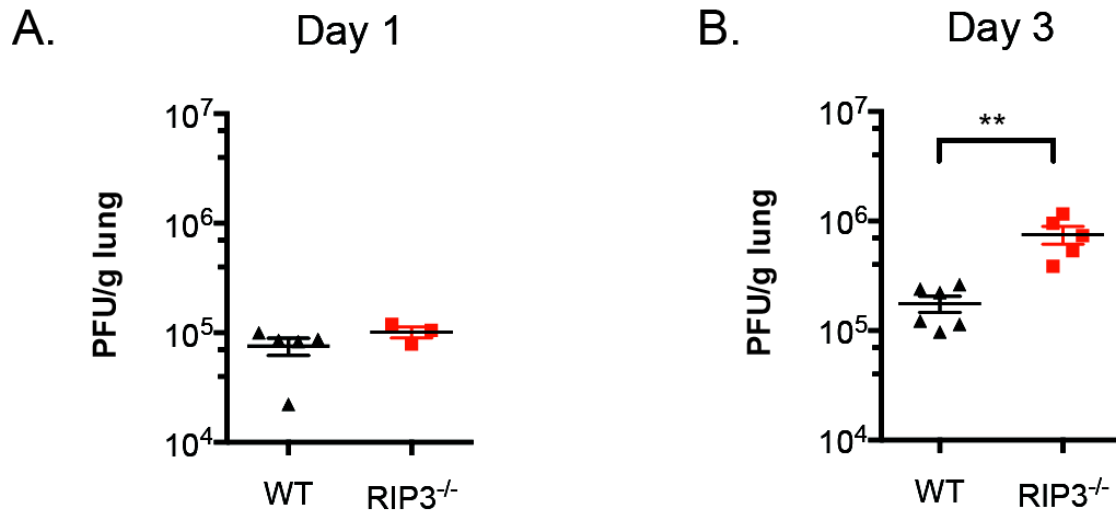


Figure 3. RIP3^{-/-} mice have higher viral titers after IAV infection

Groups of wild type mice (WT, **black triangles**) and RIP3^{-/-} mice (**red squares**) were infected with PR/8 IAV, lungs were removed one (**A**) (WT n =5 and RIP3^{-/-} n=3) or three (**B**) (WT n =6 and RIP3^{-/-} n=5) days post-infection and assayed for infectious virus by plaque assay. The data represent the average of at least five biological replicates ± S.E. of one experiment.

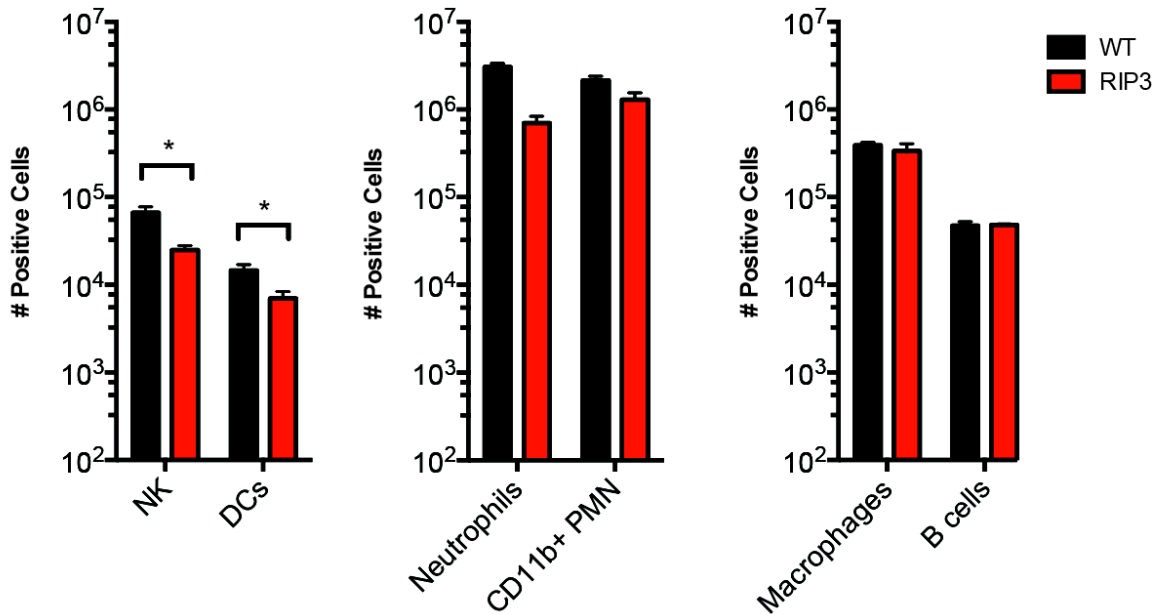
had significantly higher viral titers (RIP3^{-/-}: $7.5 \times 10^5 \pm 1.4 \times 10^5$ PFU/ml vs. WT: $1.8 \times 10^5 \pm 3.0 \times 10^4$ PFU/ml, $p \leq 0.01$) (Figure 3.B). This suggests that RIP3^{-/-} mice cannot control viral replication to the same extent as wild type, and suggesting that the exacerbated pathology is due to a delayed immune response in knockout mice.

RIP3^{-/-} mice a dysregulation of pulmonary infiltrates after IAV infection

Next, I examined the immune infiltrate in RIP3^{-/-} and wild type infected lungs in order to measure the degree of immune activation. I infected mice with PR/8 and removed the lung airway associated cells by bronchoalveolar lavage (BAL) three days post-infection (Figure 4A). RIP3^{-/-} mice had significantly fewer NK cells (RIP3^{-/-}: $2.5 \times 10^4 \pm 3 \times 10^3$ vs. WT: $6.7 \times 10^4 \pm 1 \times 10^4$ cells, $p \leq 0.05$) and fewer CD11b⁺, CD11c⁺ dendritic cells (RIP3^{-/-}: $1.9 \times 10^4 \pm 3 \times 10^3$ vs. WT: $3 \times 10^4 \pm 3 \times 10^3$ cells, $p \leq 0.05$) (Figure 4A left panel). RIP3^{-/-} mice also had slightly fewer neutrophils (PMNs, 7/4 and Ly6G double positive), but the difference was not significant ($p = 0.07$). Furthermore, wild type and RIP3^{-/-} mice had the same levels of activated PMNs (7/4, Ly6G and CD11b triple positive) (Figure 4A middle panel), pulmonary macrophages (F4/80 and CD11b double positive), and B-cells (B220 positive) (Figure 4A right panel). The differences in BAL leukocytes are not overly dramatic, but NK cells are thought aid in the early lysis and control of IAV infected cells. DCs are important for priming the adaptive immune response. The decrease of these two populations may explain the higher viral titers and histopathology in RIP3^{-/-} mice. In addition, at this time point post-infection, a sizable portion of leukocytes may be in the perivascular space, which a BAL would not collect, and RIP3^{-/-} mice may have less perivascular leukocytes as well.

Figure 4 RIP3^{-/-} mice have dysregulated leukocyte influx after IAV infection.

A.



B.

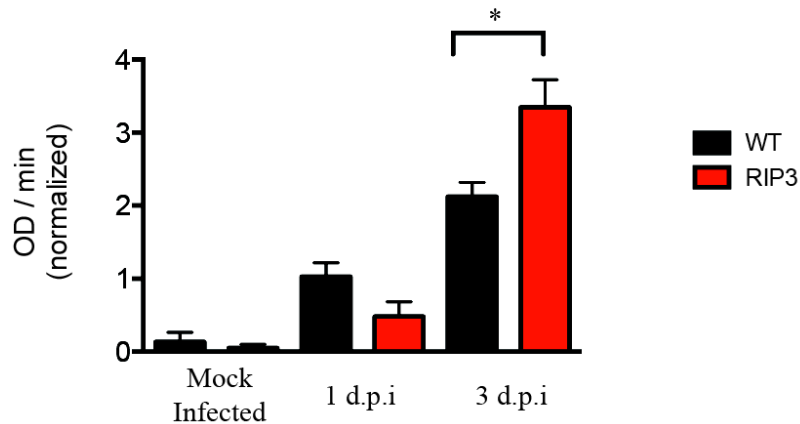


Figure 4 RIP3^{-/-} mice have dysregulated leukocyte influx after IAV infection.

A, Wild type (**black**) and RIP3^{-/-} mice (**red**) were infected with PR/8 IAV and BALs were harvested three days post infection, three mice per group. BAL cells were kept as independent samples and stained for the leukocyte surface markers as described in Materials and Methods. Cells are expressed as number of cells based on the percent positive cells of the total counted cells. **B**, Wild type and RIP3^{-/-} mice lungs were harvested one or three days post infection and tested for MPO activity. Mock-infected mice received saline.

FACs analysis of BAL cells will also overlook dead cells. It is possible that RIP3^{-/-} mice have increased amounts of non-programmed cell death, which could result from lytic IAV replication. Therefore, to investigate the total number of PMNs, dead and alive, I assayed wild type and RIP3^{-/-} lungs for myeloperoxidase (MPO) levels (Figure 4B). MPO is a peroxidase enzyme highly expressed in PMNs. MPO can be tested as an indirect readout of the number of PMNs in a tissue. Without infection, RIP3^{-/-} lungs had normal MPO levels, identical to wild-type lungs. After infection, MPO levels increased for both RIP3^{-/-} and wild type, but one day post-infection, lungs from RIP3^{-/-} mice had slightly less MPO (RIP3^{-/-}: 0.48 ± 0.21 vs. WT: 1.03 ± 0.19 OD/min, p = 0.086). Three days post-infection, RIP3^{-/-} lungs had significantly higher MPO levels than wild type (RIP3^{-/-}: 3.34 ± 0.38 vs. WT: 2.12 ± 0.20 OD/min, p ≤ 0.01). These data suggest that RIP3^{-/-} mice may have a delayed initial response and cellular influx to IAV, followed by excessive PMN influx. Additionally, PMN cell death may be higher in the RIP3^{-/-} mice as evidenced by the higher MPO levels but lower PMN BAL numbers. Neutrophils are important during IAV infection, and a reduction of functioning pulmonary PMNs results in worse outcomes from IAV (Tumpey, Garcia-Sastre et al. 2005). Furthermore, dead PMNs may release their granule components non-specifically, causing pathology, which may be the cause of enhanced RIP3^{-/-} pathology seen above.

IAV induces less early cytokine and chemokine production in mice lacking RIP3

Proinflammatory cytokines and chemokines are required to recruit leukocytes into the infected lung, and to establish an anti-viral state. Ablation of proinflammatory cytokines during IAV infection leads to higher viral titers and lower survival (Schmitz, Kurrer et al. 2005). However, IAV isolates that stimulate excessive cytokine production, or a ‘cytokine storm’ as

seen with the 1918 pandemic IAV, cause elevated pathology and increased mortality (Tumpey, Garcia-Sastre et al. 2005; Seki, Kohno et al. 2010). Therefore I examined the pulmonary cytokine profile of wild type and RIP3^{-/-} mice after IAV infection. I found that mice lacking RIP3 had a general, delayed cytokine response to IAV (Figure 5). Several key cytokines were lower than wild type levels one day post-infection, but regained wild type levels three days post-infection. The inflammasome cytokine IL-1 α was decreased over 2 fold in knockout animals. The granulocyte growth factor, G-CSF, was decreased two and a half fold. IP-10 (CXCL10) was reduced two fold and is a chemokine for monocytes, NK cells and DCs, the latter two of which are decreased in RIP3^{-/-} mice. IL-1Ra was also significantly reduced, down two and a half fold in RIP3^{-/-} mice (Figure 5). The inflammasome cytokine IL-1 β also trended down slightly, as did the proinflammatory cytokines MCP1 and IL-6 (data not shown). All of these cytokines had come back to wild type levels three days post infection. The mouse PMN recruitment cytokine KC also trended lower one day post-infection, but unlike the other cytokines, it was significantly elevated three days post-infection (Figure 5). Together with G-CSF, this may explain the reduced numbers of live PMN in the RIP3^{-/-} mice; chemokines are recruiting PMNs, but the decreased survival signals in the lung to keep them from undergoing apoptosis. These data may explain the elevated MPO levels and decreased PMN BAL numbers three days post-infection.

Figure 5 RIP3^{-/-} mice have a delayed cytokine profile early after IAV infection.

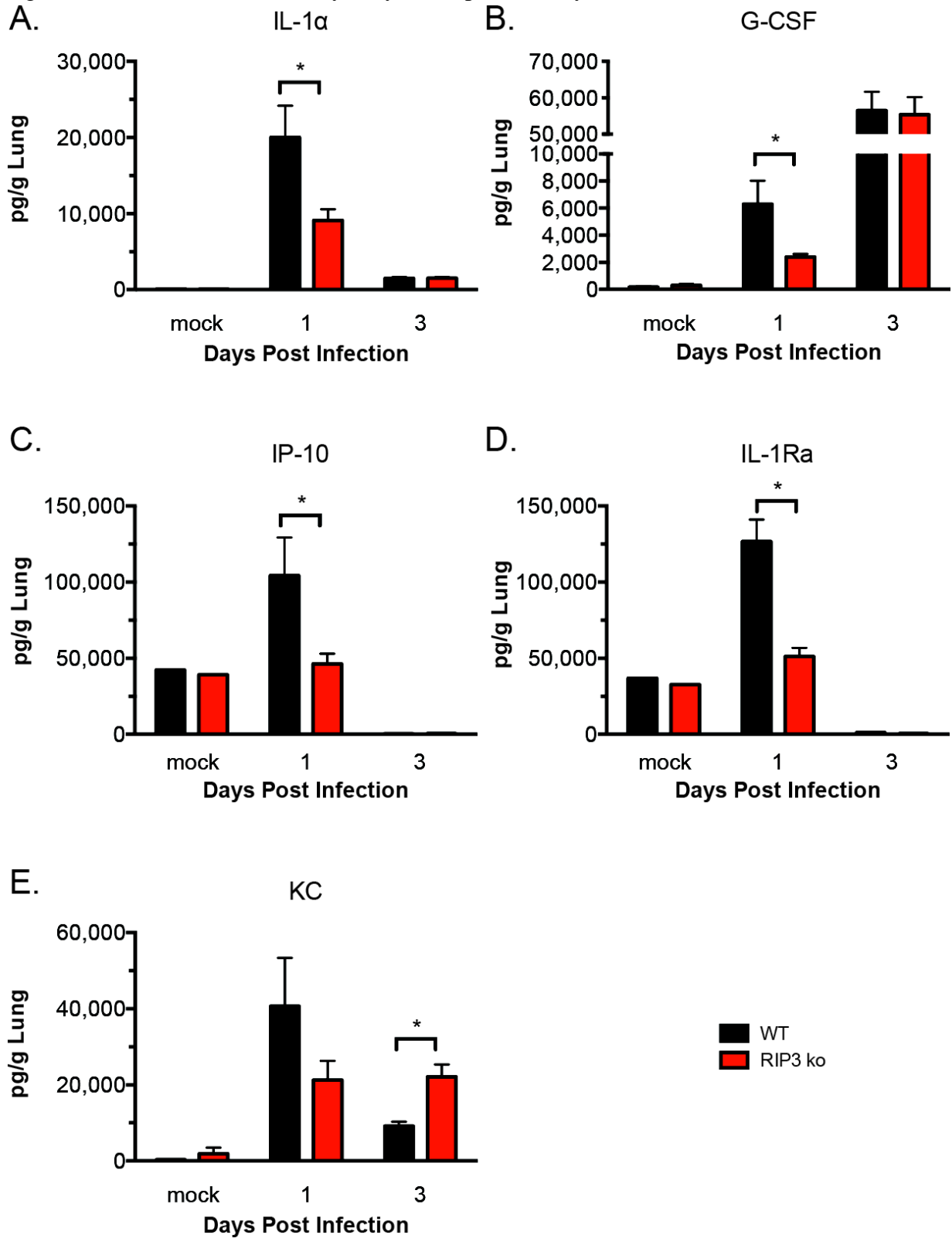


Figure 5 RIP3^{-/-} mice have a delayed cytokine profile early after IAV infection.

Wild type (**black**) and RIP3^{-/-} mice (**red**) were infected with PR/8 IAV, and lungs were harvested one or three days post infection and tested for cytokine and chemokine levels. Mock-infected mice received saline. RIP3^{-/-} mice had significantly less IL-1 α (**A**), G-CSF (**B**), IP-10 (**C**), and IL-1Ra (**D**) one day post-infection. RIP3^{-/-} mice also had significantly elevated levels of KC (**E**) three-days post infection. Each time point represents groups of at least 5 mice.

RIP3-dependent programmed necrosis is required for a proper danger signal during influenza A virus infection

Discussion

The data presented here begin to delve into the role of a specific danger signal during IAV infection. The mechanism of pathogen associated molecular patterns (PAMPs) has been well described; conserved regions of pathogens are recognized by germ-line encoded innate receptors and initiate an immune response. However, a second mechanism of immune activation has recently been elucidated, the release and recognition of danger-associated molecular patterns (DAMPs). DAMPs are specific host molecules, often nuclear or cytosolic proteins, that when released from a necrotic cell, activate bystander cells to initiate and perpetuate an immune response. Essentially they alert the immune response to danger, either from sterile injury or from a pathogen that has blocked innate immune recognition (Rubarcelli and Lotze 2007). Furthermore, RIP3-dependent necrosis has been shown to release DAMPs (Seya, Shime et al. 2012). My data generated with mice lacking RIP3-dependent necrosis demonstrate that knockout mice have elevated lung pathology, higher viral loads and a delayed cytokine response immediately following infection.

The delayed cytokine phenotype is resolved quickly, by day three post-infection, but, the delay is enough to cause a significant reduction of NK and DC cells in the infected lung, and slightly fewer neutrophils. NK cells, via the receptors NKp46 and NKp44 have been shown to bind to IAV HA, and this suggests that NK cells may be important for killing infected cells early in IAV infection (Arnon, Lev et al. 2001; Mandelboim, Lieberman et al. 2001), and DCs are the critical for priming the adaptive immune system. PMNs have also been shown to be important during IAV infection. The combined loss of cytokines and infiltrating leukocytes negatively affects the antiviral state, failing to control viral infection by three days post-infection.

The observed delay in the RIP3^{-/-} immune response was not sufficient to cause a reproducible mortality phenotype. This is due, most likely, to the many innate PRRs present in the lungs. Many PRRs are redundant, knocking out a single receptor alone does not result in an overt mortality phenotype with IAV, but ablation of both receptors significantly increases mortality (Seo, Kwon et al. 2010). Likewise, the loss of DAMP release in RIP3^{-/-} mice may not be enough to cause a reproducible mortality phenotype. In addition, the loss of cytokine production only immediately after infection is indicative of redundant PRRs signaling in RIP3^{-/-} mice compensating after viral replication increases the number of PAMPs in the lung.

References

- Adamson, P., S. Thammawat, et al. (2012). "Diversity in glycosaminoglycan binding amongst hMPV G protein lineages." *Viruses* 4(12): 3785-3803.
- Allen, I. C., M. A. Scull, et al. (2009). "The NLRP3 inflammasome mediates in vivo innate immunity to influenza A virus through recognition of viral RNA." *Immunity* 30(4): 556-565.
- Amonsén, M., D. F. Smith, et al. (2007). "Human parainfluenza viruses hPIV1 and hPIV3 bind oligosaccharides with alpha2-3-linked sialic acids that are distinct from those bound by H5 avian influenza virus hemagglutinin." *J Virol* 81(15): 8341-8345.
- Anders, E. M., C. A. Hartley, et al. (1990). "Bovine and mouse serum beta inhibitors of influenza A viruses are mannose-binding lectins." *Proc Natl Acad Sci U S A* 87(12): 4485-4489.
- Arnon, T. I., M. Lev, et al. (2001). "Recognition of viral hemagglutinins by NKp44 but not by NKp30." *Eur J Immunol* 31(9): 2680-2689.
- Asher, D. R., A. M. Cerny, et al. (2005). "The erythrocyte viral trap: transgenic expression of viral receptor on erythrocytes attenuates coxsackievirus B infection." *Proc Natl Acad Sci U S A* 102(36): 12897-12902.
- Aung, S., Y. W. Tang, et al. (1999). "Interleukin-4 diminishes CD8(+) respiratory syncytial virus-specific cytotoxic T-lymphocyte activity in vivo." *J Virol* 73(11): 8944-8949.
- Baumgart, T., S. T. Hess, et al. (2003). "Imaging coexisting fluid domains in biomembrane models coupling curvature and line tension." *Nature* 425(6960): 821-824.
- Blume, G. and G. Cevc (1993). "Molecular mechanism of the lipid vesicle longevity in vivo." *Biochim Biophys Acta* 1146(2): 157-168.
- Bolte, S. and F. P. Cordelières (2006). "A guided tour into subcellular colocalization analysis in light microscopy." *J Microsc* 224(Pt 3): 213-232.
- Bot, A., A. Holz, et al. (2000). "Local IL-4 expression in the lung reduces pulmonary influenza-virus-specific secondary cytotoxic T cell responses." *Virology* 269(1): 66-77.
- Carragher, D. M., D. A. Kaminski, et al. (2008). "A novel role for non-neutralizing antibodies against nucleoprotein in facilitating resistance to influenza virus." *J Immunol* 181(6): 4168-4176.
- Chames, P., M. Van Regenmortel, et al. (2009). "Therapeutic antibodies: successes, limitations and hopes for the future." *Br J Pharmacol* 157(2): 220-233.
- Chandrasekaran, A., A. Srinivasan, et al. (2008). "Glycan topology determines human adaptation of avian H5N1 virus hemagglutinin." *Nat Biotechnol* 26(1): 107-113.
- Cheng, P. K., A. P. To, et al. (2010). "Oseltamivir- and amantadine-resistant influenza virus A (H1N1)." *Emerg Infect Dis* 16(1): 155-156.
- Cho, Y. S., S. Challa, et al. (2009). "Phosphorylation-driven assembly of the RIP1-RIP3 complex regulates programmed necrosis and virus-induced inflammation." *Cell* 137(6): 1112-1123.
- Choi, S. K., M. Mammen, et al. (1996). "Monomeric inhibitors of influenza neuraminidase enhance the hemagglutination inhibition activities of polyacrylamides presenting multiple C-sialoside groups." *Chem Biol* 3(2): 97-104.

- Clements, M. L., R. F. Betts, et al. (1986). "Serum and nasal wash antibodies associated with resistance to experimental challenge with influenza A wild-type virus." J Clin Microbiol 24(1): 157-160.
- Coderch, L., J. Fonollosa, et al. (2000). "Influence of cholesterol on liposome fluidity by EPR. Relationship with percutaneous absorption." J Control Release 68(1): 85-95.
- Collins, P. J., L. F. Haire, et al. (2008). "Crystal structures of oseltamivir-resistant influenza virus neuraminidase mutants." Nature 453(7199): 1258-1261.
- Corti, D., J. Voss, et al. (2011). "A neutralizing antibody selected from plasma cells that binds to group 1 and group 2 influenza A hemagglutinins." Science 333(6044): 850-856.
- Cox, N. J. and K. Subbarao (2000). "Global epidemiology of influenza: past and present." Annu Rev Med 51: 407-421.
- Dawood, F. S., A. D. Iuliano, et al. (2012). "Estimated global mortality associated with the first 12 months of 2009 pandemic influenza A H1N1 virus circulation: a modelling study." Lancet Infect Dis.
- Deol, P. and G. K. Khuller (1997). "Lung specific stealth liposomes: stability, biodistribution and toxicity of liposomal antitubercular drugs in mice." Biochim Biophys Acta 1334(2-3): 161-172.
- Deyde, V. M., X. Xu, et al. (2007). "Surveillance of resistance to adamantanes among influenza A(H3N2) and A(H1N1) viruses isolated worldwide." J Infect Dis 196(2): 249-257.
- Dharan, N. J., L. V. Gubareva, et al. (2009). "Infections with oseltamivir-resistant influenza A(H1N1) virus in the United States." JAMA 301(10): 1034-1041.
- Douagi, I., C. Gujer, et al. (2009). "Human B cell responses to TLR ligands are differentially modulated by myeloid and plasmacytoid dendritic cells." J Immunol 182(4): 1991-2001.
- Eichelberger, M. C., M. L. Wang, et al. (1991). "Influenza virus RNA in the lung and lymphoid tissue of immunologically intact and CD4-depleted mice." J Gen Virol 72 (Pt 7): 1695-1698.
- Eisen, M. B., S. Sabesan, et al. (1997). "Binding of the influenza A virus to cell-surface receptors: structures of five hemagglutinin-sialyloligosaccharide complexes determined by X-ray crystallography." Virology 232(1): 19-31.
- Ennis, F. A., A. H. Rook, et al. (1981). "HLA restricted virus-specific cytotoxic T-lymphocyte responses to live and inactivated influenza vaccines." Lancet 2(8252): 887-891.
- Feldman, S. A., S. Audet, et al. (2000). "The fusion glycoprotein of human respiratory syncytial virus facilitates virus attachment and infectivity via an interaction with cellular heparan sulfate." J Virol 74(14): 6442-6447.
- Feldman, S. A., R. M. Hendry, et al. (1999). "Identification of a linear heparin binding domain for human respiratory syncytial virus attachment glycoprotein G." J Virol 73(8): 6610-6617.
- Fields, B. N., D. M. Knipe, et al. (2013). Fields virology. Philadelphia, Wolters Kluwer/Lippincott Williams & Wilkins Health.
- Fleischer, B., H. Becht, et al. (1985). "Recognition of viral antigens by human influenza A virus-specific T lymphocyte clones." J Immunol 135(4): 2800-2804.

- Foo, J. J., V. Chan, et al. (2003). "Contact deformation of liposome in the presence of osmosis." Ann Biomed Eng 31(10): 1279-1286.
- Fritz, R. S., F. G. Hayden, et al. (1999). "Nasal cytokine and chemokine responses in experimental influenza A virus infection: results of a placebo-controlled trial of intravenous zanamivir treatment." J Infect Dis 180(3): 586-593.
- Gambaryan, A. S., A. B. Tuzikov, et al. (2002). "Polymeric inhibitor of influenza virus attachment protects mice from experimental influenza infection." Antiviral Res 55(1): 201-205.
- Gamian, A., M. Chomik, et al. (1991). "Inhibition of Influenza-a Virus Hemagglutinin and Induction of Interferon by Synthetic Sialylated Glycoconjugates." Canadian Journal of Microbiology 37(3): 233-237.
- Gerdil, C. (2003). "The annual production cycle for influenza vaccine." Vaccine 21(16): 1776-1779.
- Gerhard, W., K. Mozdzanowska, et al. (1997). "Role of the B-cell response in recovery of mice from primary influenza virus infection." Immunol Rev 159: 95-103.
- Glaser, L., J. Stevens, et al. (2005). "A single amino acid substitution in 1918 influenza virus hemagglutinin changes receptor binding specificity." J Virol 79(17): 11533-11536.
- Glick, G. D., P. L. Toogood, et al. (1991). "Ligand recognition by influenza virus. The binding of bivalent sialosides." J Biol Chem 266(35): 23660-23669.
- Govorkova, E. A., T. Baranovich, et al. (2013). "Antiviral resistance among highly pathogenic influenza A (H5N1) viruses isolated worldwide in 2002-2012 shows need for continued monitoring." Antiviral Res 98(2): 297-304.
- Gowdy, K. M., Q. T. Krantz, et al. (2010). "Role of oxidative stress on diesel-enhanced influenza infection in mice." Part Fibre Toxicol 7: 34.
- Gower, T. L., M. K. Pastey, et al. (2005). "RhoA signaling is required for respiratory syncytial virus-induced syncytium formation and filamentous virion morphology." J Virol 79(9): 5326-5336.
- Graham, M. B. and T. J. Braciale (1997). "Resistance to and recovery from lethal influenza virus infection in B lymphocyte-deficient mice." J Exp Med 186(12): 2063-2068.
- Gubareva, L. V., A. A. Trujillo, et al. (2010). "Comprehensive assessment of 2009 pandemic influenza A (H1N1) virus drug susceptibility in vitro." Antivir Ther 15(8): 1151-1159.
- Guo, C. T., X. L. Sun, et al. (2002). "An O-glycoside of sialic acid derivative that inhibits both hemagglutinin and sialidase activities of influenza viruses." Glycobiology 12(3): 183-190.
- Ha, Y., D. J. Stevens, et al. (2001). "X-ray structures of H5 avian and H9 swine influenza virus hemagglutinins bound to avian and human receptor analogs." Proc Natl Acad Sci U S A 98(20): 11181-11186.
- Hagenaars, N., E. Mastrobattista, et al. (2009). "Physicochemical and immunological characterization of N,N,N-trimethyl chitosan-coated whole inactivated influenza virus vaccine for intranasal administration." Pharm Res 26(6): 1353-1364.
- Hancock, K., V. Veguilla, et al. (2009). "Cross-reactive antibody responses to the 2009 pandemic H1N1 influenza virus." N Engl J Med 361(20): 1945-1952.

- Hartshorn, K., D. Chang, et al. (1996). "Interactions of recombinant human pulmonary surfactant protein D and SP-D multimers with influenza A." Am J Physiol 271(5 Pt 1): L753-762.
- Hartshorn, K. L., E. C. Crouch, et al. (1994). "Evidence for a protective role of pulmonary surfactant protein D (SP-D) against influenza A viruses." J Clin Invest 94(1): 311-319.
- Hartshorn, K. L., K. Sastry, et al. (1993). "Human mannose-binding protein functions as an opsonin for influenza A viruses." J Clin Invest 91(4): 1414-1420.
- Hayden, F. (2009). "Developing new antiviral agents for influenza treatment: what does the future hold?" Clin Infect Dis 48 Suppl 1: S3-13.
- Henrickson, K. J., S. M. Kuhn, et al. (1994). "Epidemiology and cost of infection with human parainfluenza virus types 1 and 2 in young children." Clin Infect Dis 18(5): 770-779.
- Hensley, S. E., S. R. Das, et al. (2009). "Hemagglutinin receptor binding avidity drives influenza A virus antigenic drift." Science 326(5953): 734-736.
- Hiemenz, J. W. and T. J. Walsh (1996). "Lipid formulations of amphotericin B: recent progress and future directions." Clin Infect Dis 22 Suppl 2: S133-144.
- Hobbie, S. N., K. Viswanathan, et al. (2013). "Modular glycosphere assays for high-throughput functional characterization of influenza viruses." BMC Biotechnol 13(1): 34.
- Ibricevic, A., A. Pekosz, et al. (2006). "Influenza virus receptor specificity and cell tropism in mouse and human airway epithelial cells." J Virol 80(15): 7469-7480.
- Ichinohe, T., I. K. Pang, et al. (2010). "Influenza virus activates inflammasomes via its intracellular M2 ion channel." Nat Immunol 11(5): 404-410.
- Ikonen, N., M. Strengell, et al. (2010). "High frequency of cross-reacting antibodies against 2009 pandemic influenza A(H1N1) virus among the elderly in Finland." Euro Surveill 15(5).
- Immordino, M. L., F. Dosio, et al. (2006). "Stealth liposomes: review of the basic science, rationale, and clinical applications, existing and potential." Int J Nanomedicine 1(3): 297-315.
- Iozzo, R. V. (1998). "Matrix proteoglycans: from molecular design to cellular function." Annu Rev Biochem 67: 609-652.
- Ito, T., Y. Suzuki, et al. (1997). "Differences in sialic acid-galactose linkages in the chicken egg amnion and allantois influence human influenza virus receptor specificity and variant selection." J Virol 71(4): 3357-3362.
- Itoh, M., P. Hetterich, et al. (1995). "Suppression of Influenza-Virus Infection by an N-Thioacetylneuraminic Acid Acrylamide Copolymer Resistant to Neuraminidase." Virology 212(2): 340-347.
- Jagger, B. W., H. M. Wise, et al. (2012). "An overlapping protein-coding region in influenza A virus segment 3 modulates the host response." Science 337(6091): 199-204.
- Jing, X., C. Ma, et al. (2008). "Functional studies indicate amantadine binds to the pore of the influenza A virus M2 proton-selective ion channel." Proc Natl Acad Sci U S A 105(31): 10967-10972.

- Kaneko, T., N. Baba, et al. (1996). "Cytotoxicity of phosphatidylcholine hydroperoxides is exerted through decomposition of fatty acid hydroperoxide moiety." Free Radic Biol Med 21(2): 173-179.
- Katz, J. M., W. Lim, et al. (1999). "Antibody response in individuals infected with avian influenza A (H5N1) viruses and detection of anti-H5 antibody among household and social contacts." J Infect Dis 180(6): 1763-1770.
- Kiessling, L. L. and N. L. Pohl (1996). "Strength in numbers: non-natural polyvalent carbohydrate derivatives." Chem Biol 3(2): 71-77.
- Kingerywood, J. E., K. W. Williams, et al. (1992). "The Agglutination of Erythrocytes by Influenza-Virus Is Strongly Inhibited by Liposomes Incorporating an Analog of Sialyl Gangliosides." Journal of the American Chemical Society 114(18): 7303-7305.
- Klein, M. R., J. Veenstra, et al. (1997). "Gag-specific immune responses after immunization with p17/p24:Ty virus-like particles in HIV type 1-seropositive individuals." AIDS Res Hum Retroviruses 13(5): 393-399.
- Krause, J. C., T. Tsibane, et al. (2012). "Human Monoclonal Antibodies to Pandemic 1957 H2N2 and Pandemic 1968 H3N2 Influenza Viruses." J Virol 86(11): 6334-6340.
- Krauze, M. T., C. O. Noble, et al. (2007). "Convection-enhanced delivery of nanoliposomal CPT-11 (irinotecan) and PEGylated liposomal doxorubicin (Doxil) in rodent intracranial brain tumor xenografts." Neuro Oncol 9(4): 393-403.
- Krusat, T. and H. J. Streckert (1997). "Heparin-dependent attachment of respiratory syncytial virus (RSV) to host cells." Arch Virol 142(6): 1247-1254.
- La Gruta, N. L., K. Kedzierska, et al. (2007). "A question of self-preservation: immunopathology in influenza virus infection." Immunol Cell Biol 85(2): 85-92.
- Lachmann, P. (2009). "Anti-infective antibodies--reviving an old paradigm." Vaccine 27 Suppl 6: G33-37.
- Lakadamyali, M., M. J. Rust, et al. (2004). "Endocytosis of influenza viruses." Microbes Infect 6(10): 929-936.
- Lees, W. J., A. Spaltenstein, et al. (1994). "Polyacrylamides Bearing Pendant Alpha-Sialoside Groups Strongly Inhibit Agglutination of Erythrocytes by Influenza-a Virus - Multivalency and Steric Stabilization of Particulate Biological-Systems." J Med Chem 37(20): 3419-3433.
- LeVine, A. M., J. A. Whitsett, et al. (2001). "Surfactant protein D enhances clearance of influenza A virus from the lung in vivo." J Immunol 167(10): 5868-5873.
- Li, S., J. Y. Min, et al. (2006). "Binding of the influenza A virus NS1 protein to PKR mediates the inhibition of its activation by either PACT or double-stranded RNA." Virology 349(1): 13-21.
- Lin, Y. P., X. Xiong, et al. (2012). "Evolution of the receptor binding properties of the influenza A(H3N2) hemagglutinin." Proc Natl Acad Sci U S A 109(52): 21474-21479.
- Lu, Y., M. Wambach, et al. (1995). "Binding of the influenza virus NS1 protein to double-stranded RNA inhibits the activation of the protein kinase that phosphorylates the eIF-2 translation initiation factor." Virology 214(1): 222-228.
- Mammen, M., G. Dahmann, et al. (1995). "Effective Inhibitors of Hemagglutination by Influenza-Virus Synthesized from Polymers Having Active Ester Groups - Insight into Mechanism of Inhibition." J Med Chem 38(21): 4179-4190.

- Mandelboim, O., N. Lieberman, et al. (2001). "Recognition of haemagglutinins on virus-infected cells by NKp46 activates lysis by human NK cells." Nature 409(6823): 1055-1060.
- Mao, H., W. Tu, et al. (2009). "Influenza virus directly infects human natural killer cells and induces cell apoptosis." J Virol 83(18): 9215-9222.
- Markwell, M. A. and J. C. Paulson (1980). "Sendai virus utilizes specific sialyloligosaccharides as host cell receptor determinants." Proc Natl Acad Sci U S A 77(10): 5693-5697.
- Martin-Sosa, S., M. J. Martin, et al. (2003). "Sialyloligosaccharides in human and bovine milk and in infant formulas: variations with the progression of lactation." J Dairy Sci 86(1): 52-59.
- Martinez, I. and J. A. Melero (2000). "Binding of human respiratory syncytial virus to cells: implication of sulfated cell surface proteoglycans." J Gen Virol 81(Pt 11): 2715-2722.
- Matrosovich, M. N., A. S. Gambaryan, et al. (1993). "Probing of the receptor-binding sites of the H1 and H3 influenza A and influenza B virus hemagglutinins by synthetic and natural sialosides." Virology 196(1): 111-121.
- McDonald, N. J., C. B. Smith, et al. (2007). "Antigenic drift in the evolution of H1N1 influenza A viruses resulting from deletion of a single amino acid in the haemagglutinin gene." J Gen Virol 88(Pt 12): 3209-3213.
- Mocarski, E. S., J. W. Upton, et al. (2012). "Viral infection and the evolution of caspase 8-regulated apoptotic and necrotic death pathways." Nat Rev Immunol 12(2): 79-88.
- Mochalova, L. V., A. B. Tuzikov, et al. (1994). "Synthetic Polymeric Inhibitors of Influenza-Virus Receptor-Binding Activity Suppress Virus-Replication." Antiviral Research 23(3-4): 179-190.
- Moscona, A. (2005). "Neuraminidase inhibitors for influenza." N Engl J Med 353(13): 1363-1373.
- Murphy, B. R., E. G. Chalhub, et al. (1973). "Temperature-sensitive mutants of influenza virus. 3. Further characterization of the ts-1(E) influenza A recombinant (H3N2) virus in man." J Infect Dis 128(4): 479-487.
- Nayak, D. P., E. K. Hui, et al. (2004). "Assembly and budding of influenza virus." Virus Res 106(2): 147-165.
- O'Donnell, C. D., L. Vogel, et al. (2012). "Antibody pressure by a human monoclonal antibody targeting the 2009 pandemic H1N1 virus hemagglutinin drives the emergence of a virus with increased virulence in mice." MBio 3(3).
- Ohkura, T., Y. Kikuchi, et al. (2012). "Epitope mapping of neutralizing monoclonal antibody in avian influenza A H5N1 virus hemagglutinin." Biochem Biophys Res Commun 418(1): 38-43.
- Osterholm, M. T., N. S. Kelley, et al. (2012). "Efficacy and effectiveness of influenza vaccines: a systematic review and meta-analysis." Lancet Infect Dis 12(1): 36-44.
- Pappas, C., K. Viswanathan, et al. (2010). "Receptor specificity and transmission of H2N2 subtype viruses isolated from the pandemic of 1957." PLoS One 5(6): e11158.
- Petitou, M., J. P. Herault, et al. (1999). "Synthesis of thrombin-inhibiting heparin mimetics without side effects." Nature 398(6726): 417-422.
- Pociask, D. A., E. V. Scheller, et al. (2013). "IL-22 is essential for lung epithelial repair following influenza infection." Am J Pathol 182(4): 1286-1296.

- Popp, M. W., R. A. Karssemeijer, et al. (2012). "Chemoenzymatic site-specific labeling of influenza glycoproteins as a tool to observe virus budding in real time." PLoS Pathog 8(3): e1002604.
- Potter, C. W. (2001). "A history of influenza." J Appl Microbiol 91(4): 572-579.
- Powell, T. J., D. W. Dwyer, et al. (2006). "The immune system provides a strong response to even a low exposure to virus." Clin Immunol 119(1): 87-94.
- Pritchett, T. J., R. Brossmer, et al. (1987). "Recognition of Mono-Valent Sialosides by Influenza-Virus H-3 Hemagglutinin." Virology 160(2): 502-506.
- Reuter, J. D., A. Myc, et al. (1999). "Inhibition of viral adhesion and infection by sialic-acid-conjugated dendritic polymers." Bioconjug Chem 10(2): 271-278.
- Robb, N. C., M. Smith, et al. (2009). "NS2/NEP protein regulates transcription and replication of the influenza virus RNA genome." J Gen Virol 90(Pt 6): 1398-1407.
- Rubartelli, A. and M. T. Lotze (2007). "Inside, outside, upside down: damage-associated molecular-pattern molecules (DAMPs) and redox." Trends Immunol 28(10): 429-436.
- Rubenstein, J. L., B. A. Smith, et al. (1979). "Lateral diffusion in binary mixtures of cholesterol and phosphatidylcholines." Proc Natl Acad Sci U S A 76(1): 15-18.
- Rudneva, I., A. Ignatieva, et al. (2012). "Escape mutants of pandemic influenza A/H1N1 2009 virus: Variations in antigenic specificity and receptor affinity of the hemagglutinin." Virus Res 166(1-2): 61-67.
- Russell, R. J., D. J. Stevens, et al. (2006). "Avian and human receptor binding by hemagglutinins of influenza A viruses." Glycoconj J 23(1-2): 85-92.
- Sauter, N. K., M. D. Bednarski, et al. (1989). "Hemagglutinins from two influenza virus variants bind to sialic acid derivatives with millimolar dissociation constants: a 500-MHz proton nuclear magnetic resonance study." Biochemistry 28(21): 8388-8396.
- Scherle, P. A., G. Palladino, et al. (1992). "Mice can recover from pulmonary influenza virus infection in the absence of class I-restricted cytotoxic T cells." J Immunol 148(1): 212-217.
- Schmitz, N., M. Kurrer, et al. (2005). "Interleukin-1 is responsible for acute lung immunopathology but increases survival of respiratory influenza virus infection." J Virol 79(10): 6441-6448.
- Schneider, C. A., W. S. Rasband, et al. (2012). "NIH Image to ImageJ: 25 years of image analysis." Nat Methods 9(7): 671-675.
- Schnyder, B., C. Lima, et al. (2010). "Interleukin-22 is a negative regulator of the allergic response." Cytokine 50(2): 220-227.
- Seibert, C. W., S. Rahmat, et al. (2013). "Recombinant IgA is sufficient to prevent influenza virus transmission in guinea pigs." J Virol.
- Seki, M., S. Kohno, et al. (2010). "Critical role of IL-1 receptor-associated kinase-M in regulating chemokine-dependent deleterious inflammation in murine influenza pneumonia." J Immunol 184(3): 1410-1418.
- Seo, S. U., H. J. Kwon, et al. (2010). "MyD88 signaling is indispensable for primary influenza A virus infection but dispensable for secondary infection." J Virol 84(24): 12713-12722.
- Seya, T., H. Shime, et al. (2012). "TLR3/TICAM-1 signaling in tumor cell RIP3-dependent necroptosis." Oncoimmunology 1(6): 917-923.

- Simonsen, L., M. J. Clarke, et al. (1998). "Pandemic versus epidemic influenza mortality: a pattern of changing age distribution." *J Infect Dis* 178(1): 53-60.
- Skehel, J. J. and D. C. Wiley (2000). "Receptor binding and membrane fusion in virus entry: the influenza hemagglutinin." *Annu Rev Biochem* 69: 531-569.
- Spaltenstein, A. and G. M. Whitesides (1991). "Polyacrylamides Bearing Pendant Alpha-Sialoside Groups Strongly Inhibit Agglutination of Erythrocytes by Influenza-Virus." *Journal of the American Chemical Society* 113(2): 686-687.
- Sparks, M. A., K. W. Williams, et al. (1993). "Synthesis of Potential Inhibitors of Hemagglutination by Influenza-Virus - Chemoenzymic Preparation of N-5 Analogs of N-Acetylneuraminic Acid." *Tetrahedron* 49(1): 1-12.
- Spevak, W., J. O. Nagy, et al. (1993). "Polymerized Liposomes Containing C-Glycosides of Sialic-Acid - Potent Inhibitors of Influenza-Virus Invitro Infectivity." *Journal of the American Chemical Society* 115(3): 1146-1147.
- Strutt, T. M., K. K. McKinstry, et al. (2010). "Memory CD4+ T cells induce innate responses independently of pathogen." *Nat Med* 16(5): 558-564, 551p following 564.
- Sugimoto, K., A. Ogawa, et al. (2008). "IL-22 ameliorates intestinal inflammation in a mouse model of ulcerative colitis." *J Clin Invest* 118(2): 534-544.
- Sullivan, K. M. (1996). "Health impact of influenza in the United States." *Pharmacoeconomics* 9 Suppl 3: 26-33; discussion 50-23.
- Summerfield, A. and K. C. McCullough (2009). "Dendritic Cells in Innate and Adaptive Immune Responses against Influenza Virus." *Viruses* 1(3): 1022-1034.
- Sun, X. L., Y. Kanie, et al. (2000). "Syntheses of C-3-modified sialylglycosides as selective inhibitors of influenza hemagglutinin and neuraminidase." *European Journal of Organic Chemistry*(14): 2643-2653.
- Suwannakarn, K., T. Chieochansin, et al. (2010). "Molecular evolution of human H1N1 and H3N2 influenza A virus in Thailand, 2006-2009." *PLoS One* 5(3): e9717.
- Tejaro, J. R., D. Turner, et al. (2011). "Cutting edge: Tissue-retentive lung memory CD4 T cells mediate optimal protection to respiratory virus infection." *J Immunol* 187(11): 5510-5514.
- Toogood, P. L., P. K. Galliker, et al. (1991). "Monovalent Sialosides That Bind Tightly to Influenza-a Virus." *J Med Chem* 34(10): 3138-3140.
- Tumpey, T. M., A. Garcia-Sastre, et al. (2005). "Pathogenicity of influenza viruses with genes from the 1918 pandemic virus: functional roles of alveolar macrophages and neutrophils in limiting virus replication and mortality in mice." *J Virol* 79(23): 14933-14944.
- Tuzikov, A. B., A. S. Gambaryan, et al. (2000). "Conversion of complex sialooligosaccharides into polymeric conjugates and their anti-influenza virus inhibitory potency." *Journal of Carbohydrate Chemistry* 19(9): 1191-1200.
- Upton, J. W., W. J. Kaiser, et al. (2010). "Virus inhibition of RIP3-dependent necrosis." *Cell Host & Microbe* 7(4): 302-313.
- van de Sandt, C. E., J. H. Kreijtz, et al. (2012). "Evasion of influenza A viruses from innate and adaptive immune responses." *Viruses* 4(9): 1438-1476.
- van Steensel, B., E. P. van Binnendijk, et al. (1996). "Partial colocalization of glucocorticoid and mineralocorticoid receptors in discrete compartments in nuclei of rat hippocampus neurons." *J Cell Sci* 109 (Pt 4): 787-792.

- Visekruna, A., J. Ritter, et al. (2013). "Tc9 cells, a new subset of CD8(+) T cells, support Th2-mediated airway inflammation." Eur J Immunol 43(3): 606-618.
- von Itzstein, M., W. Y. Wu, et al. (1993). "Rational design of potent sialidase-based inhibitors of influenza virus replication." Nature 363(6428): 418-423.
- Wareing, M. D., A. B. Lyon, et al. (2004). "Chemokine expression during the development and resolution of a pulmonary leukocyte response to influenza A virus infection in mice." J Leukoc Biol 76(4): 886-895.
- Weinhold, E. G. and J. R. Knowles (1992). "Design and Evaluation of a Tightly Binding Fluorescent Ligand for Influenza-a Hemagglutinin." Journal of the American Chemical Society 114(24): 9270-9275.
- Weirich, K. L., J. N. Israelachvili, et al. (2010). "Bilayer edges catalyze supported lipid bilayer formation." Biophys J 98(1): 85-92.
- Woodle, M. C. and D. D. Lasic (1992). "Sterically stabilized liposomes." Biochim Biophys Acta 1113(2): 171-199.
- WuDunn, D. and P. G. Spear (1989). "Initial interaction of herpes simplex virus with cells is binding to heparan sulfate." J Virol 63(1): 52-58.
- Xu, D., E. I. Newhouse, et al. (2009). "Distinct glycan topology for avian and human sialopentasaccharide receptor analogues upon binding different hemagglutinins: a molecular dynamics perspective." J Mol Biol 387(2): 465-491.
- Zhang, Z., S. A. McCallum, et al. (2008). "Solution structures of chemoenzymatically synthesized heparin and its precursors." Journal of the American Chemical Society 130(39): 12998-13007.
- Zhu, W., J. Li, et al. (2011). "How does cellular heparan sulfate function in viral pathogenicity?" Biomed Environ Sci 24(1): 81-87.